Bridge Vulnerability Assessment and Mitigation against Explosions

Final Report
December 2010

IOWA STATE UNIVERSITY
Institute for Transportation

Sponsored by
University Transportation Centers Program,
U.S. Department of Transportation
(MTC Project 2007-06)
California Department of Transportation
University of Missouri-Columbia

About the MTC

The mission of the University Transportation Centers (UTC) program is to advance U.S. technology and expertise in the many disciplines comprising transportation through the mechanisms of education, research, and technology transfer at university-based centers of excellence. The Midwest Transportation Consortium (MTC) is a Tier 1 University Transportation Center that includes Iowa State University, the University of Iowa, and the University of Northern Iowa. Iowa State University, through its Institute for Transportation (InTrans), is the MTC's lead institution.

Disclaimer Notice

Non-Discrimination Statement

Technical Report Documentation Page

1. Report No. MTC Project 2007-06	**2. Government Accession No.**	**3. Recipient's Catalog No.**	
4. Title and Subtitle Bridge Vulnerability Assessment and Mitigation against Explosions		**5. Report Date** December 2010	
		6. Performing Organization Code	
7. Author(s) Kiger, Sam A., Hani A. Salim, and Ahmed Ibrahim		**8. Performing Organization Report No.**	
9. Performing Organization Name and Address National Center for Explosion Resistant Design University of Missouri-Columbia Columbia, MO 65211-2200		**10. Work Unit No. (TRAIS)**	
		11. Contract or Grant No.	
12. Sponsoring Organization Name and Address California Department of Transportation 1120 N Street P.O. Box 942873 Sacramento, CA 942873-0001	University of Missouri-Columbia Columbia, MO 65211-2200	**13. Type of Report and Period Covered** Final Report	
		14. Sponsoring Agency Code	
Midwest Transportation Consortium Institute for Transportation 2711 South Loop Drive, Suite 4700 Ames, IA 50010-8664			
15. Supplementary Notes Visit www.intrans.iastate.edu/mtc/research.cfm for color PDF files of this and other research reports.			
16. Abstract In this research, a literature review of the effect of blast loads on bridges is presented. The review indicates a need to establish design criteria for post-tensioned box girder bridges subjected to blast loads, based on numerical and analytical results. This design criterion would predict the relation between the charge size and the damage type (no damage, spall, and breach). For these needs, numerical models based on the nonlinear explicit finite element method were developed to predict the damage type. Specific conclusions and recommendations are presented.			
17. Key Words blast load effects on bridges—box girder bridge blast load resistance—bridge damage prediction— bridge explosion mitigation—bridge explosion vulnerability—critical bridge assessment—post-tensioned box girder bridge assessment		**18. Distribution Statement** No restrictions.	
19. Security Classification (of this report) Unclassified.	**20. Security Classification (of this page)** Unclassified.	**21. No. of Pages** 74	**22. Price** NA

Form DOT F 1700.7 (8-72) **Reproduction of completed page authorized**

Bridge Vulnerability Assessment and Mitigation against Explosions

Final Report
December 2010

Principal Investigators

Sam A. Kiger and Hani A. Salim
Civil and Environmental Engineering, National Center for Explosion Resistant Design
University of Missouri, Columbia, Missouri 65211-2200
KigerS@missouri.edu; SalimH@missouri.edu

Research Assistant
Ahmed Ibrahim
Civil Engineering and Construction Department
206 Jobst Hall, Bradley University, Peoria, Illinois 61625
aibrahim@Bradley.edu

Authors
Sam A. Kiger, Hani A. Salim, and Ahmed Ibrahim

Sponsored by
Midwest Transportation Consortium
a U.S. DOT Tier 1 University Transportation Center
(MTC Project 2007-06)
California Department of Transportation
University of Missouri-Columbia

A report from
Midwest Transportation Consortium
Iowa State University
2711 S. Loop Drive, Suite 4700
Ames, Iowa 50010-8664
Phone: 515-294-8103
Fax: 515-294-0467
www.mtc.iastate.edu

TABLE OF CONTENTS

LIST OF FIGURES

LIST OF TABLES

ACKNOWLEDGMENTS

The authors greatly appreciate the financial support from the Midwest Transportation Consortium (MTC) of the Institute for Transportation (InTrans) at Iowa State University, Ames, Iowa and the financial support and guidance provided by the California Department of Transportation (CalTrans), Sacramento, California.

1. Introduction

This report focuses on the structural and material response of post-tensioned box girder bridges under blast loads. The bridge is simulated using the explicit dynamic finite element hydrodynamic code LSDYNA. It is assumed that the explosive material was located on top the bridge deck. However, when an explosion occurs over the concrete deck of any bridge, the rest of the bridge superstructure could be affected due to the localized damage to the deck. The results and the analyses of various parameters of the box girder bridge on the dynamic response and failure mechanism of the bridge under blast loads are discussed in this report.

The behavior of a simply supported and a continuous post-tensioned box girder bridge of 100 ft span under blast loads is presented in this report. The main parameters of this study were the high explosive charge size, explosive location over the bridge deck, the material properties of steel and concrete used in the bridge construction, and the effect of prestressing force used in the concrete deck section as a solution to decrease the damage level. One-quarter of the simple span bridge and half scale for the continuous system were modeled taking into account the appropriate boundary symmetry conditions. The effects of above parameters on the overall behavior of the bridge (local and global) under the high velocity shock blast pressure waves were performed and evaluated in this study. The study used eight different amounts of TNT high explosive material. The explosives are represented by a multiplier of 'W', where W represents a specific amount of explosive weight, in lbs.

2. Background

The statistics of worldwide attacks against bridges were recorded by the Mineta Transportation Institute indicated that 53 terrorist attacks between 1980 and 2006, and 60% of those attacks were explosions. One of the most common bridges in California is the box girder which is one of the most flexible deck forms. It can cover a range of spans from 82 ft up to the longest non-suspended concrete decks built; of the order of 1300 ft. Single box girders may also carry decks up to 160 ft wide. For the longer span beams, beyond about 160 ft, they are almost the only practicable deck sections. For the shorter spans they are in competition with most other deck types. The advantages of the box form are principally its high structural efficiency, which minimize the post-tensioned force required to resist high moments, and torsion resistance.

The box form can be built by several methods of bridge construction that have been progressively refined over the last 50 years, such as precast or cast-in-place segmental construction with epoxy in the joints, balanced cantilever method either precast in-situ or coupled with precast segmental construction. Several threats might damage these structures like collisions, earthquakes, severe wind storms, and even explosions which could be from accidents or terrorist attacks. Blast loads are considered a special type of loading different than loading from earthquakes or wind. The later loads cause global structural response and build up over longer time periods which means the structural members can work together to resist these loads. In the case of air blast, the extremely intense blast loads last only a few milliseconds and can produce a local material response, which means that not all the structural components are available to compositely resist the blast loading.

2.1 Blast Loads

Blast loads are considered one of the extreme loads affecting structures, and even a small amount of explosive can produce severe localized damage to the structure. In some cases this localized severe damage can potentially progress to global collapse of the entire structure. An explosion starts when a high explosive material is detonated forming a detonation wave in the material. The detonation wave typically moves at velocities of 18,000 ft/s to 20,000 ft/s and is pressurized at up to 4×10^6 psi with temperatures in the range of 8,000°F. This hot gas is expanded, as a rapid release of energy occurs. A shock front moving at supersonic velocity is formed in front of this gas and is called the blast wave or shock front. This wave propagates outward in all directions from the detonation center. The front of the wave, or the shock front, travels faster that the speed of sound.

The flow of the air mass behind the shock results in an outward movement of air and debris causing drag loading on the structure and is known as the dynamic pressure. This dynamic pressure loading is a function of the structural shape, incident pressure, air density, and the explosive material. Figure 1 shows a typical curve for incident pressure and the dynamic pressure over time. As seen from Figure 1, the blast load is characterized by a positive phase which is considered in the design and a negative phase which is normally neglected as its effect is very small compared to the positive phase. The reflected pressure shown in Figure 1 is the reflected pressure loading on any structural surface the moving shock front impinges upon.

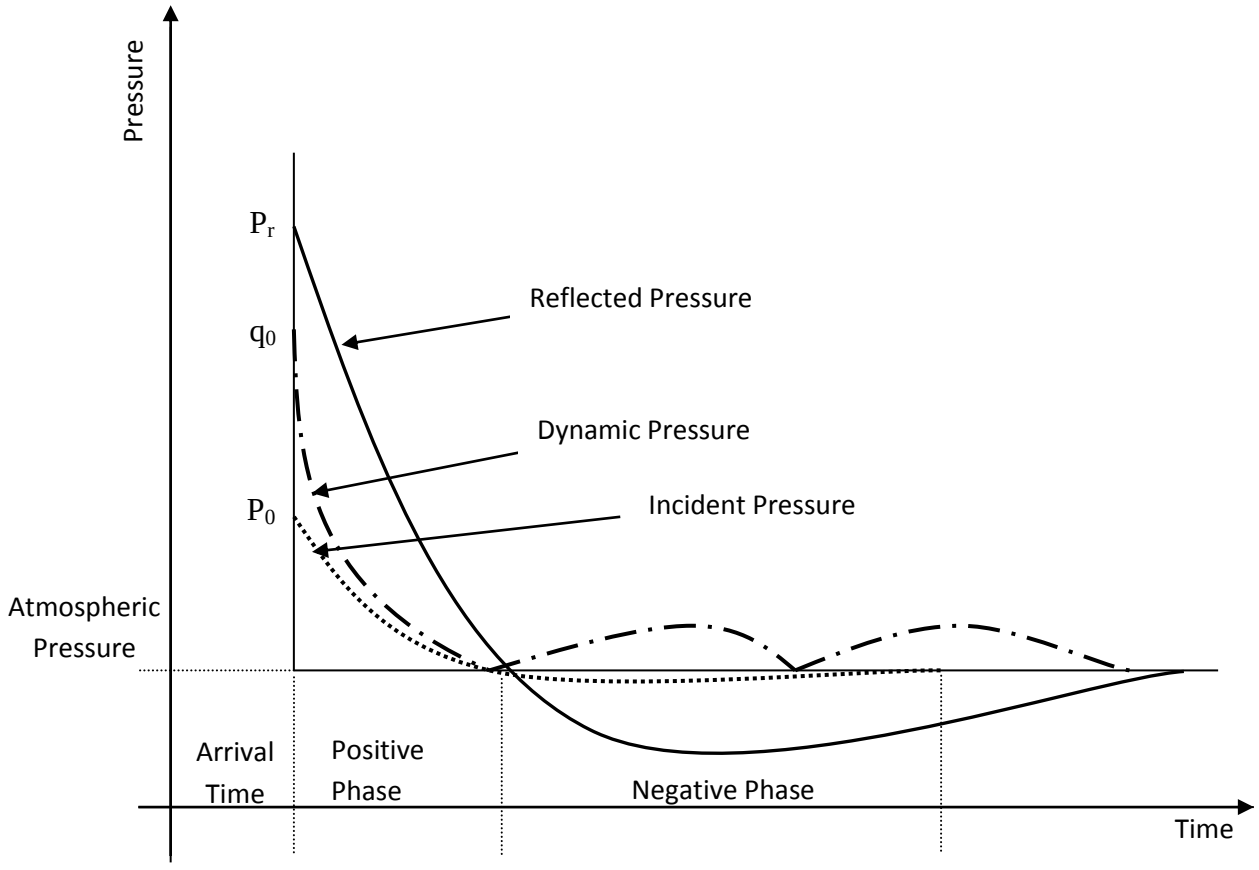

Figure 1. Variation of overpressure and dynamic pressure over time (ASCE, 1997)

2.2 Blast on Bridges

The study of the structural and material response of bridges under blast loads are conducted either by experiments or numerical simulations. However experiments are difficult to be done in full scale and are costly to perform. In addition to that, the other important factor is the difficulty of measuring the various parameters in the field for close-in detonations where the instrument is often destroyed and the failure process is difficult to document. Therefore, numerical solutions are considered an attractive approach to evaluating bridge response to explosions and are very important to support any blast experiments on bridges.

In a study conducted by Marchand et al. (2004), the structural response of bridge piers subjected to vehicular and hand placed bombs was evaluated. Various standoff distances and charge weights of vehicular bombs were analyzed while the hand placed bomb was used to investigate the impact of a single bomb versus two bombs. Counterforce bombs are a set of bombs placed on opposite sides of an object so that both sides of the object experience identical pressures (Marchand et al., 2004).

Once the loads were applied and the analysis was performed, it was determined that breaching of the concrete was the main factor that influenced the pier performance in both the vehicular blast and hand placed explosive scenarios. When 3000 and 5000 psi concrete piers were evaluated against one another, there was a 30% increase in breaching when the lower concrete strength was used. An evaluation of the piers when breaching was neglected indicated that the strength played only a small role in the performance of the columns. When breaching was neglected, there was only a 10% difference between the support rotations in the two piers (Marchand et al., 2004).

A simplified beam and spring system was used by Schleyer and Hsu (2000); however, the method of analysis and generation of transient displacement were quite different. This analysis was conducted to evaluate the maximum transient displacement of rectangular members subjected to blast loading. In this investigation, only a single beam and spring system was evaluated; however, this system could be combined together to create frames and arches. The springs were used at the end of the beam specimens to represent variable end conditions. An additional spring was used for the formation of the plastic hinge in the center of the specimen. Within the model, coupled mode shapes were used to represent the overall elastic-plastic behavior of the beam structure under blast pulse pressure loading. The loading case used for the analysis consisted of a uniformly distributed load.

The results generated from the simplified beam and spring analysis was compared with finite element models generated in ABAQUS and SDOF spring mass models. A transversely loaded rectangular beam was used for the comparison. The simplified method underestimated the maximum transient displacement of the beam; however, compared well for the remainder of the deflection results. The results generated from the single SDOF compared well with those produced with the simplified analysis since both methods assume the first mode shape. The accuracy of this method is a function of the equations used to generate the shape functions. With more complex equations, the results increased in accuracy. The drawback to this is the longer computational time (Schleyer and Hsu, 2000).

In addition to the two general types of analyses presented previously, hydrocodes and finite element analyses have also been applied to gain a better understanding of blast and impact loading. Hydrocode analysis allows for more investigation into experimental results and allows the researcher to see more details. It also gives the researcher a more cost effective manner of analysis. In addition to providing a comparison base for experimentation, these programs can also be used to validate simpler models and ensure accurate results have been generated.

Baylot et al. (2002) conducted research to determine an effective method of analyzing bridge girders with different charge sizes and locations. Through this investigation, they evaluated the effectiveness of determining a load measure. This is "a single number that includes the effects of load magnitude and distribution" (Baylot et al., 2002). If the load factor exceeded a predetermined critical value, the beam would fail. Through finite element analysis, it was determined that the load factor was proportional to the web thickness. The load factor associated with the height of the web was more complicated and was not directly proportional to the height of the web. Appropriate equations were developed to evaluate the load factor with respect to the web thickness and height. Upon evaluation of the load factor equations, it was determined that the equations would accurately predict the performance of a structure (Baylot et al., 2002).

Vulitsky et al. (2002) developed a numerical simulation using LS-DYNA to predict the effect of the detonation of high explosives on steel structures. This method was aimed at the explosive blast in the air to the structure. The simulation used Jones-Wilkins-Lee (JWL) equation of state to describe the explosive. A linear polynomial equation of state was used to simulate the behavior of air. The mix between air and explosion reaction products is modeled using LS-DYNA multi-materials capabilities. The blast pressure wave travelling through the air interacts with the structure by means of fluid-structure interface algorithms. Numerical results were compared with those from experiment and they gave maximum under-prediction deformations around 20-40%

Cimo (2007) performed background information related to loads caused by blasts and analytical modeling options, as well as a literature review of related research findings. AUTODYN, a commercially available non-linear dynamic program, was selected to conduct this modeling. A study to determine the most appropriate constitutive models considering the dynamic material properties was subsequently conducted. This resulted in the selection of four constitutive models for the four materials incorporated in the modeling – air, TNT, concrete, and steel. A mesh sensitivity analysis was also performed to determine the optimum element size to be used, considering the conflicting interests of increased accuracy and decreased processing speed and memory availability with smaller elements. For this analysis, AUTODYN results were compared against results generated using the semi-empirically based program called ConWep, as well as hand calculations, which also served as a general validation of the accuracy of the program. The results of the constitutive model studies and mesh sensitivity analyses were incorporated in developing a model of a cross-section of a two-lane bridge, where the performance of the cross-section when subjected to a below deck blast was investigated.

Within the bridge cross-section investigation, it was determined that the movement of the shock front and its interaction with the structure was greatly influenced by the girder location. Due to the reflected waves generated in confined corners, the pressure in the deck close to the girders

was increased and caused this to be the highest area of stress within the deck. Although the stresses were not enough to yield the reinforcement, the tensile strength of the concrete was exceeded and significant cracking occurred.

Williamson et al. (2006) presented the research results at the University of Texas for the design of different types of bridges to withstand blast loads. Based on the results of these analyses, performance-based design recommendations were provided to improve bridge response to blast loads to a level that is appropriate for a given threat scenario. Structural configurations considered in that research include the prestressed girder bridges, post-tensioned segmental boxes, steel bridges, trusses and cable stayed bridges. Williamson et al. (2006) concluded that practical and economical feasible design and retrofit solutions can be implemented to provide reasonable protection levels for threats from truck bombs and hand placed charges for a large number of bridges across the U.S. Bridges can be categorized based on their criticality to most effectively prioritize resources for bridges security. With this approach, the most expensive solutions are applied only to the most critical bridges. According to Williamson (2006), unimportant bridges do not need to be protected, while the most critical ones may require significant levels of protection. Less important, but still critical, bridges may require intermediate levels of protection.

Winget et al. (2005) discussed the previous develop performance–based blast load design standards tailored specifically for bridges. Based on the best practices obtained from international literature review, the research demonstrates the incorporation of physical security and site landscape principles into the design process. It then discusses the effects of blast loads on bridges and provides structural design and retrofit solutions to counter these effects.

Winget et al. (2005) showed that the study showed that bridge geometry can significantly affect the blast loads that develop below the bridge deck. For bridges with deep girders, confinement effects can greatly enhance the blast loads acting on the girders and the tops of the piers, and in some cases may result in more damage to the girders due to the formation of a Mach front. Explosions occurring near sloped abutments could possibly result in more damage than an explosion at mid-span due to the confinement effects at the abutments. Finally, round columns will experience lower loads due to the increased angle of incidence from the curved surface.

Nago et al. (2007) estimated that blast loading typically produces very high strain rate ranges of 10^2 to 10^4 s^{-1} rather than the ordinary static strain rates of 10^{-6} to 10^{-5} s^{-1}. At strain rates, the dynamic mechanical properties of the structure may be different from the mechanical properties under static loading. It is reported that the yield stress of mild steel could be doubled when the strain rate changes from 10^{-3} to 10^3 s^{-1}. Figure 2 shows the various strain rates according to the loading type, (Nago et al., 2004).

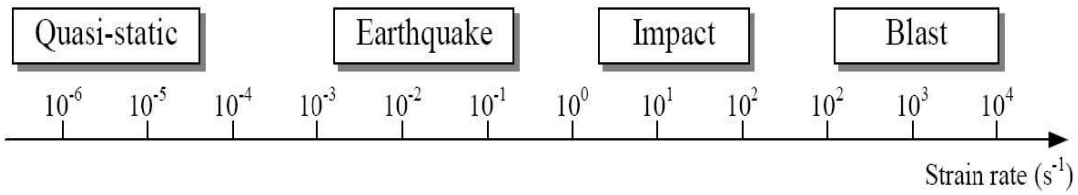

Figure 2. Strain rates versus loading type (Nago et al., 2004)

Islam et al. (2006) studied the blast capacity and protection of AASHTO girder bridges. Islam et al. (2006) stated that no specific AASHTO design guidelines exits for bridges against blast loading. The most common types of concrete bridges on interstates highways have been investigated and the capacity of critical elements was assessed. A 2-span 2-lane bridge with type III AASHTO girders was used for modeling. The girders, pier caps and columns were analyzed under blast loading to determine their capacities. The blast capacities of the AASHTO girders, piers and caps were determined and the required standoff distance of the explosion from the columns that may protect the bridge from failure was also studied**.**

The performance of cable supported bridge decks subjected to blast loads was conducted by Son (2008), who studied the behavior of steel orthotropic and composite plate girder decks subjected to blast loading. Using several materials, a design approach to protect cable supported bridges against blast events was suggested using steel orthotropic decks or orthotropic plate girder decks. Son (2008) proposed a design criterion based on the displacement of the suspended bridge under different amount of blast loads. Son (2008) concluded the following important points:

- Acceleration is the most dominant parameter affecting local behavior of a deck subjected to blast loading.
- The decks subjected to axial compressive loading could experience global progressive collapse.
- The self-anchored suspension bridges proved to be the most inferior systems among the three cable supported bridge systems with high probability of developing global progressive collapse due to their large axial load in the deck.

The effect of explosives on civil bridges was studied by Pelton (1993). It has been suggested that main load carrying members of all bridge structures can be classified into three categories:

Class One: complete ruin of the component will result in the complete destruction of the load carrying capacity of the bridge.

Class Two: complete or partial destruction of the component will diminish the load carrying capacity of the bridge, but repair will allow a reduced capability to be maintained.

Class Three: complete or partial destruction of the component will only have a localized effect on load carrying capacity, and the repair will allow the full capability to be restored.

In addition to the above research on the effect of blast loads on bridges, there are several studies on the effect of blast loads located underneath bridge decks. When the detonation occurs below the concrete deck, it is better to sacrifice the deck rather than the columns and the girders, (Winget et al., 2005). The longer the girders, the better the response to blast loads due to the mass, and the ductility. Winget et al. (2005) suggested using hinge restraint or extended column seats to prevent girders from falling.

2.3 Blast Retrofit using CFRP

Carbon Fiber Reinforced Polymer (CFRP) is considered one of the best retrofitting materials under static loads and it gave good results under blast loads due to strength- to-self -weight ratio and the large fatigue resistance. There are many different various results regarding the behavior of retrofitted structural components using CFRP but limited research exists for the behavior of

these types of material under blast loads. The following section will summarize the up-to- date results.

Kasidit et al. (2006) studied the structural behavior of Horsetail Greek Bridge strengthened by carbon reinforced polymer composites. The bridge superstructure and the substructure were modeled using the finite element code ANSYS. The bridge was analyzed under different truck loading at different locations. The results of the numerical analysis were compared to field data showing good agreement. The results presented in terms of strains in beams. Structural responses were compared for strengthened and un-strengthened bridge using the CFRP, which resulted in significant improvement to the structural performance.

The strengthening of the bridge using CFRP based on scaled truck and mass proportional loading increased the capacity by 28% and 37% respectively. The CFRP delayed the yielding of the reinforcement and the failure mode changed from sudden shear failure to flexural, which indicates ductility increased due to the CFRP composites.

The transient deformation and blast resistance of unidirectional fiber reinforced composites were studied by Betra et al. (2008). The unidirectional fibber reinforced layers were assumed perfectly bonded to each other when subject to blast load. The analyses were done using an in-house developed FORTRAN code; the code included the rate dependent damage equations for anisotropic bodies. The relative sliding between layers was modeled using the nodal releases technique. The effect of different materials and the loading parameters on damage propagation was considered. The goal of the study was to examine energy absorption and increasing the structural resistance to blast loads when unidirectional fiber reinforced composites was used.

Betra et al. (2008) concluded that the laminates deformation for close non-nuclear explosives detonations is similar to those induced by nuclear explosion. The increase in the fiber volume fraction decreases the total work done by external forces and hence decreases the kinetic energy imparted to the system.

A state-of-the-art review on blast resistance of FRP composites and polymer strengthened concrete and masonry structures was introduced by Buchan et al. (2007). The paper presented the latest and up-to-date researches on FRP and the blast effect on masonry walls. Blast resistance can be increased by adding additional concrete mass and reinforcement to the structure but the cost is one of the problems facing this technique. Another solution is using steel studs walls on the interior face of the walls facing the blast load to increase ductility and energy absorption. The choice of retrofitting materials is very important in optimizing performance and cost. Buchan et. al. (2007) summarized the material assessed in this approach for beams and slabs subject to high explosives.

The structural behavior of FRP composites bridge deck panels was studied by Alagusundaramoorthy et. al. (2006). The study evaluated the force-displacement responses of FRP composites bridge deck panels under AASHTO MS 22.5 (HS25) truck load up to failure. Several modes of failure were studied, including flexural and shear. The test results were compared with the performance criterion of Ohio Department of Transportation, the tested bridge panels gave good results with the safety factor varied from 3 to 8.

Five one-way slab specimens of decommissioned bridge in South Carolina were tested. Three of the slabs were strengthened on their soffit and the other two were taken as control specimens. The slabs were tested under monotonic and fatigue loads till failure, in addition, six half scale slabs were constructed as a model representing a bridge deck panels designed according to the LRFD manual.

Two slabs out of the six were retrofitted using CFRP grid retrofitted to their soffit. All the slabs were tested monotonically till failure. In all slab cases the ultimate load increased due to the CFRP strips which gave good improvements to the testing slabs under fatigue loads.

An analytical finite element model for study of FRP retrofitted concrete structures under blast loads was performed by Nam et al. (2009) to assess and compare a comprehensive finite element model of FRP that can be properly used in the simulation techniques. Four analytical models were tested to assess the behavior of the FRP sheets in retrofitted concrete structures. The models were isotropic linear elastic shell element, orthotropic linear elastic shell elements without shear deformations, orthotropic linear elastic shell elements with shear deformations, and linear elastic beam element model.

All the previous mentioned models were tested by using them in the simulation of RC slabs subject to blast load to validate the blast analysis technique. The finite element analysis was conducted using the explicit finite element code LS-DYNA with the appropriate models for concrete and steel taking the strain rate effect into consideration. The results showed that the orthotropic linear elastic shell elements without shear deformations gave stable convergence, independent of mesh size as well as giving most appropriate description of the dynamic behavior of the FRP.

Wu et al. (2009) investigated the blast resistance of ultra–high performance fiber reinforced concrete (UHPRC) and FRP-retrofitted concrete slabs, normal concrete slabs were tested as control specimens. The pressure and displacement were recorded at the middle point of the slab and the results were compared with TM5-1300. Wu et al. (2009) added the CFRP to the compression face of the slabs which increased the ductility and the blast resistance as well. The UHPFC samples suffered the least damage between all the specimens.

Mosalam et al. (2001) conducted a computational model using the finite element method to study the nonlinear transient behavior of reinforced concrete slab subjected to blast loading and retrofitted with CFRP composites. The model was used to investigate the effect of loading duration and the effect of the CFRP on the slabs damage accumulations. The study showed that using of CFRP prevents the total failure of the slab systems against the cracking and crushing of the as-built slabs. The load carrying capacity of the retrofitted slabs was increased by 200%. Retrofitting the two way slab systems by CFRP limited the spread of yielding in the steel reinforcement.

3. Post-Tensioned Box Girder Bridge Model

The bridge selected for this study is a post-tensioned concrete box girder type as shown in Figures 3-5. The bridge section was designed under conventional loads using the maximum truck live load conditions to obtain the safest section dimensions and the required area of prestressing and conventional steel that are common in the construction industry of these types of bridges.

The span length of the bridge is 100 ft (30.48 meters), the bridge deck width is 45.33 ft (13.81 meters), and the cross section dimensions are shown in Figure 4.

The bridge was designed using current AASHTO HL-93 truck loading, which consists of a design truck, design tandem, and a design lane load. Those loads were used to design the bridge cross section dimensions and reinforcements. The loads and properties used in the study are shown in Table 1.

The bridge under consideration was designed according the ultimate strength, and serviceability limit states using the above mentioned loads following the AASHTO LRFD specifications. Starting with the design of the concrete deck, then the live load force effects, preliminary choice of the prestressing tendons, prediction of the cables losses, checking the stresses at the transfer and service conditions, estimating the immediate and the long term deflection, and finally the profile of the tendons was designed. The post-tensioned steel profile was assumed to be straight strands at the lower portion of the vertical webs.

The bridge model was constructed in the nonlinear dynamic finite element code LS-DYNA after the hand calculations were performed under dead and live loads. The details of the material models and finite element mesh will be discussed in the next section.

Table 1. AASHTO HL-93 loading

Load Type	Design Loads of The Box Girder Bridge	Design Loads for the Concrete Deck
Design Truck	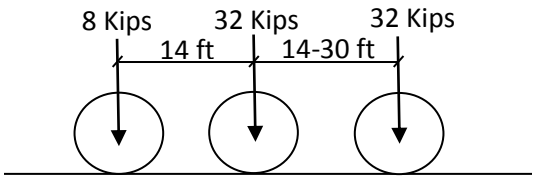	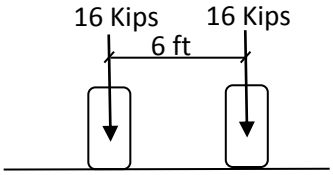
Design Tandem	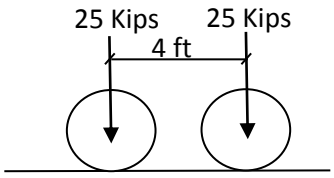	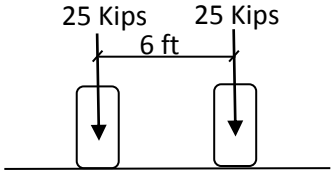
Design Lane	Uniform load equals 0.64 kip/ft/lane	N/A

4. Finite Element Model of Bridge Deck

The box girder bridge was modeled using the nonlinear finite element code LS-DYNA, the material properties of the bridge components are presented next taking into consideration the strain rate effect for all the used materials, also the material prosperities of the high explosives as well as for the air.

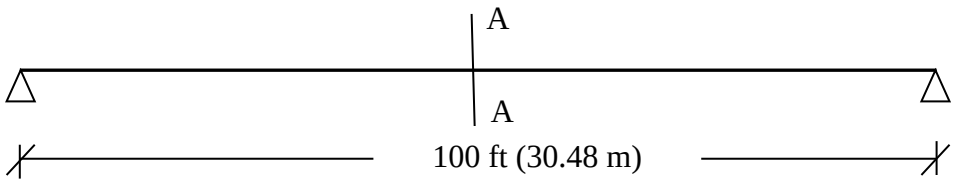

Figure 3. Bridge span

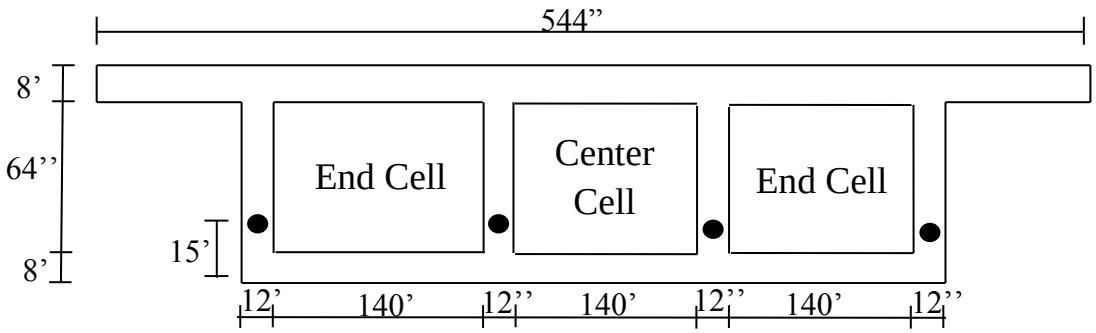

Figure 4. Bridge cross section with concrete dimensions (section A-A)

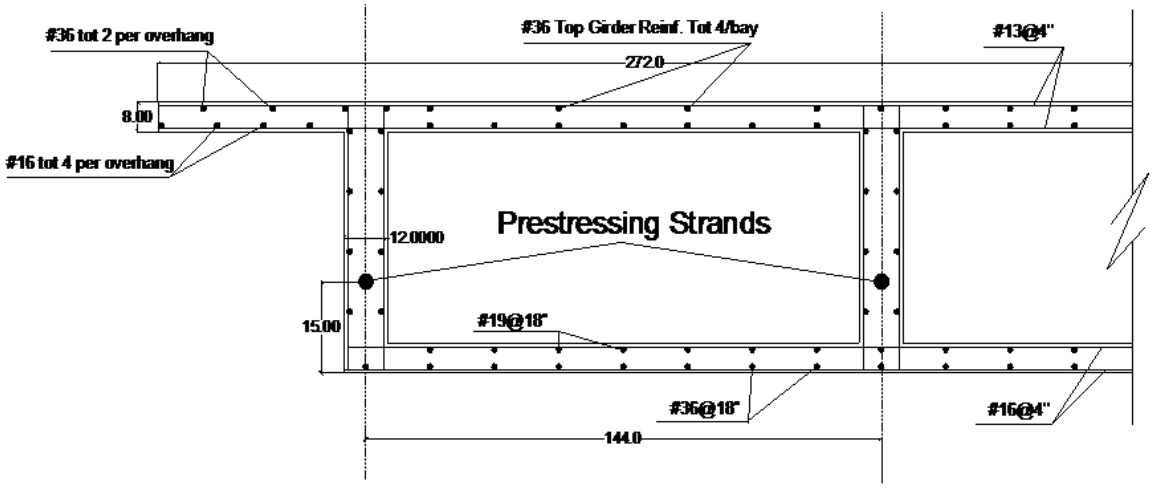

Figure 5. Bridge cross section with reinforcement details

The box girder bridge was modeled using quarter symmetry option by assigning the appropriate boundary conditions; the mesh was built using the available elements in ANSYS-LSDYNA. The concrete was modeled by the material WINFRITH_CONCRETE, which was originally developed for modeling the local and global response of reinforced concrete structures to accidental impact and blast loadings, Broadhouse (1995). The Winfrith Concrete model is a smeared crack (sometimes known as pseudo crack), smeared rebar model, implemented in the 8-node single integration point continuum element including internally the strain rate effect. The hydrostatic stress state in the concrete was input as a pressure-volumetric strain curve versus the concrete uniaxial compressive strength f_C'f`c taken as 7 ksi (49.2 MPa) and 10 ksi (70 MPa).

The deviatoric stresses are incremented elastically, using a locally rate dependent modulus and are limited by the yield surface (Ottosen, 1975). The form of this yield surface is typical of the response of most concretes. Up to three orthogonal cracks can be formed in any element. If failure is indicated in tri-axial compression, the concrete is deemed to be crushed, and three closed cracks are generated so that the material has no tensile capacity (Broadhouse, 1995). The material model takes into account the volumetric strain versus pressure.

The conventional and post-tensioned steel were simulated using material type 3 (MAT_PLASTIC_KINEMATIC) in LS-DYNA, which is a bi-linear elastic-plastic constitutive relationship that contains formulations incorporating isotropic and kinematic hardening. Since reinforcing steel shows more evident strain rate effect and for simplicity, the only input parameters of the material model are: mass density, Young's modulus, Poisson's ratio, yield stress, and tangent modulus. The strain rate effect for all types of steel included in the code according to the equation of Cowper and Symonds (1957), which scales the yield stress with the following factor:

$$1 + \left(\frac{\dot{\varepsilon}}{C}\right)^{\frac{1}{P}}$$

Where $\dot{\varepsilon}$ is the strain rate, and *C* and *P* are coefficients of strain rate.

The conventional steel was modeled using the discrete beam element formulation with the PLASTIC_KINAMATIC material model. The steel yield stress was taken as 50, 70, and 100 ksi (415, 482.6, 600 MPa) according to ASTM A588. The low relaxation post-tensioned steel strands were considered in the analysis using the ASTM A416 Grade 270. The post-tensioned forces were modeled using the INITIAL_STRESS_BEAM available in LS-DYNA. The assigned forced to the beam elements was calculated and assumed constants throughout the analysis time. The effect of self weight on the results was also taken by considering the CONTROL_DYNAMIC_RELAXATION option, where it is used to initialize stresses and deformations in a model as a preload (gravity load). After the preload state is achieved, the time was reset to zero and the solution automatically started from the preloaded state. Table 2 lists the LS-DYNA material types and mechanical properties of concrete, steel as well as the prestressing strands.

Table 2. LS-DYNA material names and mechanical properties

Material	LS-DYNA material models and mechanical properties of each, units are in inch, second and psi						
	Material Name/ Properties	Ro	E	PR	SIGY	ETAN	failure strain
Concrete	WINFRITH_CONCRETE	0.088	3.4E7	0.18	-	-	0.005
Reinforcing Steel	PLASTIC_KINAMETIC	0.258	29E6	0.33	60E3	100	0.15
Prestressing Steel	PLASTIC_KINAMETIC	0.258	28E6	0.33	120E3	200	0.17

The finite element model of the bridge is shown in Figure 6. It consists of a regular mesh of hexagonal solid elements of a typical aspect ratio of 1.0. The simply supported bridge was

modeled by taking advantage of the symmetry, so only a quarter of the bridge was modeled. The boundary conditions along the transverse and longitudinal directions were taken into account as shown in Figure 7. The high explosive material was assumed at a height of 30 inches (0.762 m) above the bridge deck and the explosives were assumed at different locations along the transverse and longitudinal direction of the bridge deck.

The parametric study includes the weight of the high explosives, the location of the high explosive, the steel grade, the concrete uniaxial compressive strength, the tendons profile, and finally the effect of using carbon fiber reinforced polymer material on the blast resistance of the bridge system. Table 3 shows the different parameters investigated in this research. Three different steel grades were used in the study (ASTM A588 Grade 50, ASTM A852 Grade 70, and ASTM A514 Grade 100) to predict the behavior of the steel bridge under the blast loads. On the other hand, one type of prestressing steel was used; namely Grade270 low relaxation steel. The conventional and prestressing steel properties are shown in Table 3. Figure 8 shows the steel reinforcement mesh for the bridges investigated in this report.

Table 3. Steel properties used in the study

Steel Types	Yield Stress (ksi)	Ultimate Strength (ksi)	Maximum Plastic Strain (in/in)	Hardening Modulus (ksi)
ASTM A588 Grade50	50	70	0.15	130
ASTM A852 Grade 70	70	100	0.15	200
ASTM A514 Grade 100	100	120	0.075	260
ASTM A416 Grade 270	120	270	0.17	200

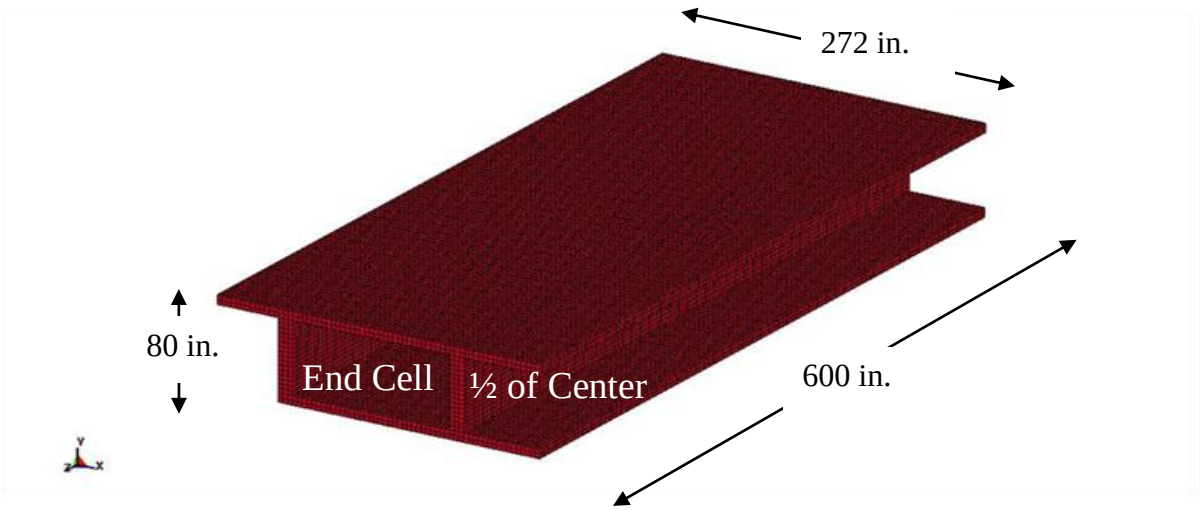

Figure 6. Isometric view showing the dimensions of the 1/4 bridge model

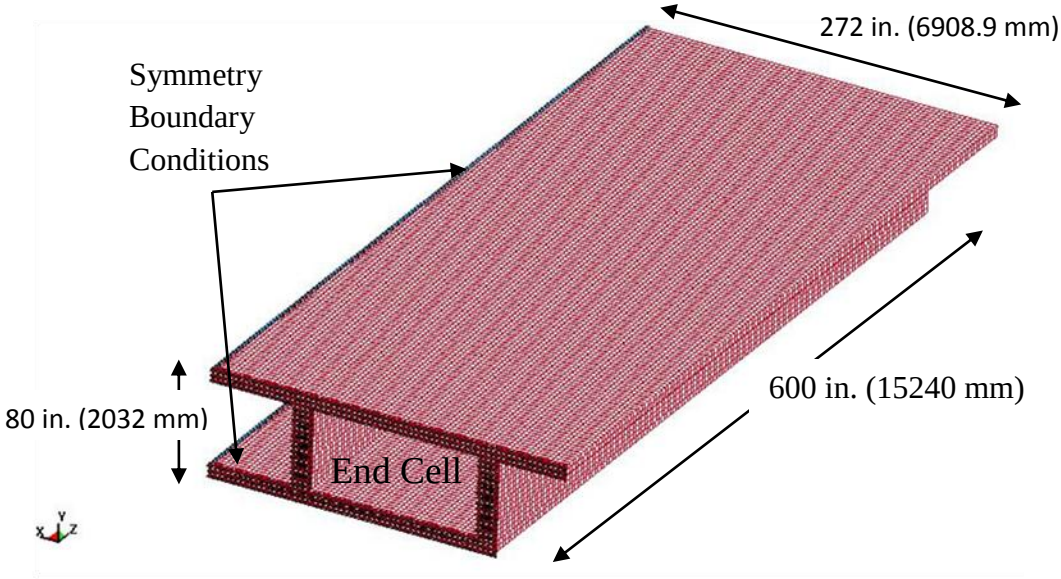

Figure 7. Isometric view showing the FE mesh of the bridge quarter symmetry

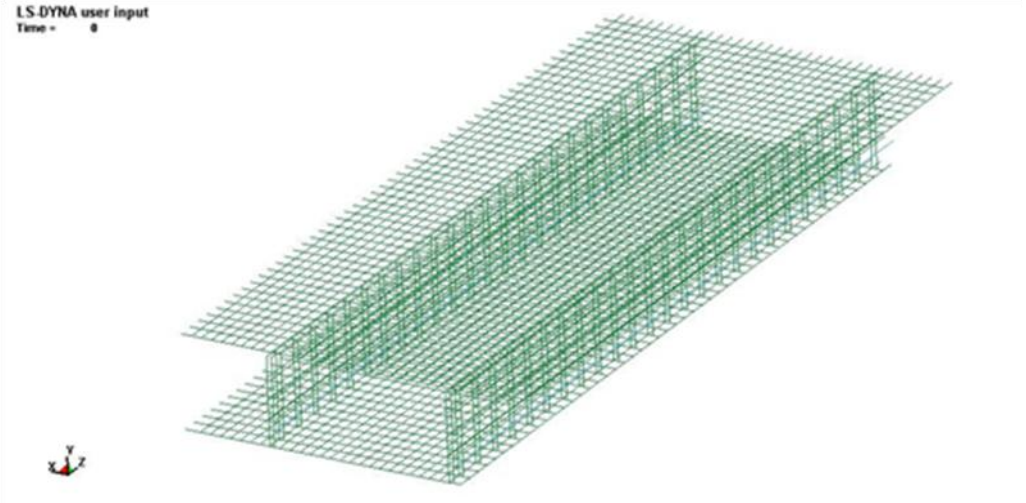

Figure 8. Isometric view showing the reinforced steel mesh of the model

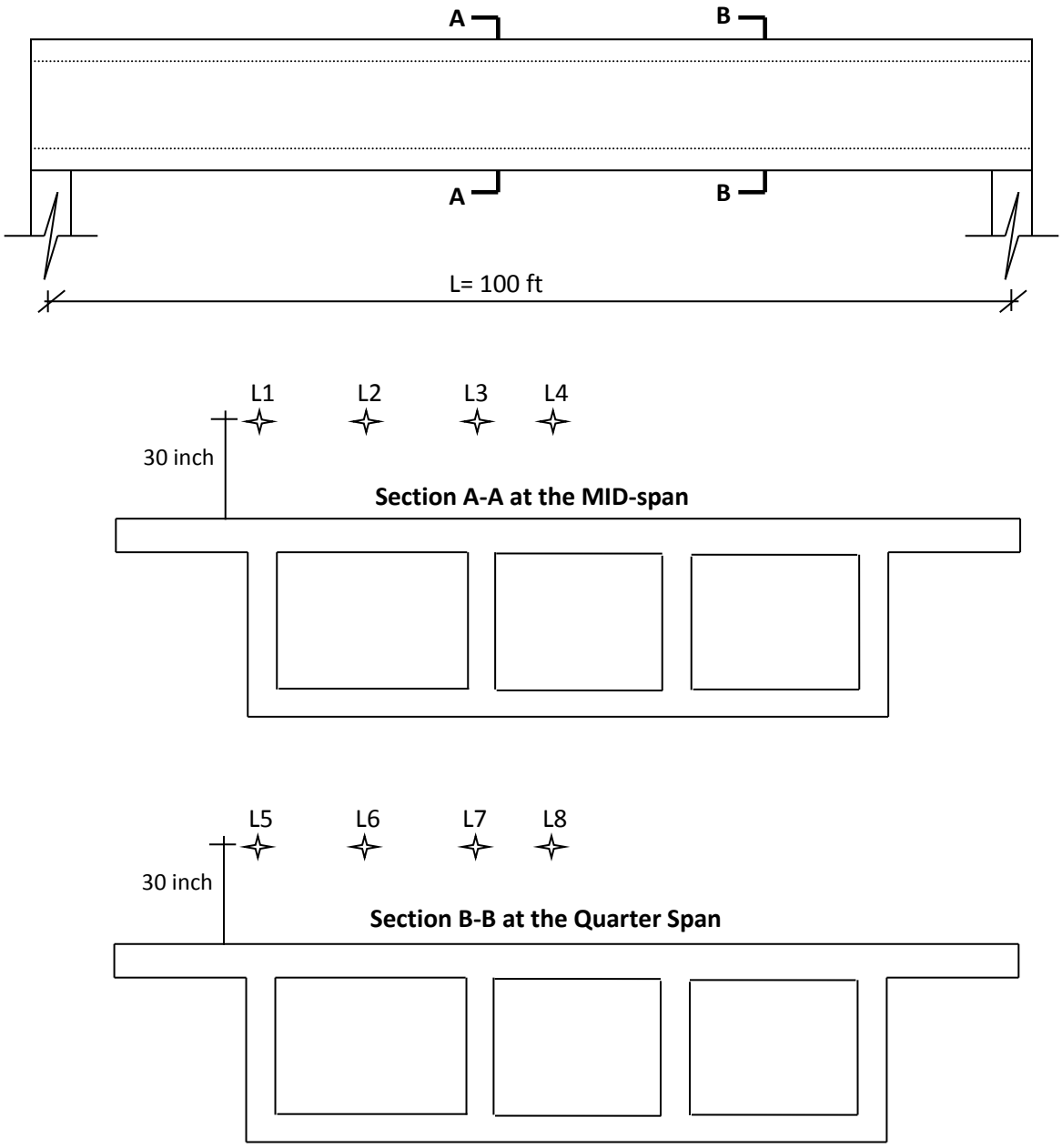

Figure 9. Selected High Explosive (HE) charge locations along the bridge and across the width

Table 4. Simply supported box girder bridge cases investigated

Case	HE Location	Charge Weight	Concrete Strength (psi)	Steel Grade	Standoff Distance (in)
1	L1	0.2W	7000	Grade50	30
2	L2	0.2W	7000	Grade50	30
3	L3	0.2W	7000	Grade50	30
4	L4	0.2W	7000	Grade50	30
5	L5	0.2W	7000	Grade50	30
6	L6	0.2W	7000	Grade50	30
7	L7	0.2W	7000	Grade50	30
8	L8	0.2W	7000	Grade50	30
9	L1	2W	7000	Grade50	30
10	L2	2W	7000	Grade50	30
11	L3	2W	7000	Grade50	30
12	L4	2W	7000	Grade50	30
13	L5	2W	7000	Grade50	30
14	L6	2W	7000	Grade50	30
15	L7	2W	7000	Grade50	30
16	L8	2W	7000	Grade50	30
17	L1	4W	7000	Grade50	30
18	L2	4W	7000	Grade50	30
19	L3	4W	7000	Grade50	30
20	L4	4W	7000	Grade50	30
21	L5	4W	7000	Grade50	30
22	L6	4W	7000	Grade50	30
23	L7	4W	7000	Grade50	30
24	L8	4W	7000	Grade50	30
25	L1	6W	7000	Grade50	30
26	L2	6W	7000	Grade50	30
27	L3	8W	7000	Grade50	30
28	L4	6W	7000	Grade50	30
29	L5	6W	7000	Grade50	30
30	L6	6W	7000	Grade50	30
31	L7	6W	7000	Grade50	30
32	L8	6W	7000	Grade50	30
33	L1	10W	7000	Grade50	30
34	L2	10W	7000	Grade50	30
35	L3	10W	7000	Grade50	30
36	L4	10W	7000	Grade50	30
37	L5	10W	7000	Grade50	30
38	L6	10W	7000	Grade50	30
39	L7	10W	7000	Grade50	30
40	L8	10W	7000	Grade50	30
41	L1	30W	7000	Grade50	30

42	L2	30W	7000	Grade50	30
43	L3	30W	7000	Grade50	30
44	L4	30W	7000	Grade50	30
45	L5	30W	7000	Grade50	30
46	L6	30W	7000	Grade50	30
47	L7	30W	7000	Grade50	30
48	L8	30W	7000	Grade50	30
49	L1	60W	7000	Grade50	30
50	L2	60W	7000	Grade50	30
51	L3	60W	7000	Grade50	30
52	L4	60W	7000	Grade50	30
53	L5	60W	7000	Grade50	30
54	L6	60W	7000	Grade50	30
55	L7	60W	7000	Grade50	30
56	L8	60W	7000	Grade50	30
57	L1	6W	10000	Grade50	30
58	L1	6W	10000	Grade70	30
59	L1	6W	10000	Grade100	30
60	L1	6W	10000	Grade50	30
61	L1	6W	15000	Grade50	30
62	L1	6W	10000	Grade100	30
63	L1	6W	10000	Grade100	40
64	L1	6W	10000	Grade100	60

Sixty four cases were analyzed for the simple span model using various parameters as shown in Table 4. The location of the HE is shown in Figure 9. The results were compared with each others to assess the local and the global damage to the bridge. The blast load was applied using the available commands for blast loads in LSDYNA. The concrete was modeled using the hexagonal solid element with one point of integration and the WINFRITH_CONCRETE material model was assigned to these elements. The WINFRITH_CONCRETE model is capable of capturing the concrete behavior under impulsive loads, (Broadhouse, 1995). The conventional and post-tensioned steel was modeled as discrete elements immersed in the concrete mesh taking the advantage of the coupling (constrained) between them using the LAGRANGE_IN_SOLID command available in LS-DYNA. All the steel reinforcement and the post-tensioned strands material were modeled using the PLASTIC_KINEMATIC model. The damping effect used in all the analysis cases was a 2% modal damping ratio, although the damping has a very little effect on structures subjected to blast loads. The effect of the gravity loads as an initial stress or preload was taken into consideration utilizing the DYNAMIC_RELAXATION option available in LS-DYNA.

5. Verification of Reflected Pressure and Element Responses

In this simulation, the blast load was assumed above the bridge deck. The load command defines an airblast function for the application of pressure loads due to explosives (LS-DYNA, 2009). This option calculates the pressure values when used with the LOAD_SEGMENT command, with these segments normal pointing toward the charge. The maximum predicted reflected pressure using TM5-1300 is compared to the values obtained from LS-DYNA as shown in

Figure 10. The calculated pressure from LS-DYNA was measured at the nearest element to the ignition point which is considered as a reflected pressure. The minimum and maximum differences between the maximum predicted pressure values using TM5-1300 and LS-DYNA were 8.7% and 30% respectively, which gave good prediction of the reflected pressure over bridge deck. In this study, the most important factor is the reflected pressure not the imparted impulse because the detonation is considered very close to the bridge deck and the material is expected to respond before the whole structure does. It is expected that at these extreme close-in pressures the local material will respond (fail by breaching) long before the entire structure can be mobilized and begin to move as a structure.

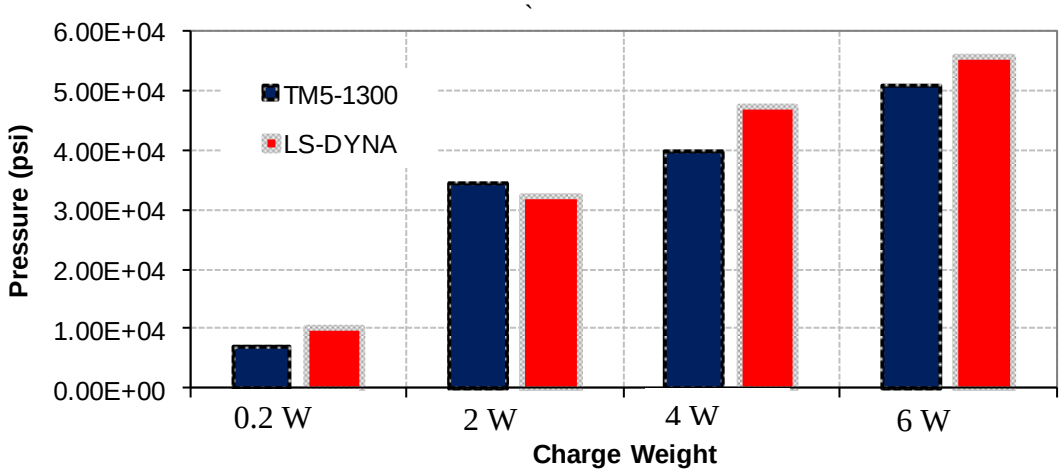

Figure 10. Comparison between the TM5-1300 and LS-DYNA

6. Structural Response of Bridge Deck to Blast Loads-Comparative Study

The effects of the various parameters identified in this study on the local response of the bridge deck under blast are presented in this section. This includes the location of the charge along and across the bridge deck, the concrete compressive strength, steel reinforcement strength, prestressing tendons profile, standoff distance, and charge weight.

6.1 Effect of Charge Weight and Location

The location of the charge above the bridge deck is varied (see Figure 9) to study its effect on deck response under blast. Eight different locations, L1-L8, are discussed next.

6.1.1 HE Location L1

The local response of the nearest point and element to the damage (crater) center was traced for different charge weights over the bridge cross section. The response was drawn as a time history of displacement, velocity, acceleration, plastic strain, the effective stresses, and the damage size. The response of the bridge was terminated at a time of 0.1 seconds for charge weights ranging from 0.2W to 60W, when the effect of the bridge has diminished. The explosive weights were chosen to predict different material responses starting from no failure and ending with a global bridge failure. In this comparative study the concrete compressive strength and the steel yield stress were assumed 7 ksi and 50 ksi respectively.

Figure 11 shows the local response time history of the bridge under the different charge weights at the first location (L1). As shown from Figure 11 the maximum response of the closest element to damage (crater) center is reached after .001 seconds and followed by a quick decay. This emphasizes that the blast load effect was a very high incident pressure in the air immediately after the explosion and then the incident pressure is increased by a reflection factor when it hits the structure. Figure 11(a) shows the displacement time history, as expected, when the charge weight increases the displacement of the nearest element to the damage center or to the detonation center increases. The maximum displacement of charge weight 0.2W is 0.6 in (0.015 m), while the maximum displacement for the charge weight 60W is 47in (1.79 m), which indicates a global failure under that load. The displacement increased gradually from 0.2W to 30W and then dramatic increase occurred due to load of 60W.

Figures 11(b) and (c) show the velocity and acceleration time histories of the closest point to the charge before failure. It can be seen that the behavior is the same. The acceleration value reached a maximum at time 0.001 seconds before the maximum velocity, which occurred at 0.007 seconds. This indicates the importance of acceleration in the damage mechanism. The velocity and acceleration values at the largest load case were 5,050 in/sec (128.27m/sec) and 7×10^{6} in/sec^{2} (1.77×10^{5} m/sec^{2}) respectively as shown in Figures 11 (b) and (c).

Figure 11 (d) shows the effective stress time history for the different high explosive weights. The stresses were drawn also for the closest undamaged element to the explosion center. It can be seen that as the charge weight increases the effective stresses increase; these cases were for concrete uniaxial compressive strength of 7,000 psi. Case 0.2W gave maximum stresses of 3,440 psi, which indicates no crushing or damage occurred to the bridge deck. On the other hand, case 30W shows effective stresses of 38,000 psi which indicates that crushing occurred to the concrete at early time of 0.002 seconds. The effect of the strain rate due to the blast loads can be seen from Figure 11 (d), where a dynamic increase factor of 5.42 was captured for the largest load case. The dynamic increase factor is defined as the ratio of the maximum dynamic concrete stresses to the static uniaxial compressive stresses. For the plastic strain results, it can be seen from Figure 11 (e) that the ultimate strain for case 60W is 0.45 in/in whereas the maximum dynamic plastic strain of concrete was assumed to be 0.005in/in in the whole study. The elements around the crater reached the maximum strain immediately after the detonation process, almost at 0.00096 seconds. That explains the effect and the importance of the strain rate factor that should be taken in the design of concrete structures subject to blast loads. Table 5 shows the damage results for the box girder bridge section at location L1 subjected to the various blast loads, ranging from 0.2W to 60W.

Table 5. Damage size for HE location L1

Case	Charge	Damage Size (in)
1	0.2W	No Failure (scabbing)
9	2W	161.50
17	4W	178.31
25	6W	189.37
33	10W	331.97
41	30W	443.32
49	60W	465.28

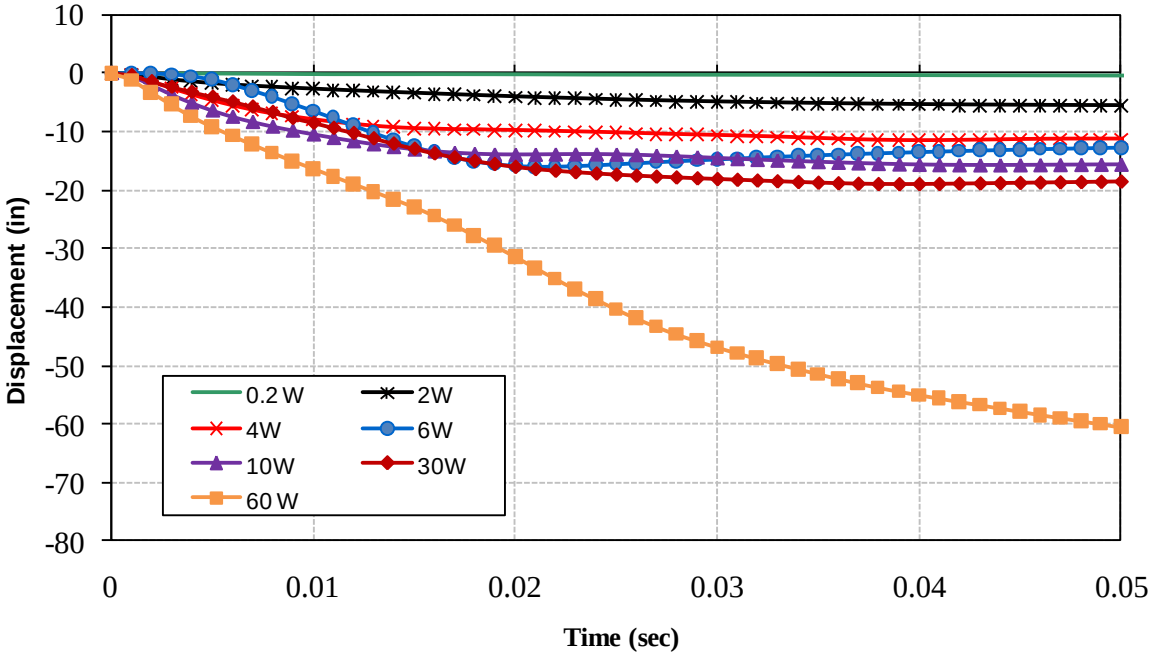

(a) Vertical Displacement

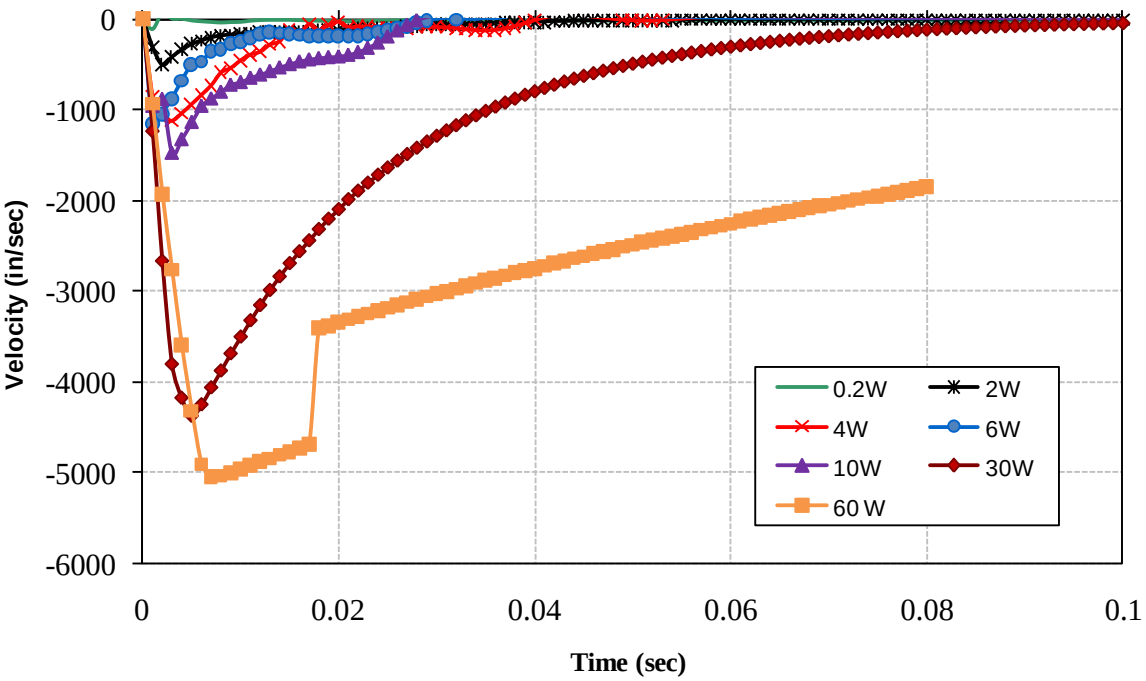

(b) Vertical Velocity

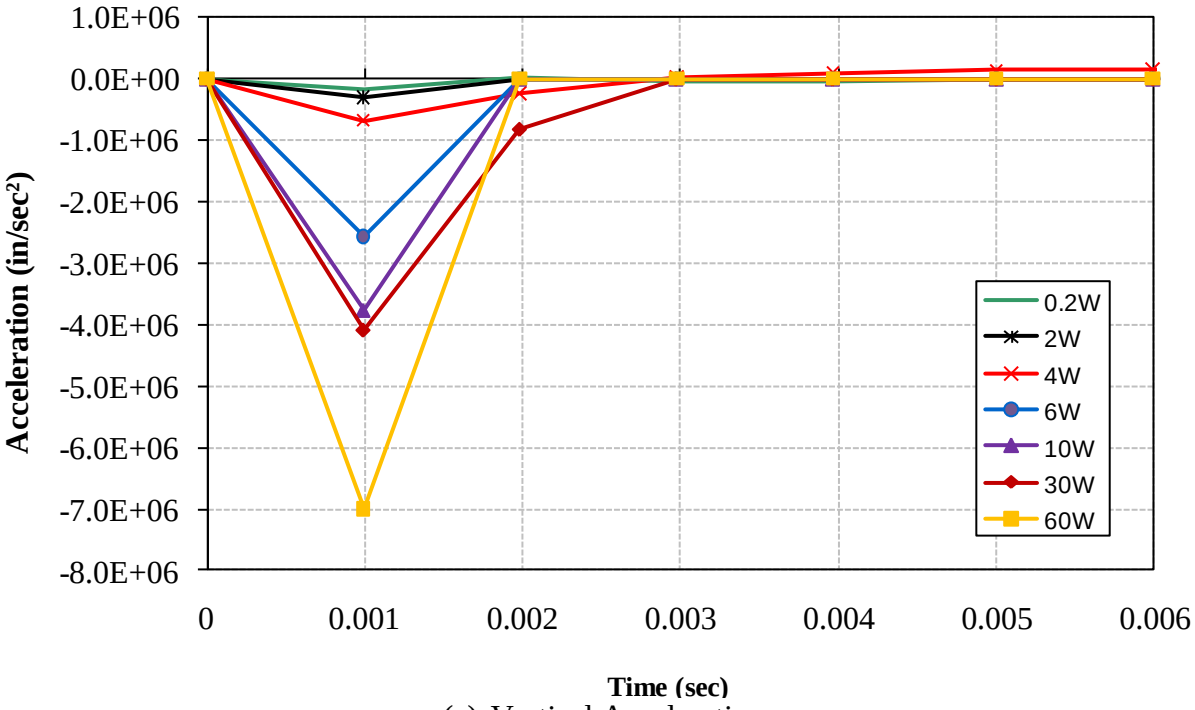

(c) Vertical Acceleration

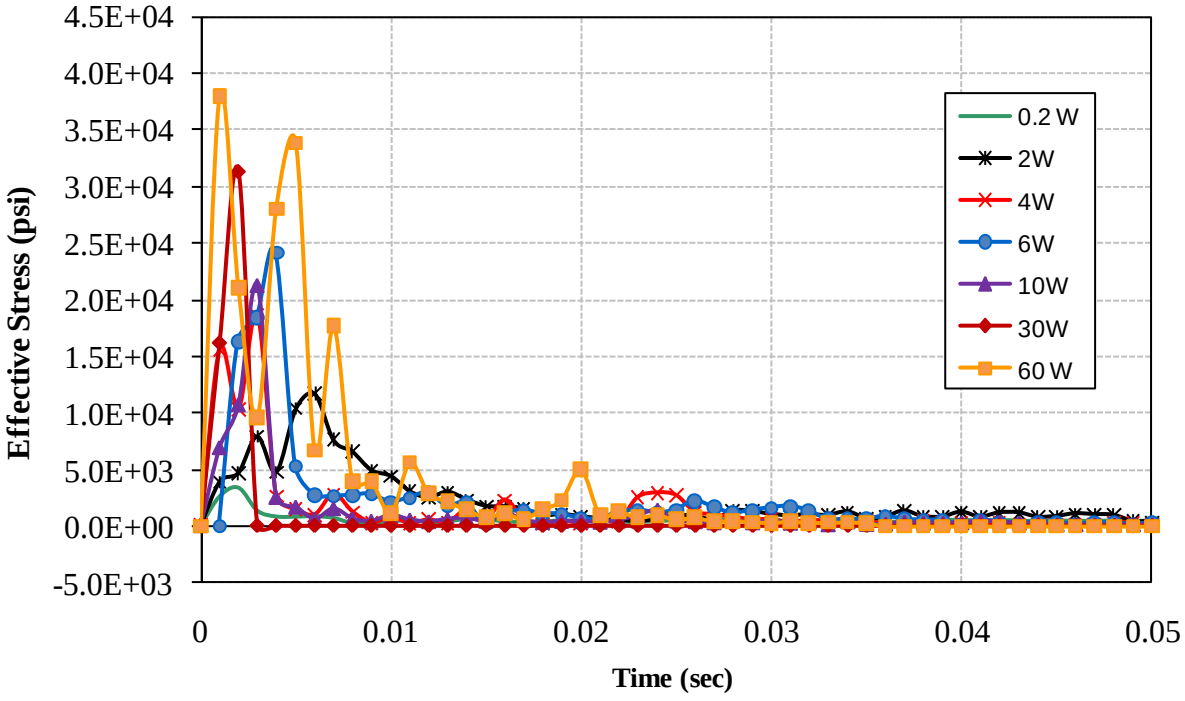

(d) Effective Stress

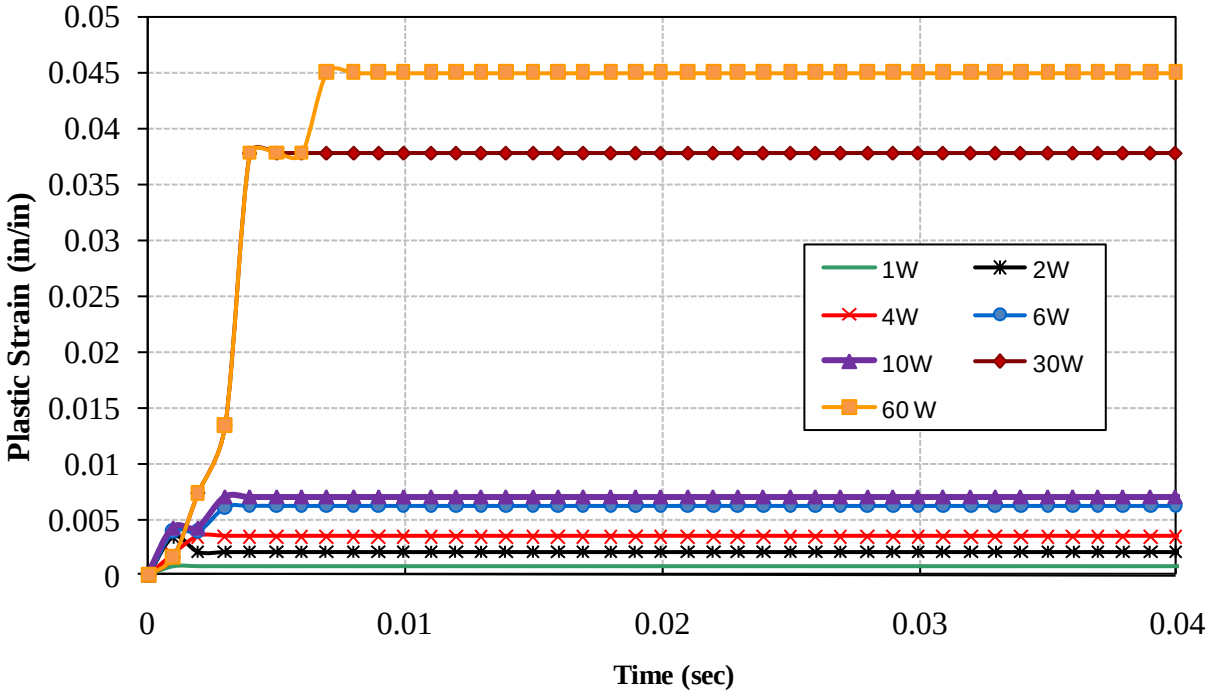

(e) Plastic Strain

(f)

Figure 11. Displacement, velocity, acceleration, effective stress, and plastic strain time histories for HE location L1

6.1.2 HE Location L2

Figure 12 shows the local response time history of the bridge under the different charge weights at the second location (L2). As shown from Figure 12, the maximum response of the closest element to damage (crater) center is reached after .001 seconds and then decayed very quickly due to the instantaneous effect of blast load. Figure 12(a) shows the displacement time history, as expected, when the charge weight increases the displacement of the nearest element to the damage center or to the detonation center increases. The maximum displacement of charge weight 0.2W is 1.03 in (0.026 m), while the maximum displacement for the charge weight 60W is 68.7in (1.74 m). For the charge weight 60W the simulation was terminated as seen from the displacement profile, which did not continue until the end of the simulation time, which indicates a global failure under that load has occurred.

Figures 12 (b) and (c) show the velocity and acceleration time histories of the closest point to the charge before failure. Noticed that the actual filed tests of close-in detonations, the velocity and acceleration profiles are very difficult to measure due to the damage of the instruments. Therefore, it is very useful to develop a good numerical model which can capture theses profiles. The acceleration reached a maximum at time 0.001 seconds, well before the maximum velocity which occurred at 0.007 seconds. The profiles plotted for different charge weights show a dramatic increase for the charge weight 60W .The velocity and acceleration values at the largest load case was 6,140 in/sec (156m/sec) and 1.45×10^{7} in/sec^2 (3.68×10^{6} m/sec^2) respectively as shown in Figures 12 (b) and (c).

The effective stress time history for different high explosive weights is shown in Figure 12 (d). The stresses were drawn also for the closest undamaged element to the explosion center. It can be seen that as the charge weight increases the effective stresses increase; these cases were for concrete uniaxial compressive strength of 7000 psi. Case 0.2W gave maximum stresses of 2,840 psi, which indicates no significant effect due to that load. On the other hand, case 60W shows effective stresses of 41,200 psi which indicates that failure occurred to the concrete at an early time of 0.003 seconds. The effect of the strain rate due to the blast loads can be seen in Figure 12 (d), where a dynamic increase factor of 5.85 was captured for the largest load case. For the plastic strain results, it can be seen from Figure 12 (e) that the ultimate strain for case 60W is 0.0.15 in/in. The elements around the crater reached the maximum strain early after the detonation process, almost at 0.00096 sec. Table 6 shows the damage results for the box girder bridge section at location L2 and subjected to the various blast loads, ranging from 0.2W to 60W.

Table 6. Damage size for HE location L2

Case	Charge	Damage Size (in)
2	0.2W	No Failure (scabbing)
10	2W	143.62
18	4W	161.52
26	6W	176.6
34	10W	207.8
42	30W	394.25
50	60W	463.93

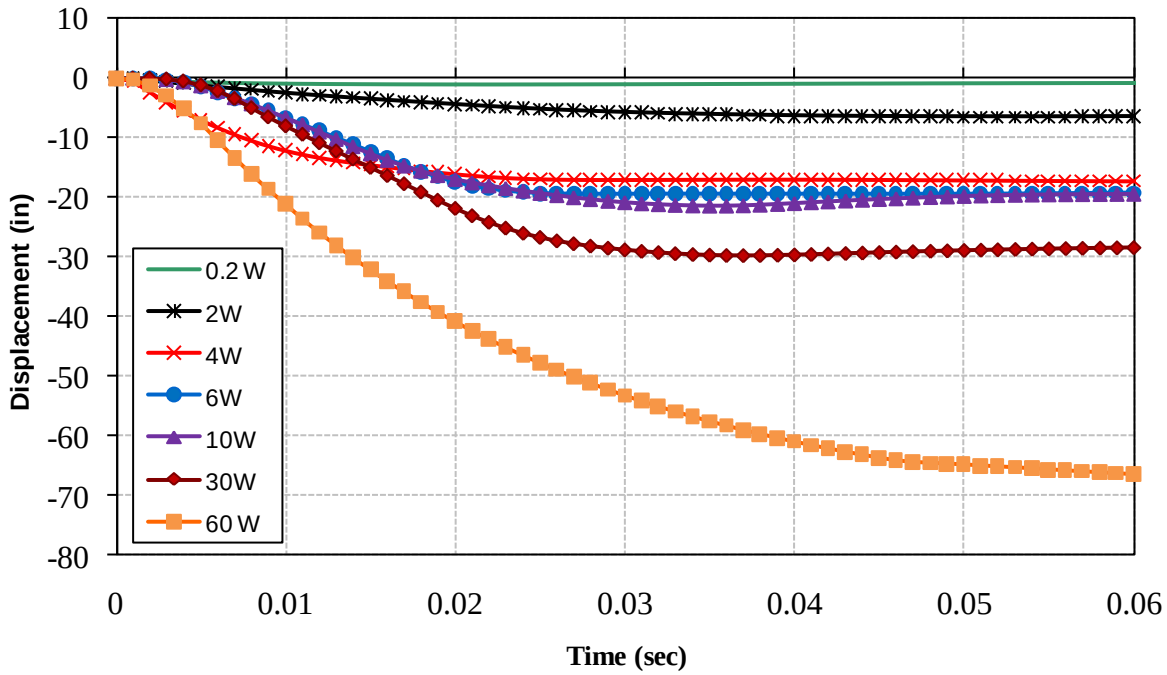

(a) Displacement

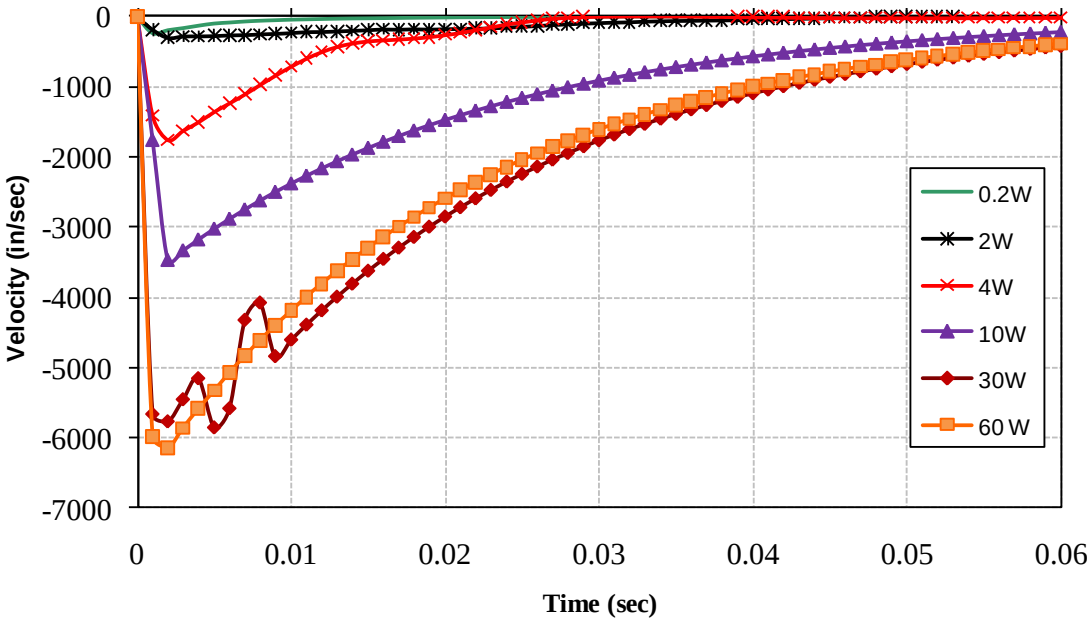

(b) Velocity

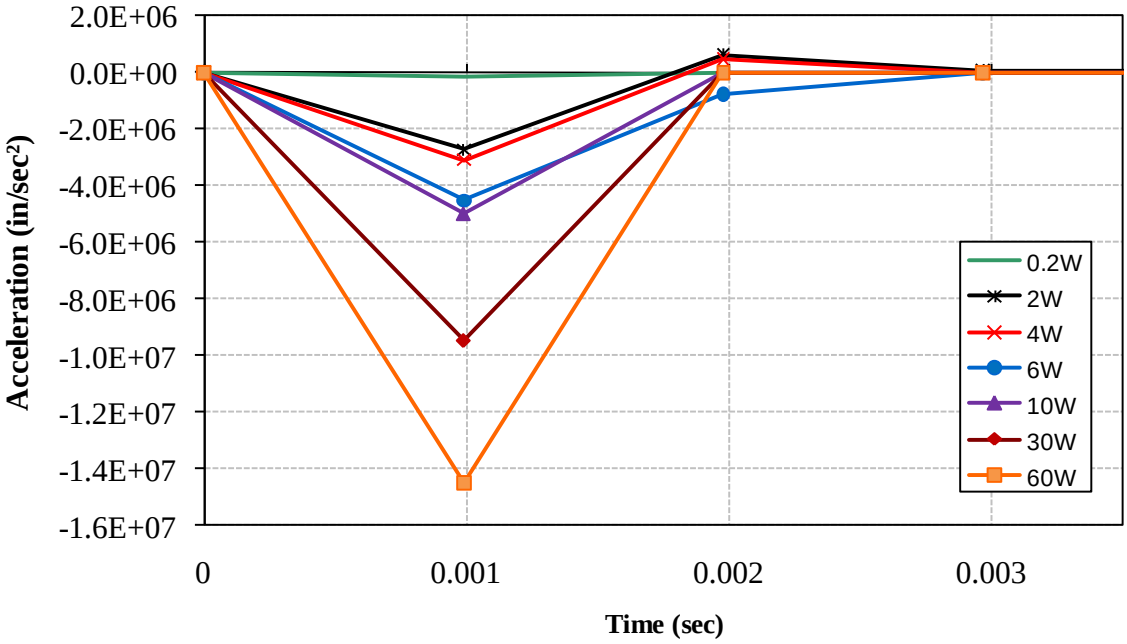

(c) Acceleration

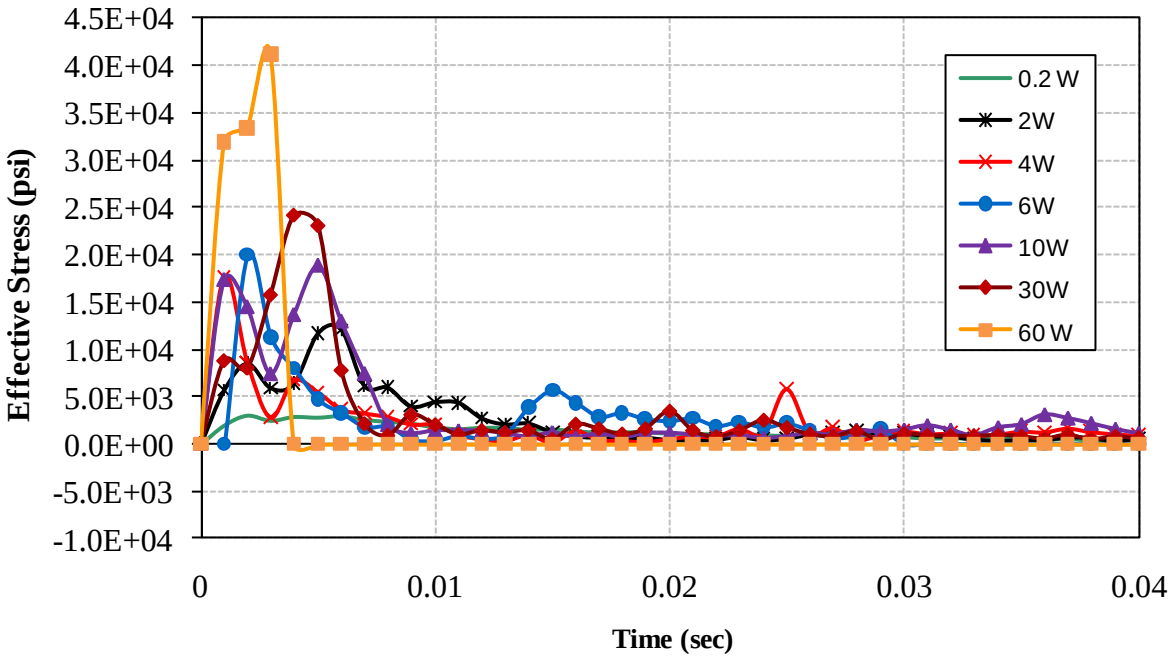

(d) Effective Stresses

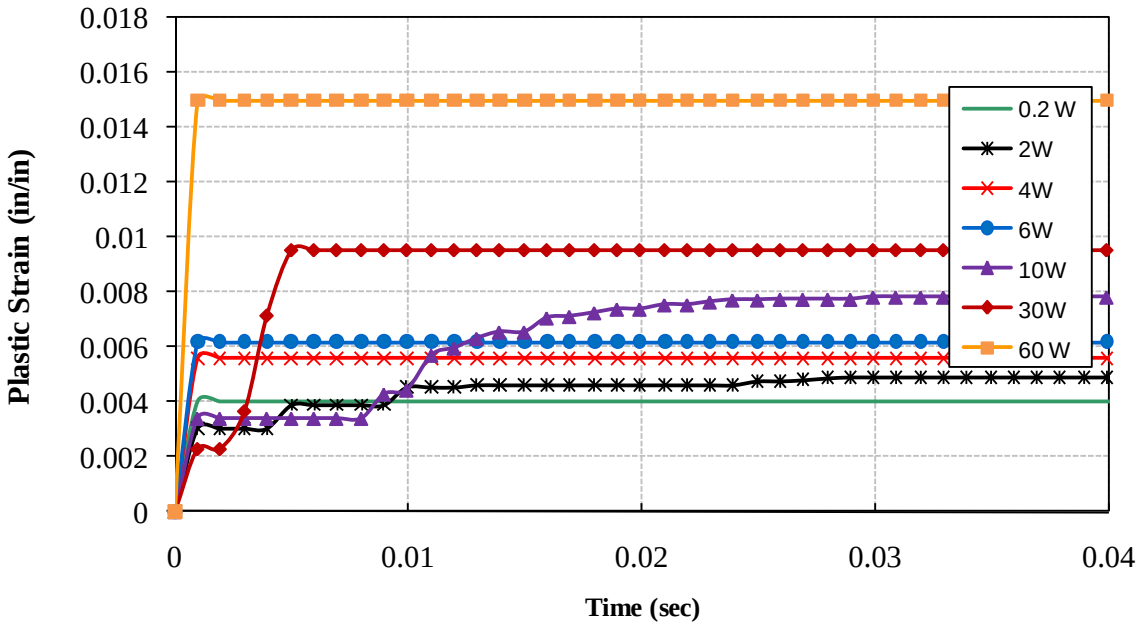

(e) Plastic Strain

(f)

Figure 12. Displacement, velocity, acceleration, effective stress, and plastic strain time histories for HE location L2

6.1.3 HE Location L3

Figure 13 shows the local response time history of the bridge under the different charge weights at the third location (L3) where the charge was placed over the interior web of the bridge section. Figure 13 (a) shows the displacement time history, which indicates that when the charge weight

increases the displacement increases. The maximum displacement the charge weight 1W is 0.64 in (0.0163 m), while the maximum displacement for charge weight 60W is 66 in (1.67 m), which indicates global failure under that load has occurred.

Figures 13 (b) and(c) show the velocity and the acceleration time histories of the closest element to damage (crater) center or the undamaged elements. The time histories of the flying debris were many times larger than what is shown in Fig. 13. It can be seen that the behavior is the same, where the acceleration and velocity values reached the maximum values almost at the same time of .0015 seconds for the different charge weights from 0.2W to 30W and then a sudden increase occurred for the charge weight 60W .The velocity and acceleration values at the biggest load case was 7,140 in/sec (181.35m/sec) and 6.5e6 in/sec^2 (1.65e6 m/sec^2).

Figure 13 (d) shows the Effective stress time history for the different charge cases. The stresses were drawn also for the closest undamaged element to the explosion center. It can be seen that as the charge weight increases the effective stresses increase. The case 0.2W gave maximum stresses of 2,450 psi, which is less than the un-axial compressive stress of concrete. On the other hand, case 60W shows effective stresses of 45,000, which signify that crushing, occurred to the concrete at the early time of 0.0019 seconds. Table 7 shows the damage results for the box girder bridge section at location L3 and subjected to the various blast loads, ranging from 0.2W to 60W.

Table 7. Damage size for HE location L3

Case	Charge	Damage Size (in)
3	0.2W	No Failure
11	2W	136.2
19	4W	177
27	6W	207
35	10W	252.8
43	30W	346.9
51	60W	505.8

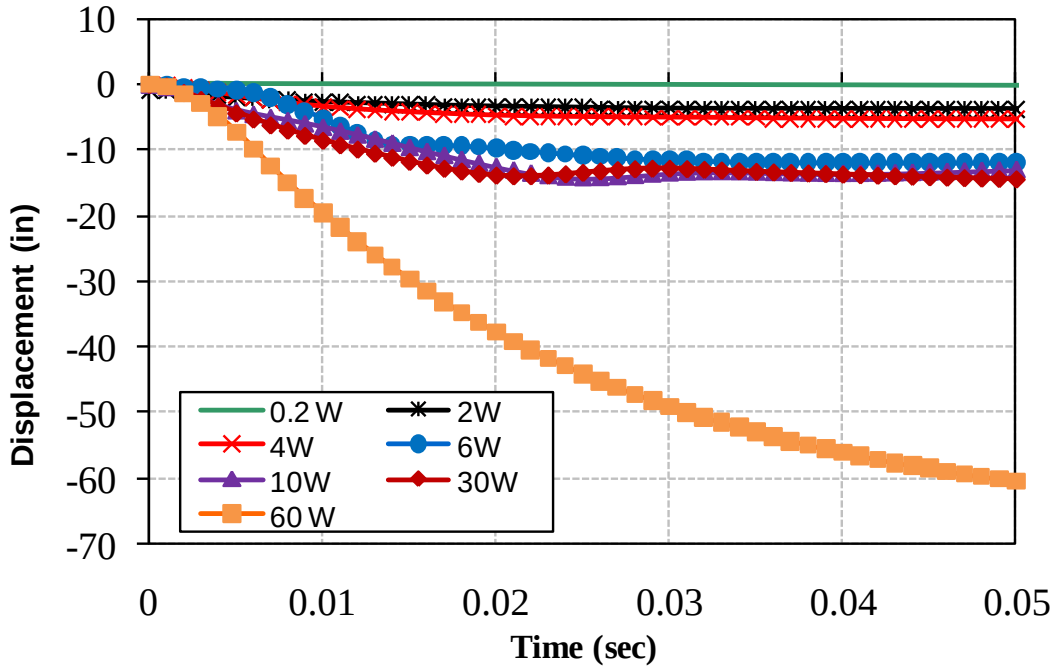

(a) Displacement

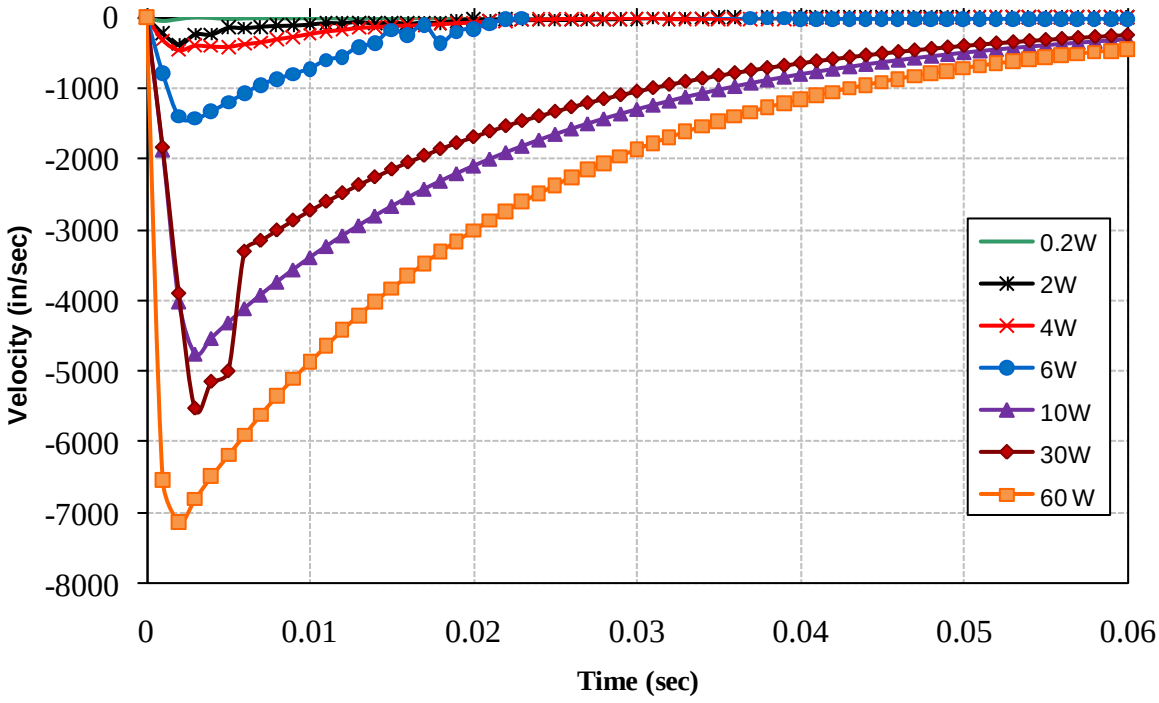

(b) Velocity

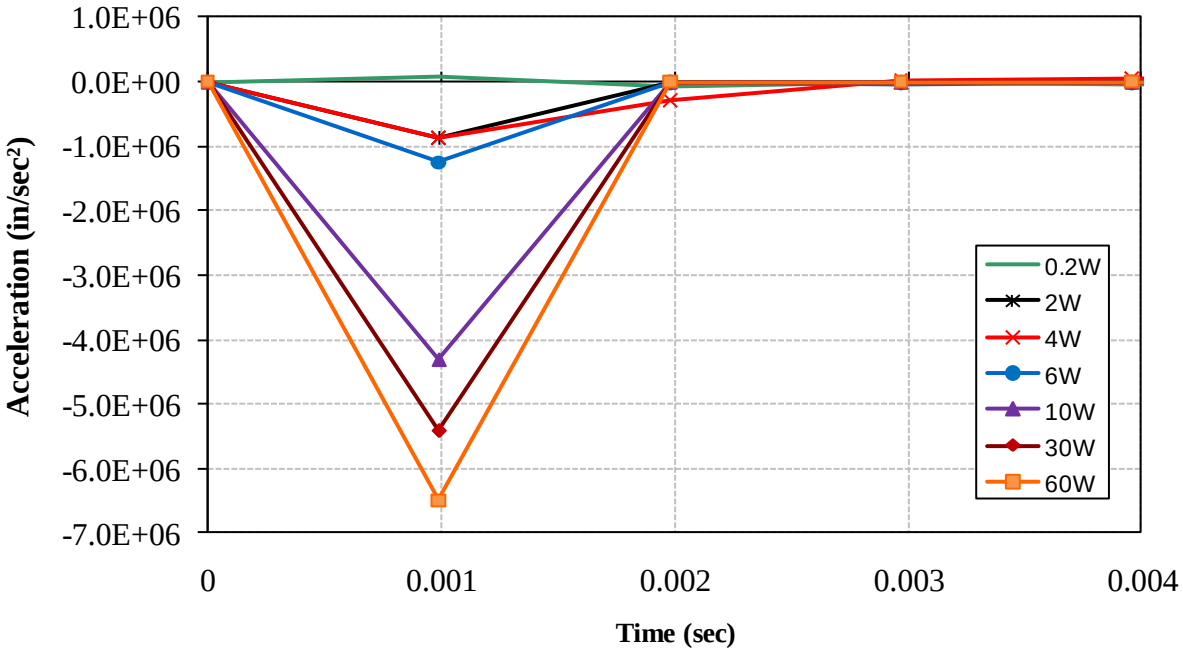

(c) Acceleration

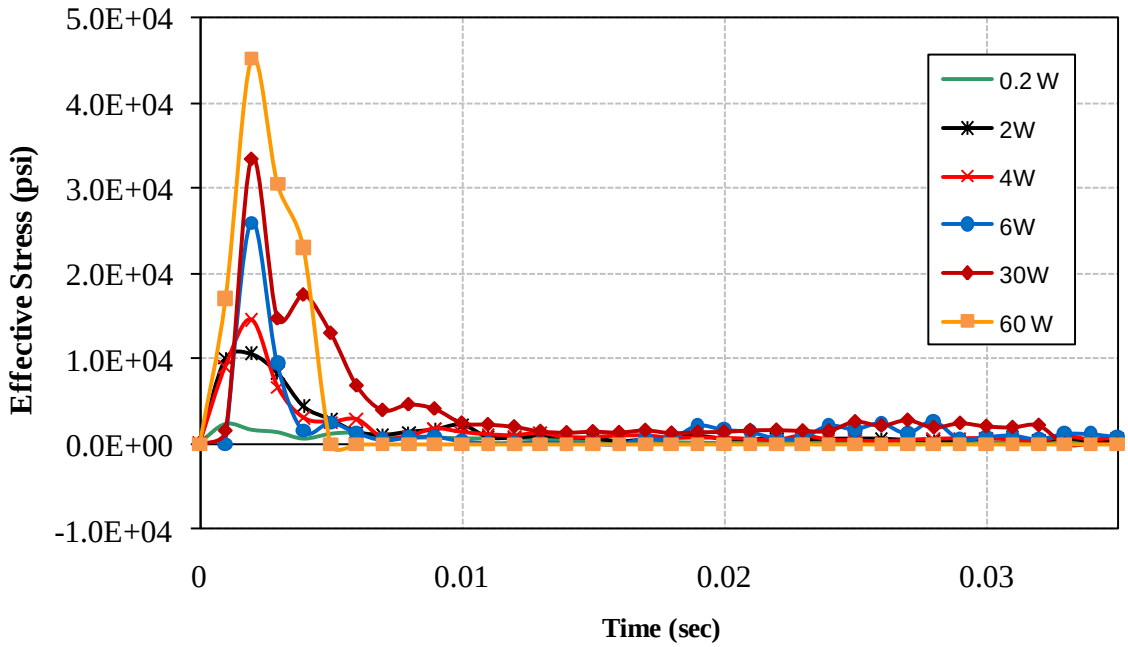

(d) Effective Stresses

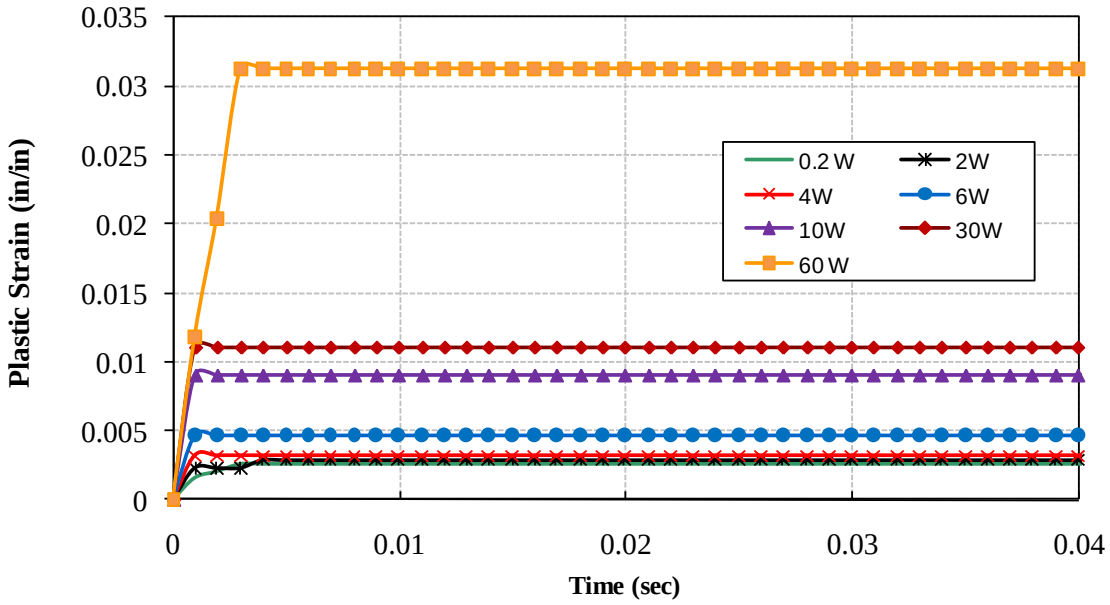

(e) Plastic Strain

Figure 13. Displacement, velocity, acceleration, effective stress, and plastic strain time histories HE location L3

6.1.4 HE Location L4

Figure 14 shows the local response time history of the bridge under the different charge weights at the first location (L4) where the high explosive weight was placed between the interior webs of the bridge section. Fig. 14 (a) shows the displacement time history; it is shown that when the charge weight increases the displacement increases. The maximum displacement for charge weight 0.2W is 1.01in (0.053 m), while the maximum displacement for the charge weight 60W is 70 in (1.76 m), which indicates a global failure under that load. That displacement is measured for the element which is attached to the bridge body and not for the flying fragments.

Figures 14 (b) and (c) show the velocity and the acceleration time histories of the closest element to damage (crater) center or the undamaged elements. It can be seen that the behavior is the same, where the acceleration and velocity values reached the maximum values almost at the same time of 0.0099 seconds for the different charge weights from 0.2W to 30W. This was followed by sharp increase for the charge weight 60W. The velocity and acceleration values at the biggest load case were 4,120 in/sec (104.6 m/sec) and 2.7×10^{7} in/sec^2 (6.85×10^{6} m/sec^2).

Figures 14 (d) shows the effective stress time history for the different charge cases. The stresses were drawn also for the closest undamaged element to the explosion center. The load case 0.2W gave maximum stresses of 3,080 psi, which did not affect significantly on the deck behavior; on the other hand, the case 60W shows effective stresses of 40,080 psi which caused the local failure of the bridge deck due to the crushing of the concrete elements at early time of 0.002 seconds. The effect of the strain rate due to the blast loads can be seen from Fig. 14 (d), where a dynamic increase factor of 5.72 was captured for the largest load case. For the plastic strain results, it can be seen from Fig. 14 (e) that the ultimate strain for the case 60W is 0.009 in/in. The elements around the crater reached the maximum quickly after the detonation process, almost at

0.001 seconds. Table 8 shows the damage results for the box girder bridge section at location L4 subjected to the various blast loads, ranging from 0.2W to 60W.

Table 8. Damage Size for HE location L4

Case	Charge	Damage Size (in)
4	0.2W	No Failure
12	2W	161.2
20	4W	177.5
28	6W	189.62
36	10W	247
44	30W	311
52	60W	404.5

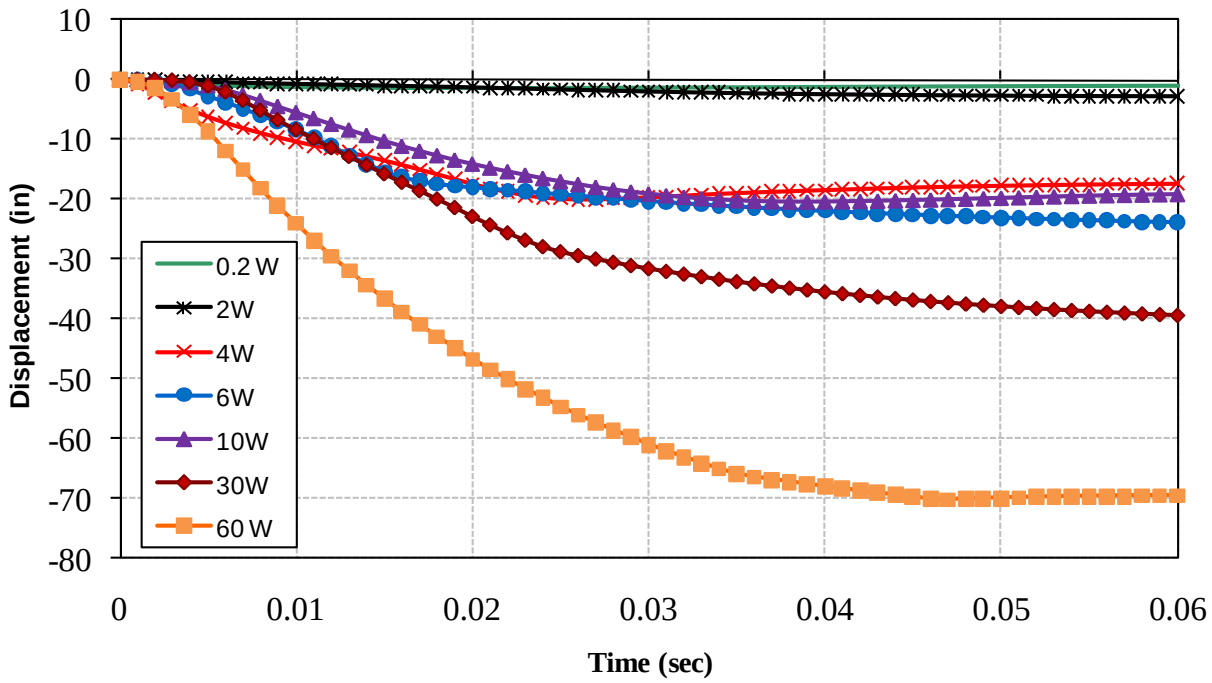

(a) Displacement

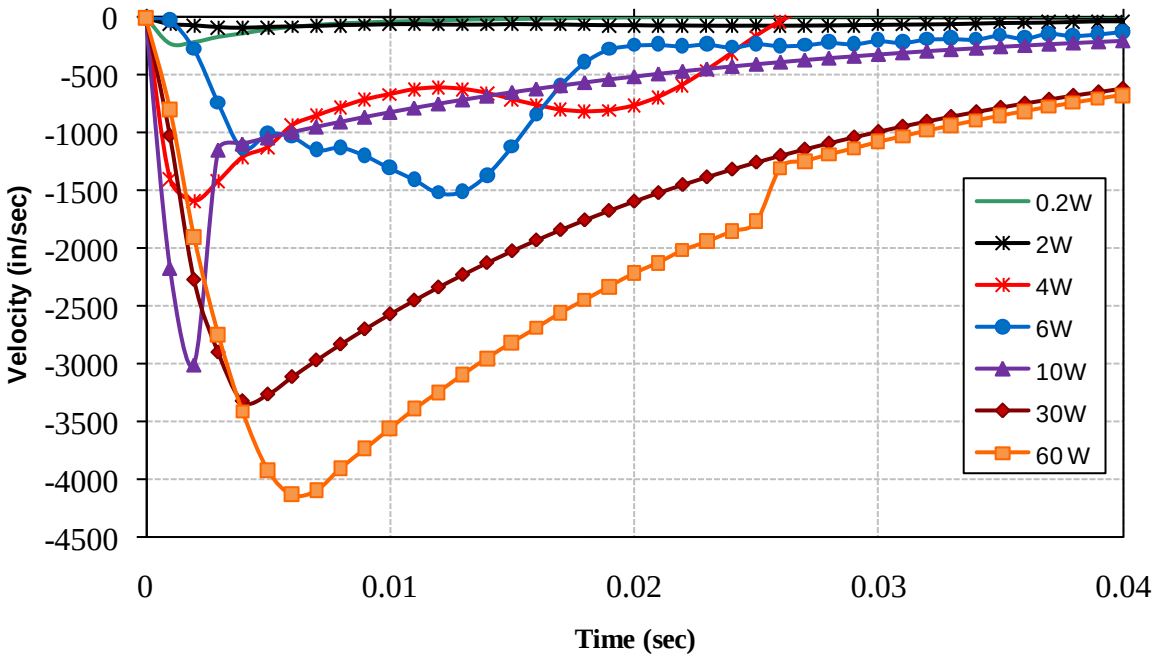

(b) Velocity

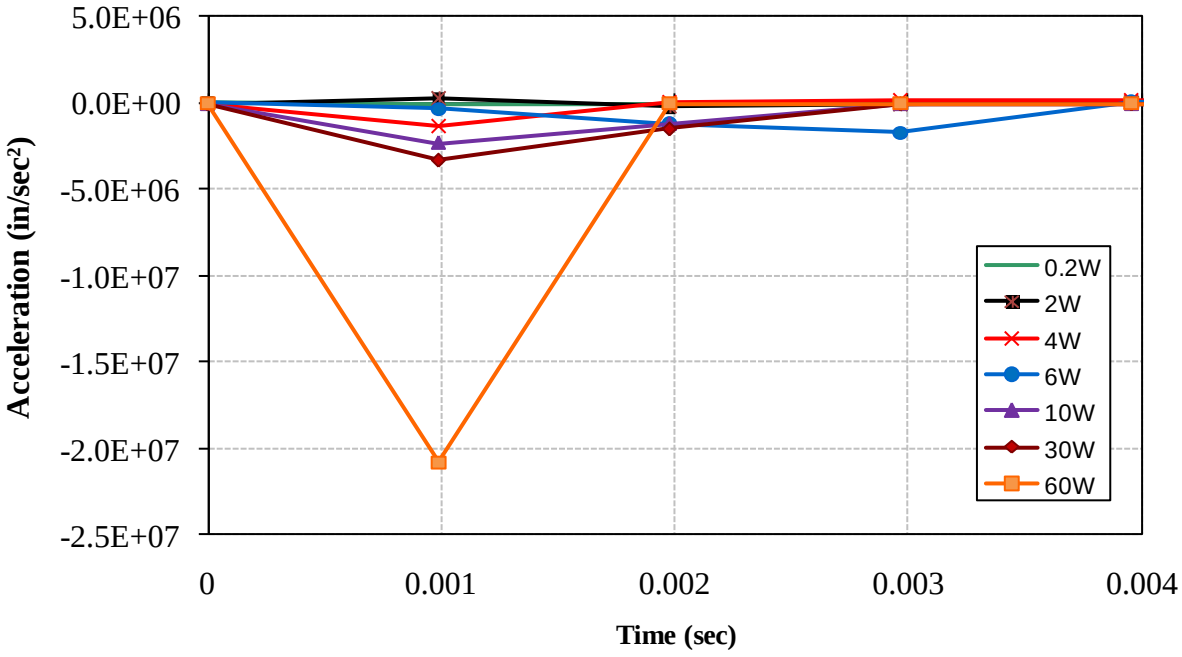

(c) Acceleration

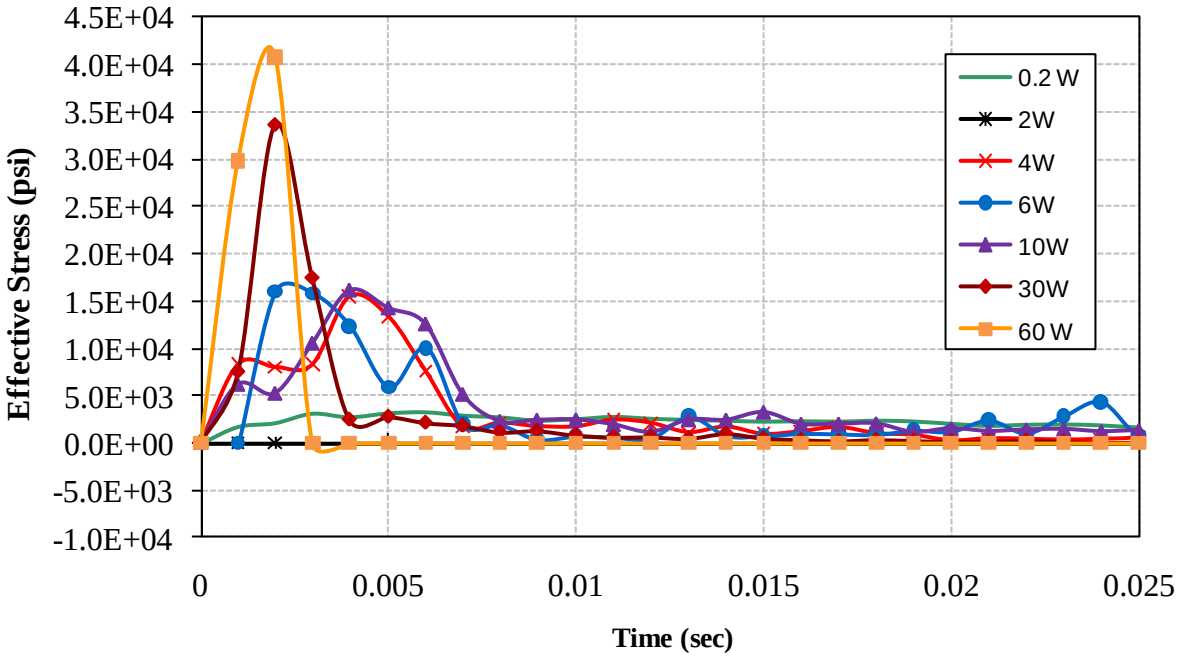

(d) Effective Stresses

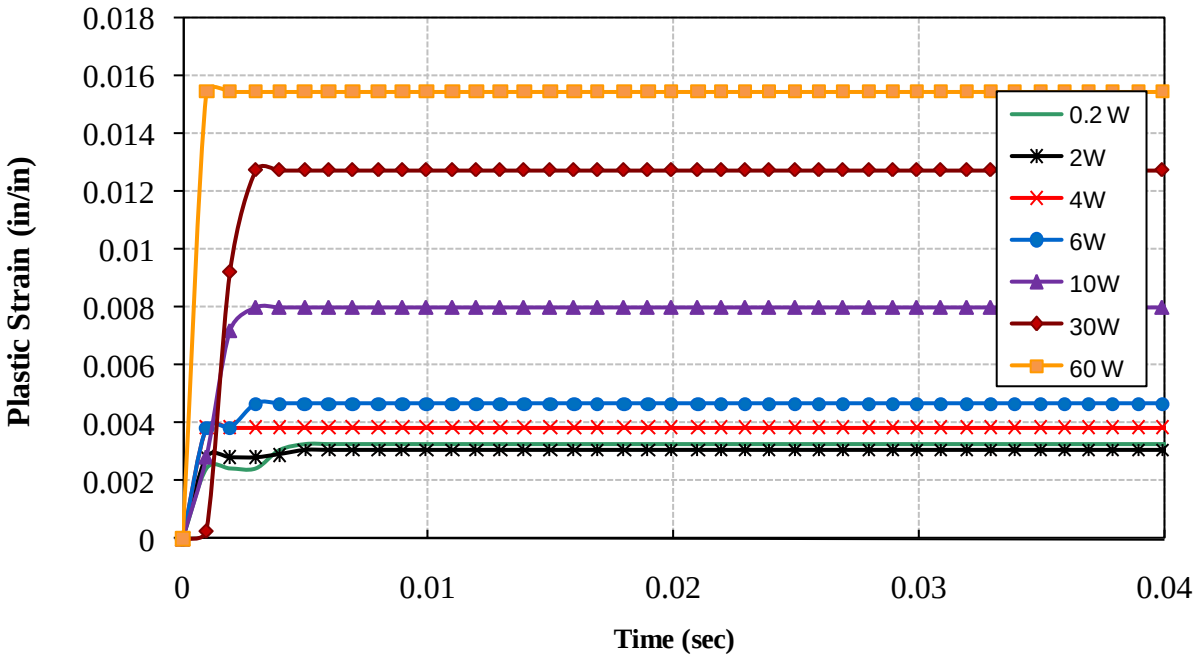

(e) Plastic Strain

Figure 14. Displacement, velocity, acceleration, effective stress, and plastic strain time histories for HE location L4

6.1.5 HE Location L5

Figure 15 shows the local response time history of the bridge under different charge weights at the fifth location (L5). As shown in Fig. 15(a), as the charge weight increases the displacement of the element closest to the damage center or to the detonation center increase. The maximum displacement of charge weight 0.2W is 0.3 in (0.007 m), while the maximum displacement for the charge weight 60W is 22in (0.56 m), which indicates a global failure under that load has occurred.

Figures 15 (b) and (c) show the velocity and acceleration time histories of the closest point to the charge before failure. The acceleration value reached the maximum at time 0.001 seconds before the maximum velocity which occurred at 0.007 seconds, which signifies the importance of the acceleration in the damage mechanism. The velocity and acceleration values at the biggest load case were 5310 in/sec (134.8m/sec) and 1.28×10^{7} in/sec^2 (3.2×10^{5} m/sec^2) respectively as shown in Figs. 15 (b) and (c).

Figure 15 (d) shows the effective stress time history for the different high explosive weights. The stresses were drawn also for the closest undamaged element to the explosion center. It can be seen that as the charge weight increases as the effective stresses increase, these cases were for concrete uniaxial compressive strength of 7000 psi. Case 0.2W gave maximum stresses 2,970 psi, which indicates that no crushing or damage occurred to the bridge deck. On the other hand, case 30W shows effective stresses of 57,800 psi which indicates that crushing occurred to the concrete at early time of 0.002 seconds. The effect of the strain rate due to the blast loads can be seen from Fig. 15 (d), where a dynamic increase factor of 8.25 was captured for the largest load case. The dynamic increase factor is defined as the ratio of the maximum dynamic concrete stresses to the static uniaxial compressive stresses. For the plastic strain results, it can be seen from Fig. 15 (e) that the ultimate strain for case 60W is 0.55 in/in whereas the maximum dynamic plastic strain of concrete was assumed to be 0.005 in this study. Table 9 shows the damage results for the box girder bridge section at location L5 subjected to the various blast loads, ranging from 0.2W to 60W.

Table 9. Damage size for HE location L5

Case	Charge	Damage Size (in)
5	0.2W	No Failure
13	2W	283.3
21	4W	308.31
29	6W	300
37	10W	326.4
45	30W	342
53	60W	648.3

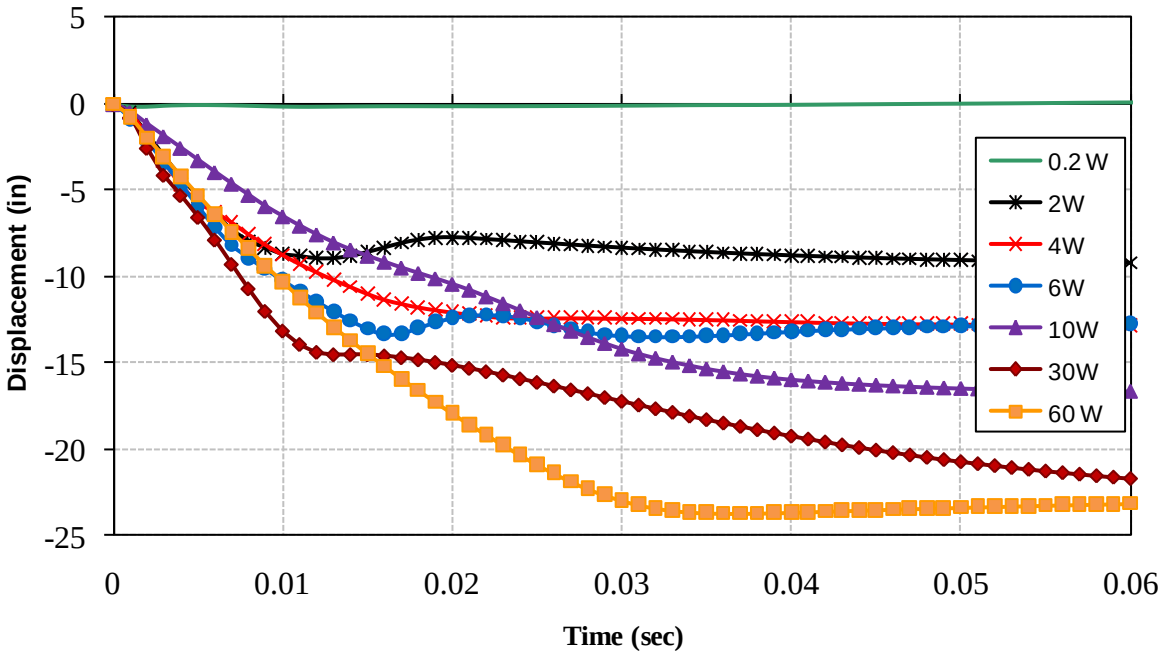

(a) Displacement

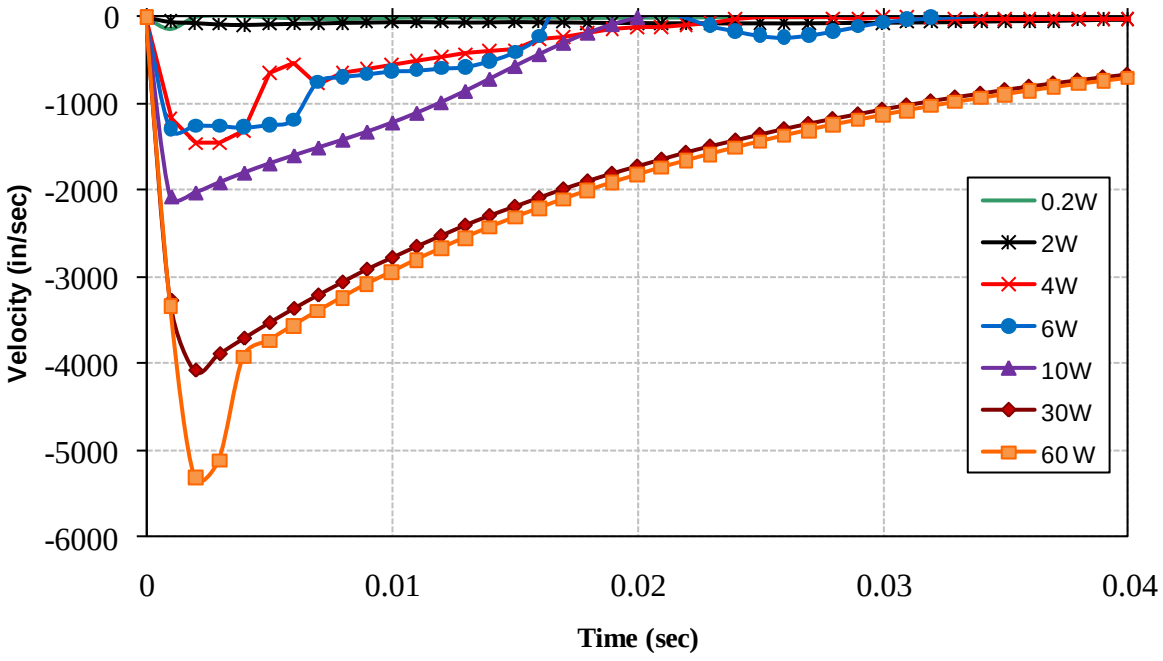

(b) Velocity

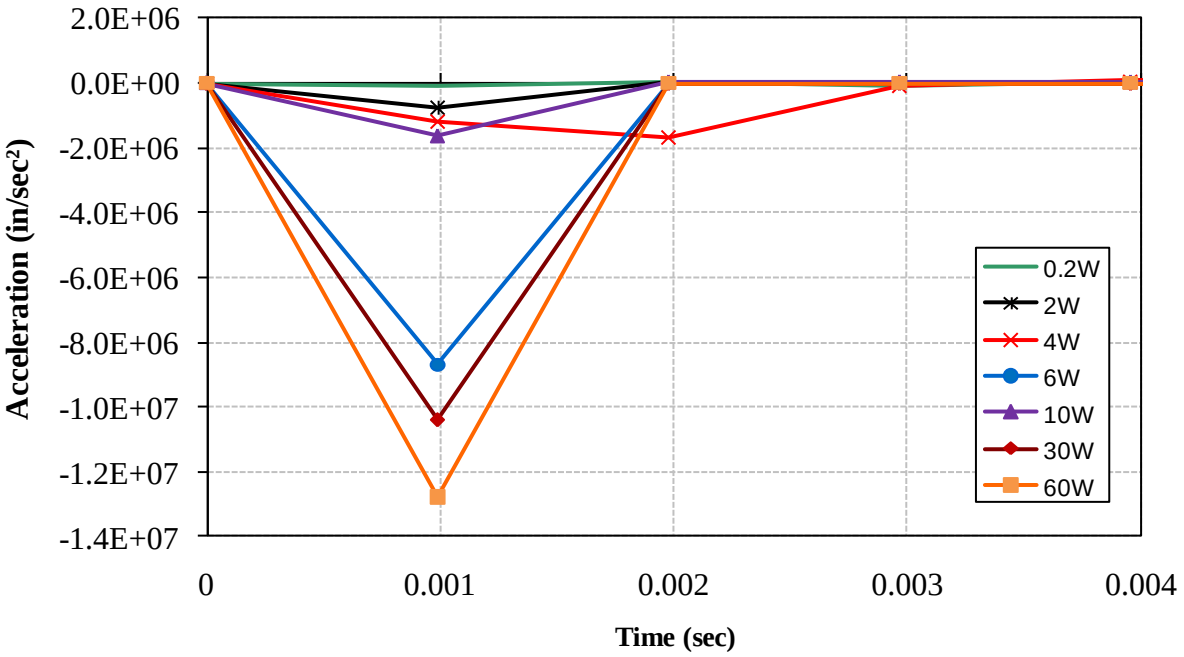

(c) Acceleration

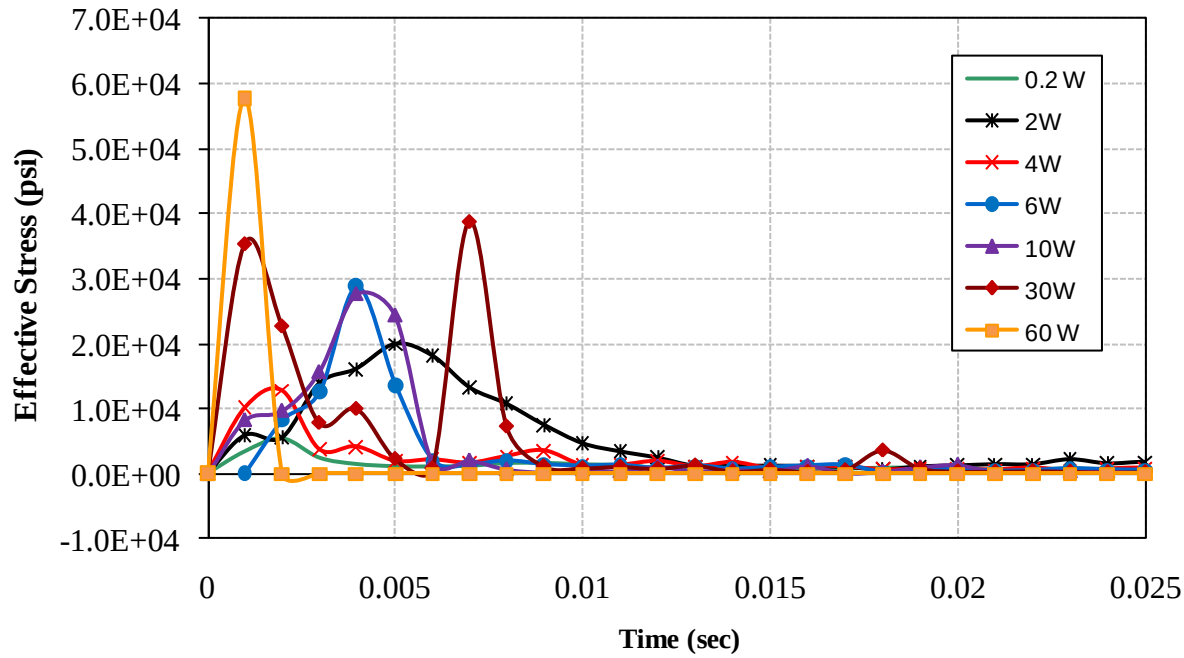

(d) Effective Stresses

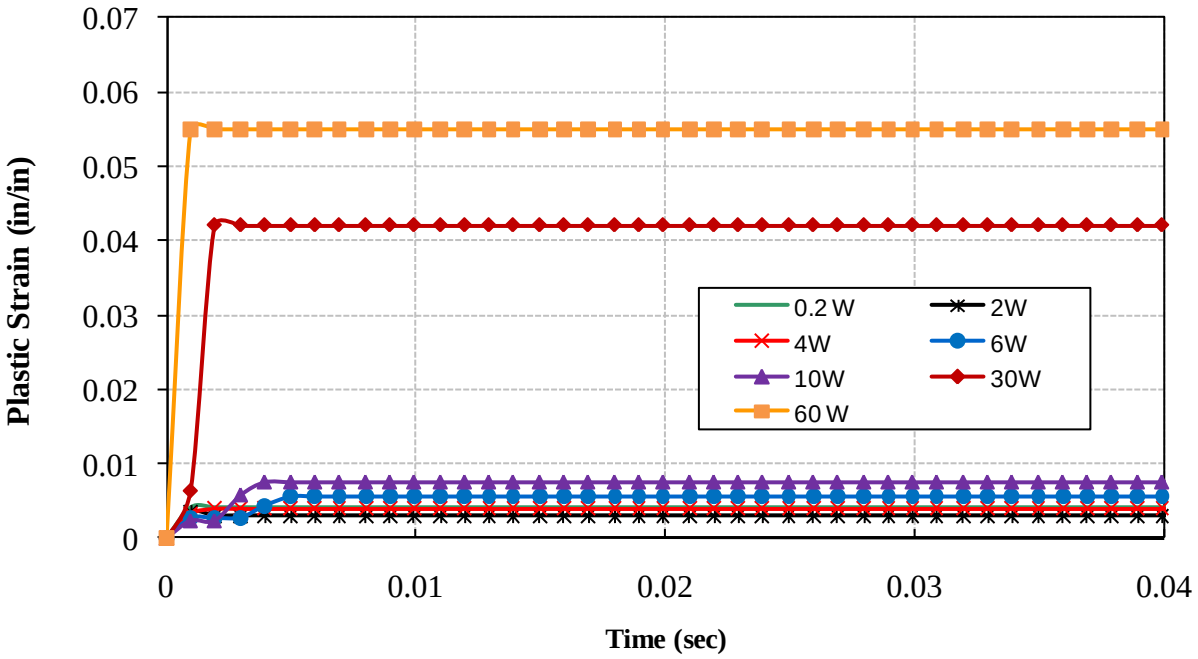

(e) Plastic Strain

Figure 15. Displacement, velocity, acceleration, effective Stress, and plastic strain time histories for HE Location L5

6.1.6 HE Location L6

The local response time history of the bridge under the different charge weights at the sixth location (L6) are shown in Fig. 16. Figure 16 (a) shows the displacement time history, which indicates that as the charge weight increases the displacement increases. The maximum displacement for charge weight 0.2W is 0.5 in (0.01 m), while the maximum displacement for charge weight 10W is 58.8 in (1.44 m), which indicates global failure under that load has occurred.

Figures 16 (b) and (c) show the velocity and the acceleration time histories of the closest element to damage (crater) center or the undamaged elements. It can be seen that the behavior is almost the same for the different charge weights from 1W to 20W: the velocity reached a maximum almost at the same time of 0.002 seconds. Dramatic increase occurred for charge weight 10W .The velocity and acceleration values at the largest load case was 5,250 in/sec (133.5m/sec) and 6.6×10^{6} in/sec^2 (1.6×10^{5} m/sec^2).

Figure 16 (d) shows the effective stress time history for the different charge weights. It can be seen that as the charge weight increases the effective stresses increase. Case 0.2W gave maximum stresses 5,400 psi, which indicates that a failure occurred to the bridge deck. On the other hand, case 60W shows effective stresses of 72,900 psi, which indicates crushing has occurred to the concrete at an early time of 0.00099 seconds. The effect of the strain rate due to the blast loads can be seen from Fig. 16 (d), where a dynamic increase factor of 5.86 was

captured for the largest load case. For the plastic strain results, it can be seen from Fig. 16 (e) that the ultimate strain for case 10W is 0.009 in/in whereas the maximum dynamic plastic strain of concrete was assumed to be 0.005 in this study. The elements around the crater reached the maximum strain rapidly after the detonation process, almost at 0.003 seconds. Table 10 shows the damage results for the box girder bridge section at location L5 subjected to the various blast loads, ranging from 0.2W to 60W.

Table 10. Damage size for HE location L6

Case	Charge	Damage Size (in)
6	0.2W	No Failure (scabbing)
14	2W	180.39
22	4W	262.85
30	6W	262.32
38	10W	280.15
46	30W	465.33
54	60W	600.15

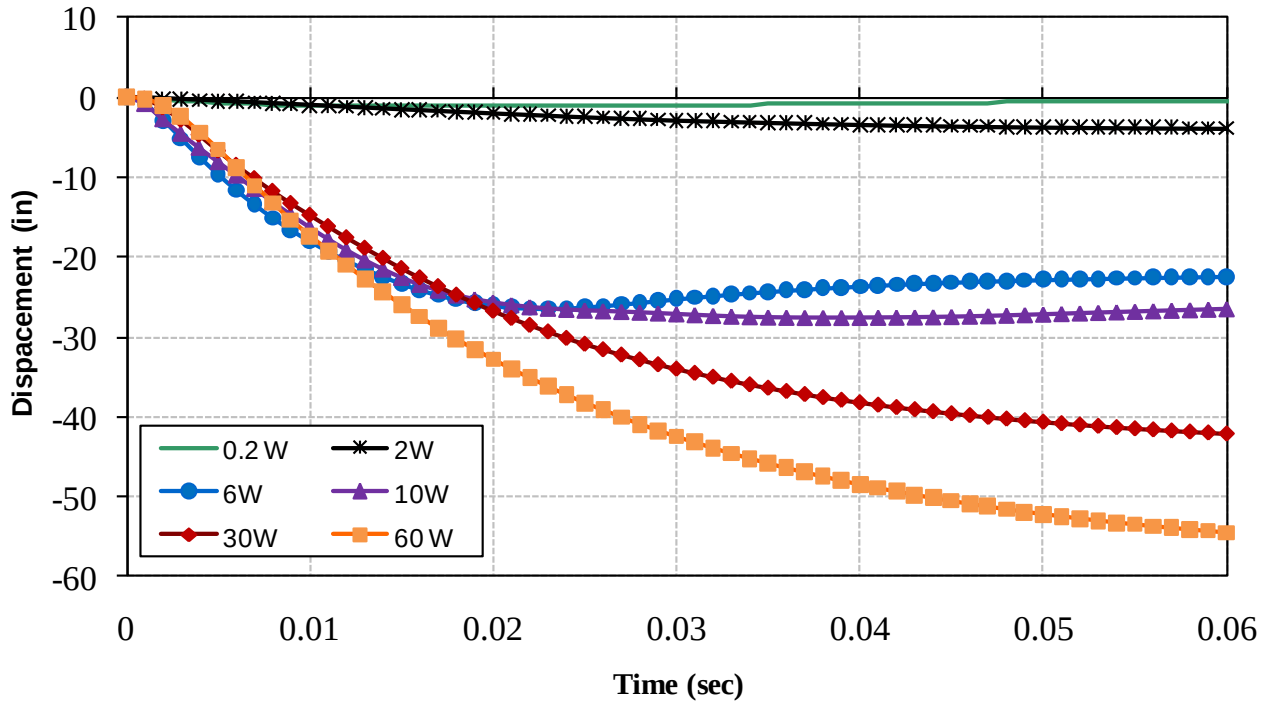

(a) Displacement

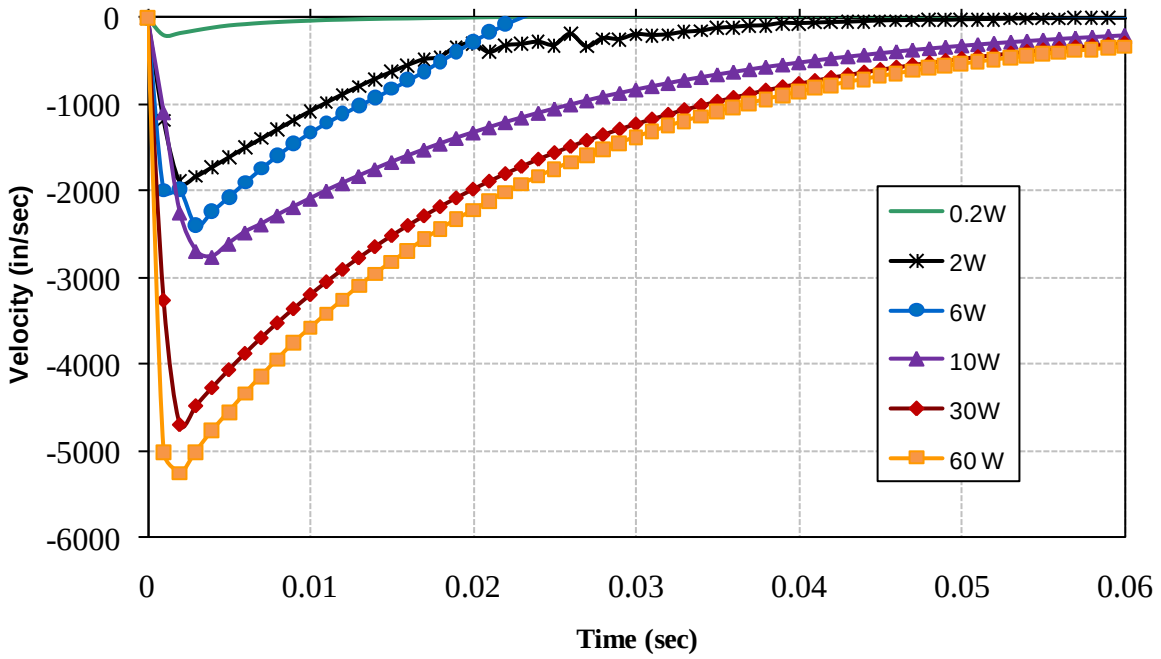

(b) Velocity

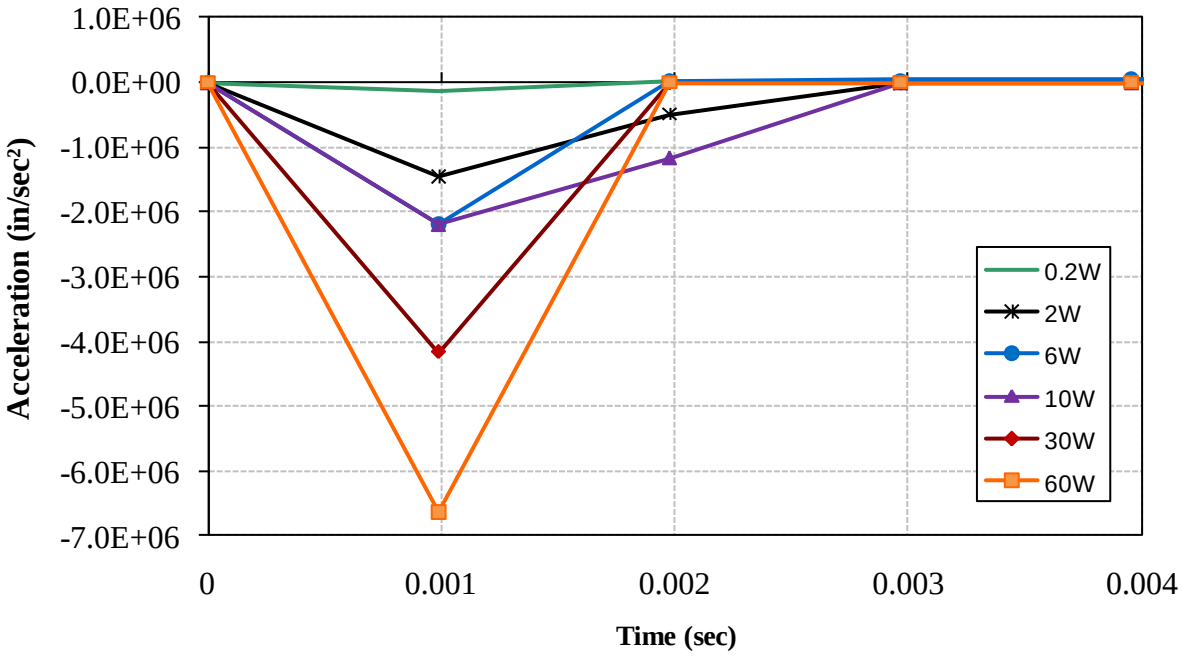

(c) Acceleration

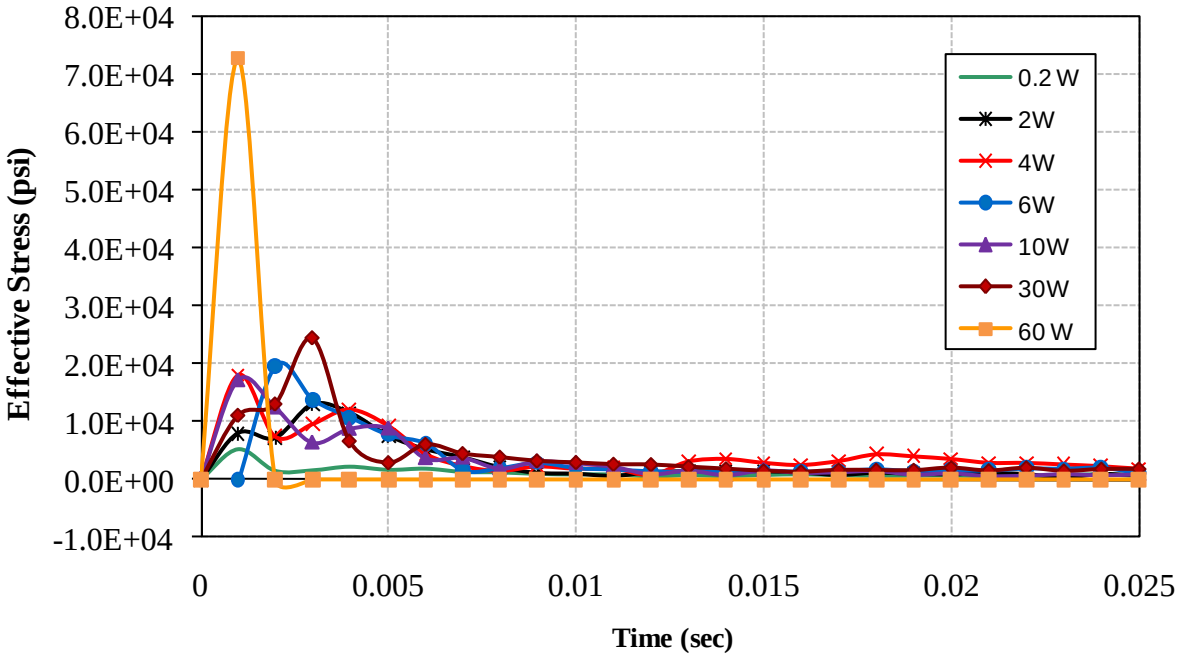

(d) Effective Stresses

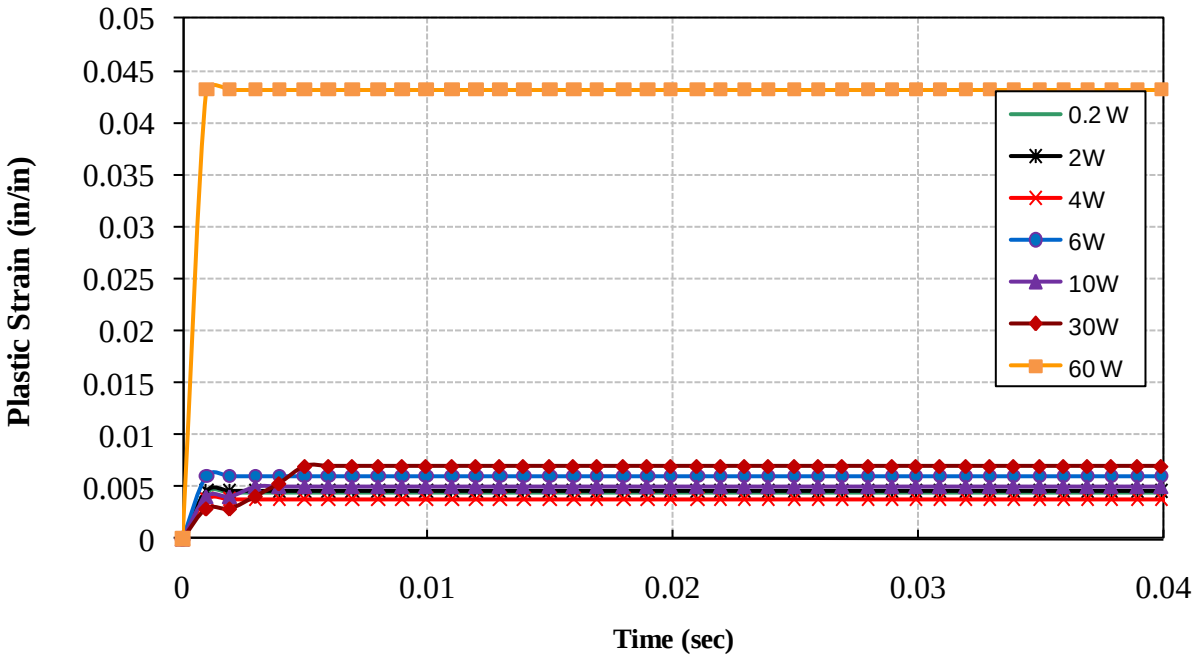

(e) Plastic Strain

Figure 16. Displacement, velocity, acceleration, effective stress, and plastic strain time histories for HE location L6

6.1.7 HE Location L7

Figure 17 shows the local response time history of the bridge under the different charge weights at the seventh location (L7). As shown from Fig. 17, the maximum response of the closest element to damage (crater) center is reached after 0.001 seconds and then decayed very quickly due to the almost instantaneous effect of blast load. Fig. 17 (a) shows the displacement time history increases, when the charge weight increases. The maximum displacement of charge weight 0.2W is 0.352 in (0.089 m), while the maximum displacement for charge weight 60W is 62in (1.57 m) and as seen the displacement profile did not continue until the end of the simulation time which indicates a global failure under that load has occurred.

Figure 17 (b) and (c) show the velocity and acceleration time histories of the closest point to the charge before failure. The acceleration value reached maximum at time 0.001 seconds before the maximum velocity which occurred at 0.007 seconds, which demonstrates the importance of the acceleration in the damage mechanism. The velocity and acceleration values at the largest load case were 4,430 sec (112.5 m/sec) and 1.17×10^{7} in/sec^2 (2.9×10^{6} m/sec^2) respectively as shown in Fig.17 (b) and (c).

The effective stress time history for the different high explosive weights is shown in Fig. 17 (d). The stresses were plotted also for the closest undamaged element to the explosion center. It can be seen that as the charge weight increases the effective stresses increase. Case 0.2W gave maximum stresses 2,620 psi, which indicates that, no significant damage occurred due to that load. On the other hand, the case 60W shows effective stresses of 95,000 psi, which indicates that failure, occurred to the concrete at an early time of 0.003 seconds. For the plastic strain results, it can be seen from Fig. 17 (e) that the ultimate strain for the case 60W is 0.047 in/in. The elements around the crater reached to the maximum strain rapidly after the detonation process, almost at 0.0008. Table 11 shows the damage results for the box girder bridge section at location L2 and subjected to the various blast loads, ranged from 0.2W to 60W

Table 11. Damage Size for HE location L7

Case	Charge	Damage Size (in)
7	0.2W	No Failure (scabbing)
15	2W	225.4
23	4W	310.62
31	6W	316
39	10W	320
47	30W	364.3
55	60W	523.5

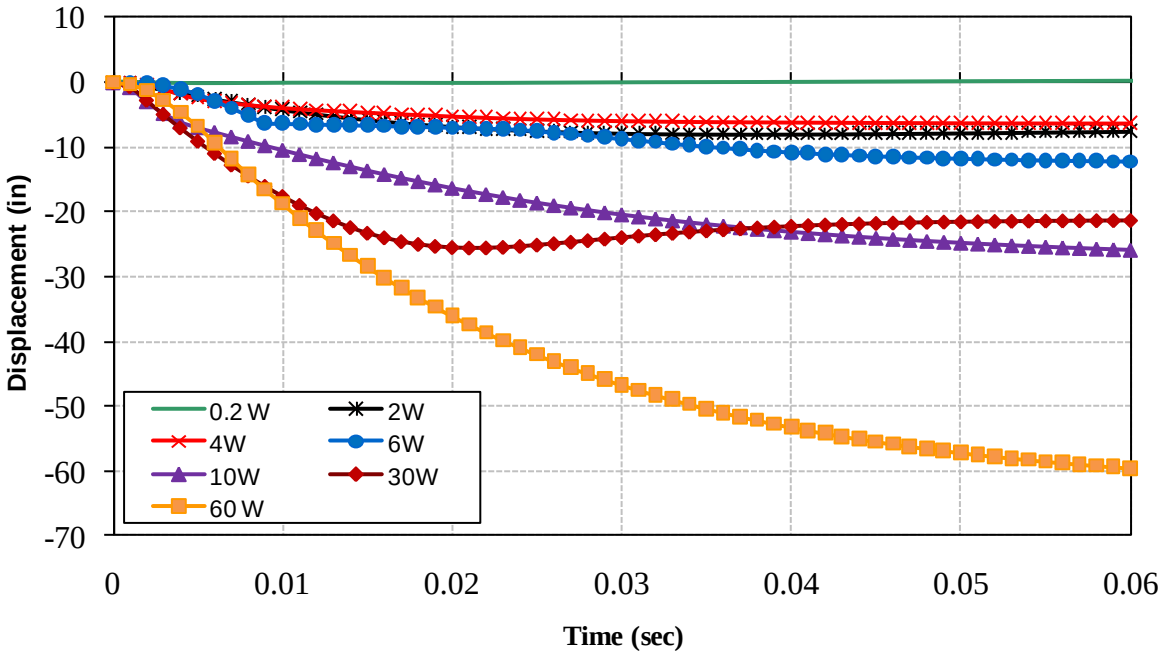

(a) Displacement

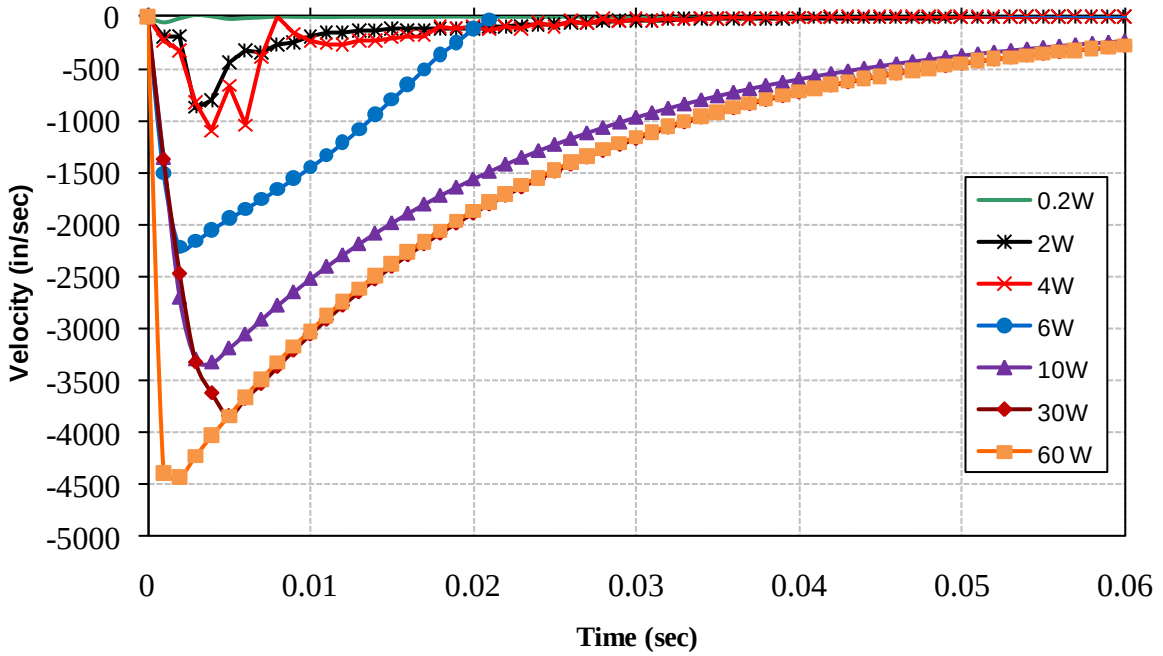

(b) Velocity

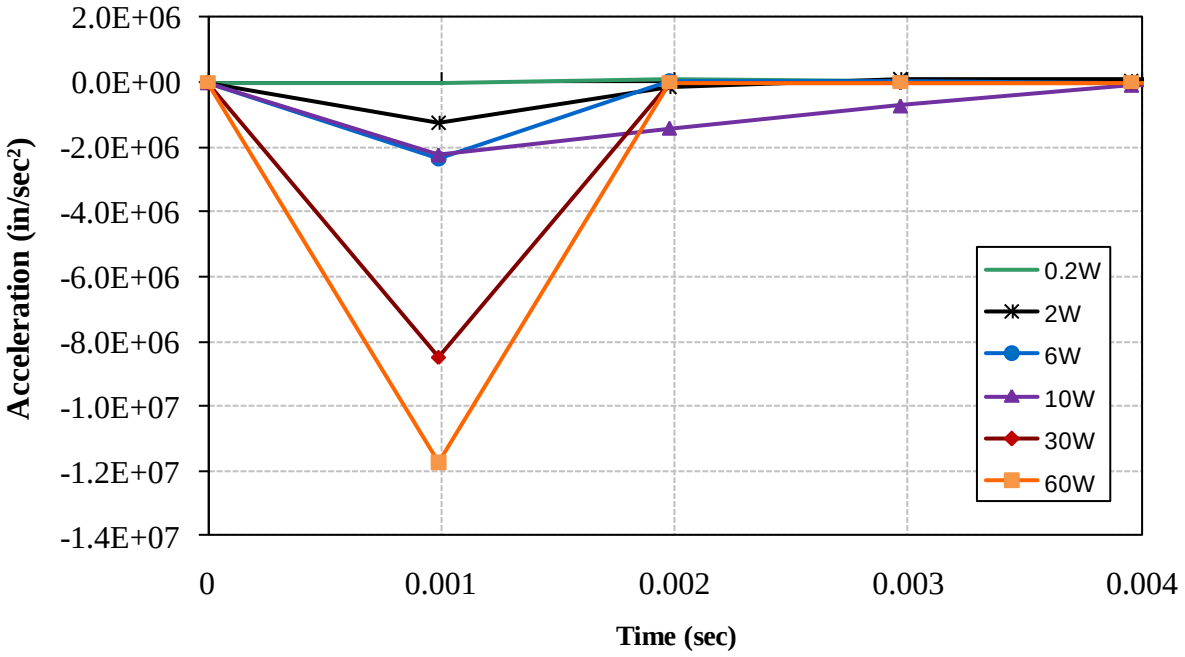

(c) Acceleration

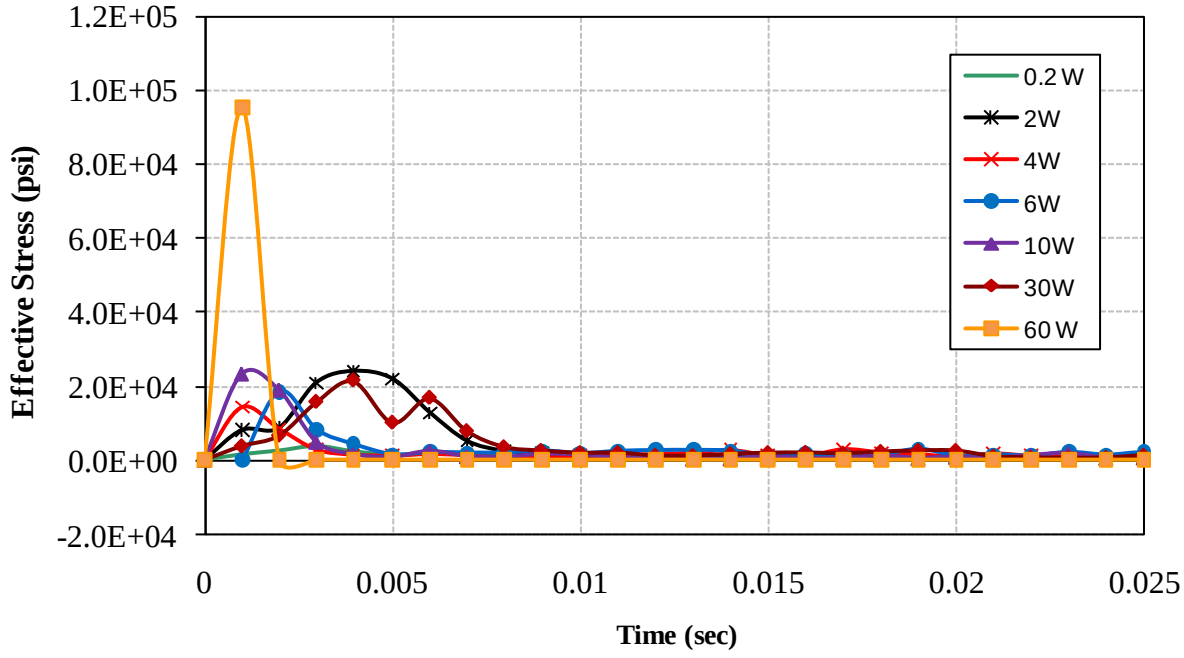

(d) Effective Stresses

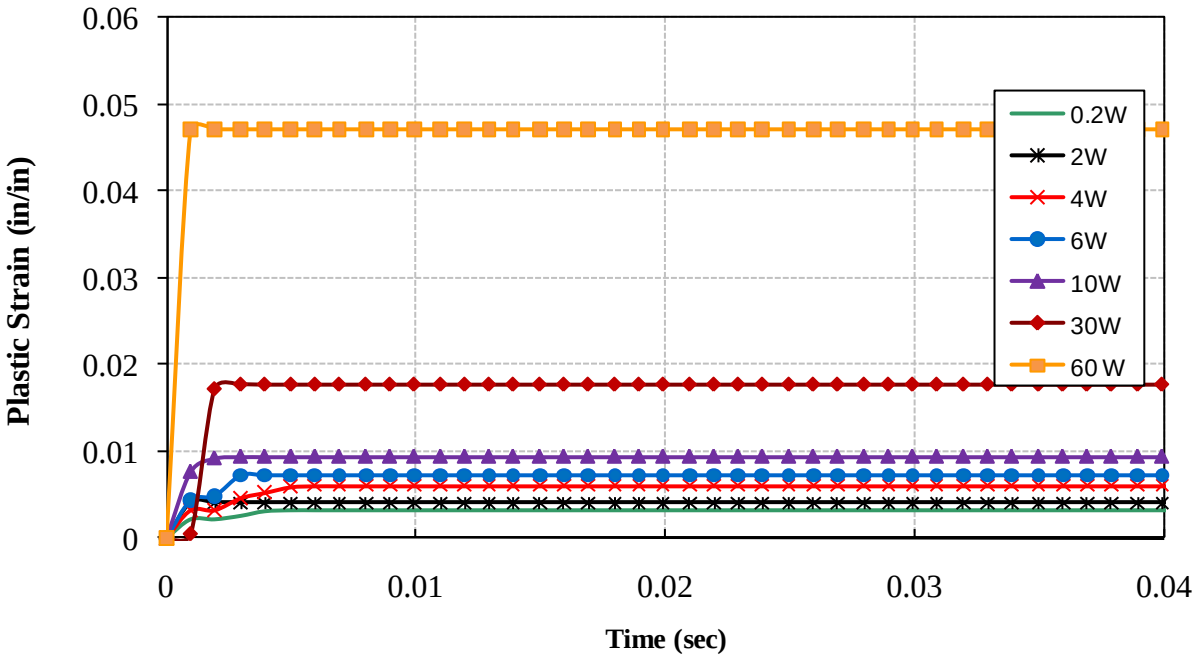

(e) Plastic Strain

Figure 17. Displacement, velocity, acceleration, effective stress, and plastic strain time histories for HE location L7

6.1.8 HE Location L8

Figure 18 shows the local response time history of the bridge under the different charge weights at the eighth location (L8). Figures 18 (a) and (b) shows the velocity and the acceleration time histories of the closest element to damage (crater) center or the undamaged. It can be seen that for the different charge weights from 0.2W to 30W, the velocity values reached maximum almost at the same time of 0.002 seconds. Sharp increase in these values occurred for charge weight 60W. The velocity and acceleration values at the largest load case were 347 in/sec (8.8 m/sec) and 5.37×10^{6} in/sec^2 (1.4×10^{6} m/sec^2), respectively.

Figure 18 (d) shows the effective stress time history for the different charge cases. The stresses were drawn also for the closest undamaged element to the explosion center. It can be seen that as the charge weight increases the effective stresses increase. Case 0.2W gave maximum stresses of 3,620 psi, which indicates that no failure occurred to the bridge deck. On the other hand, the case 10W shows effective stresses of 93,000 psi, which indicate the crushing, occurred to the concrete at the early time of 0.003 seconds. Table 12 shows the damage results for the box girder bridge section at location L2 and subjected to the various blast loads, ranging from 0.2W to 60W.

Table 12. Damage size for HE location L8

Case	Charge	Damage Size (in)
8	0.2W	No Failure (scabbing)
16	2W	239.6
24	4W	310.62
32	6W	330
40	10W	332.5
48	30W	442
56	60W	500

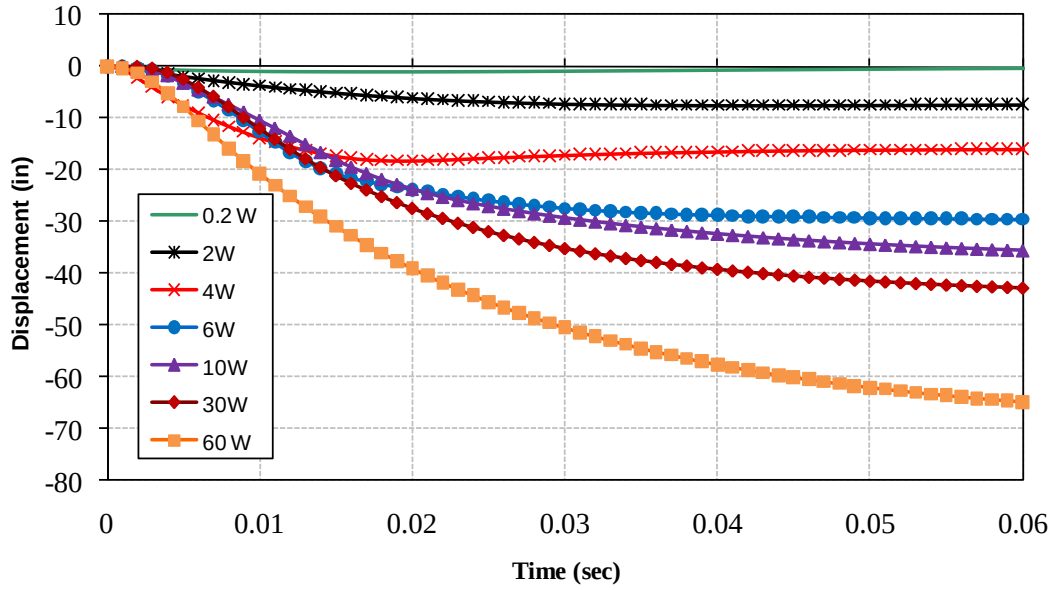

(a) Displacement

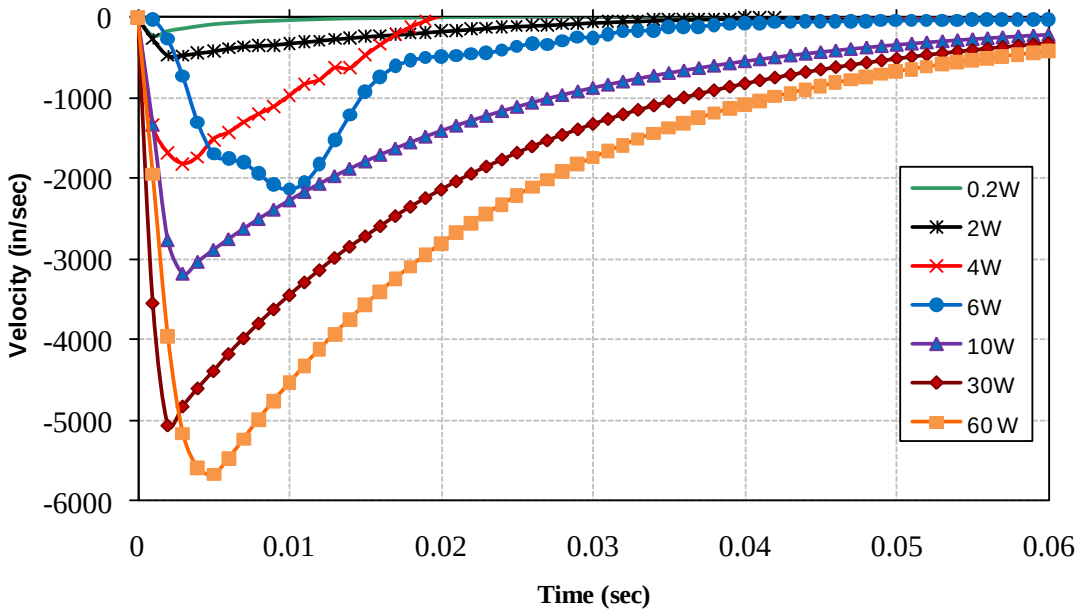

(b) Velocity

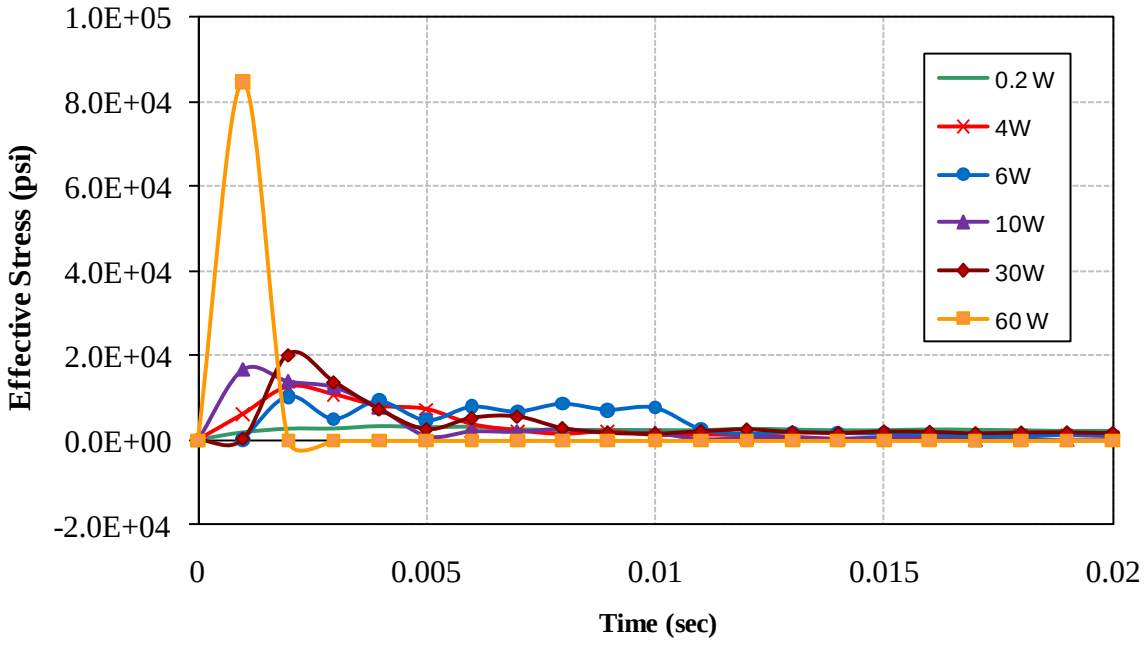

(c) Effective Stresses

Figure 18. Displacement, velocity, and effective stress time histories for HE location L8

Figure 19 shows a snapshot of the bridge section under 0.2W and 30W blast loads. It can be seen that the 0.2W produced a local failure in the form of a crater in the top flange only. Whereas 30W caused failure to the whole bridge. The top and bottom flanges as well as the girders were severly damaged under this load. In all the above cases, the blast load caused an early damage to the concrete either in the top and botom falnge accoording to the weight of the high explosive. The steel reinforcement and the post-tensioned starnds were not completely destryed, but the steel mesh was either failed or suffered large plastic deformation.

(a) Damage due to 0.2W

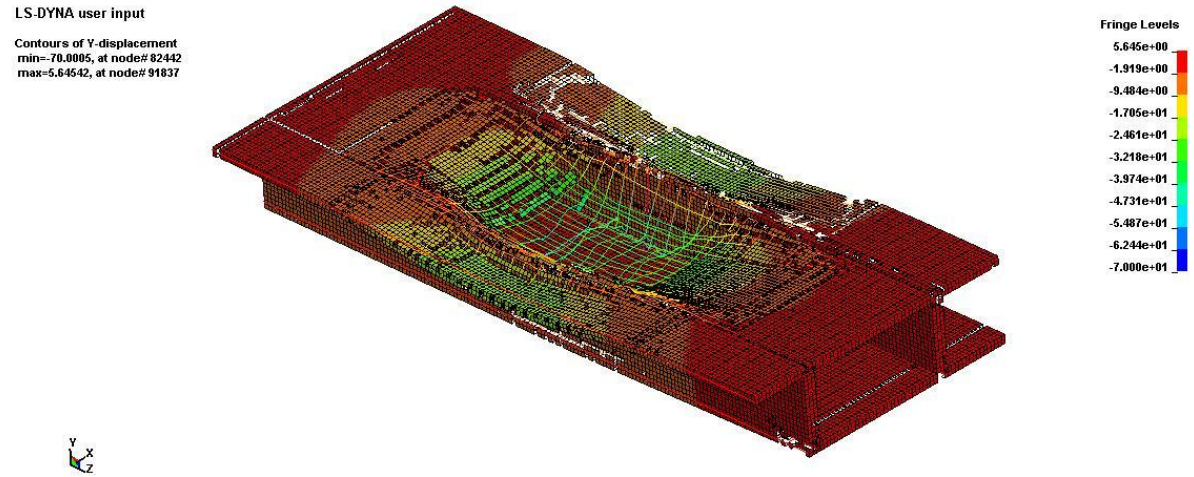

(b) Damage due to30W

Figure 19. Snapshot of the damge caused by two different HE charge sizes

6.2 Effect of Reinforced Concrete Compressive Strength

Three types of concrete compressive strengths were evaluated in this study; moderate high, and ultra high strength concrete. The uniaxial compressive strengths were 7, 10, and 15 ksi (48.3, 67, 103.4 MPa). The bridge segment was designed according to the LRFD strength limit state I using an f´c of 7000 psi. This study was conducted for the same bridge deck cross section under the same explosive size of 30W, where the high explosive charges was placed at the same location (L1). The modulii of elasticity of moderate and the high strength concrete were calculated from the following equations:

For the moderate weight concrete when $21 \leq f'_c \leq 83$ MPa:

$$E_c = (3320\sqrt{f`c} + 6900)\left(\frac{w}{2346}\right)^{1.5} \quad \textit{(ACI 363\& Martinez)}$$

where *w* is the unit weight of concrete

and for the high strength concrete, when $55 \leq f'_c \leq 125$ MPa (*ACI 363*) :

$$E_c = 4700\, C_{ca}\sqrt{f`c}$$

where C_{ca} is an empirical coefficient to account for the type of coarse aggregates, and is taken as 0.92, 0.97 or 0.82 for limestone, quartzite, and granite, respectively.

The comparison of responses in terms of time histories of vertical accelerations, velocities, and effective stresses is presented in this section. Figure 20 (a) shows the acceleration time history of the bridge using 3 different types of concrete at 0.008 seconds. It can be seen that as the concrete compressive strength increases from 7ksi to 10 ksi, no significant increase in the response was obtained. But on the other hand, a significant increase occurred to the acceleration of concrete with strength of 15 ksi. All the maximum acceleration values occurred around the same time of 0.001 seconds.

Figure 20 (b) shows the velocities time history for the three cases. It can be seen that under the same load (30W) located at location L1, the maximum values of velocities were equal to 6,780, 7,600, and 8,520 in/sec (172.2 and 193, and 216.4 m/sec) for the 7, 10, and 15 ksi (48.3 and 69, and103 MPa), respectively. All the above velocities were measured at the nearest point to the detonation (almost at the nearest point to the steel reinforcement since the concrete failed at very early time). Increasing the concrete strengths from 7 to 10 and 15 ksi, increased the velocity by 12% and 22.8% respectively as shown in Fig.20 (b). The effective stresses for the 15 ksi concrete were 1.53 and 2.52 times larger than those for the 10 and 15 ksi concrete respectively.

It is concluded from this section that increasing the compressive strength of concrete, increases the effective stresses dramatically, which causes the crushing process in concrete to be faster in high strength concrete than normal concrete. The damage size, which is measured in this section by the mass lost after the detonation for the bridge section using three different concrete strengths, is shown in Fig. 20 (c). It can be seen that when the concrete strength increased from 7 to 10 and 15 ksi, the mass loss decreased by 27% and 33%, respectively. In conclusion, using the high strength concrete in blast resistant structures will decrease the damage size and the mass loss.

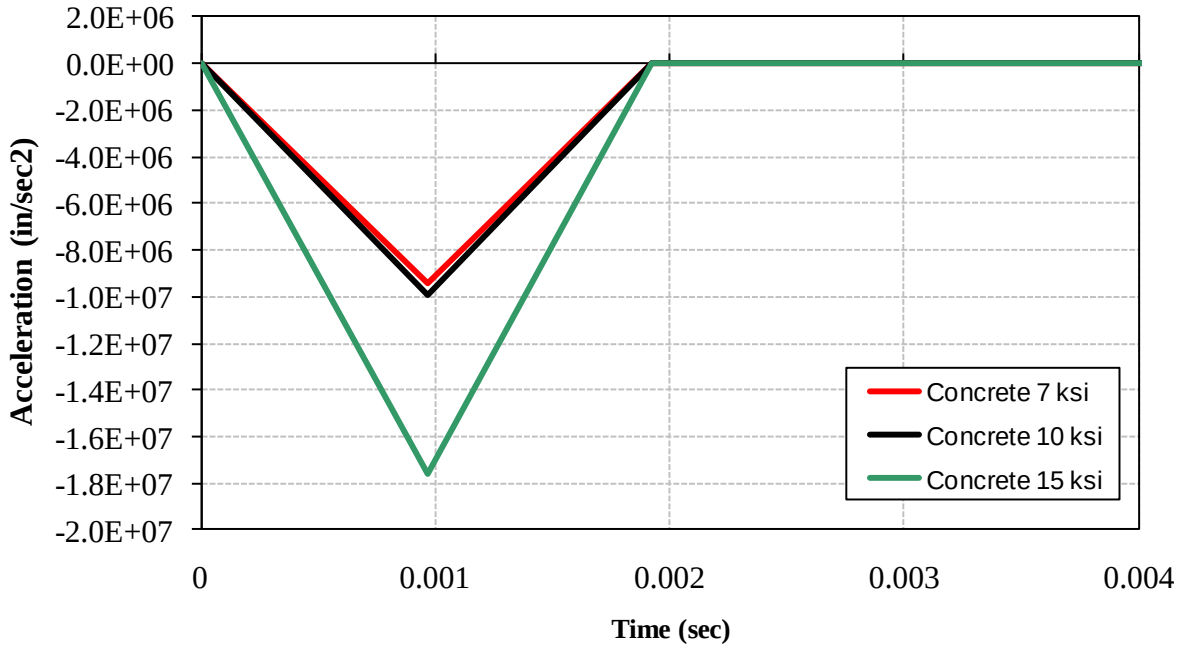

(a) Vertical Acceleration

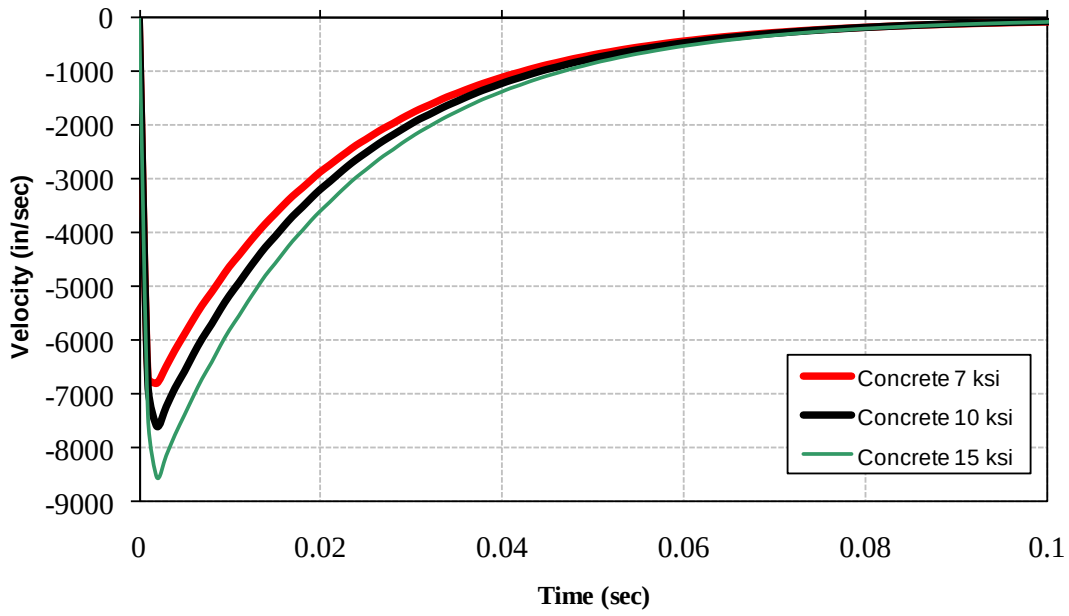

(b) Vertical Velocity

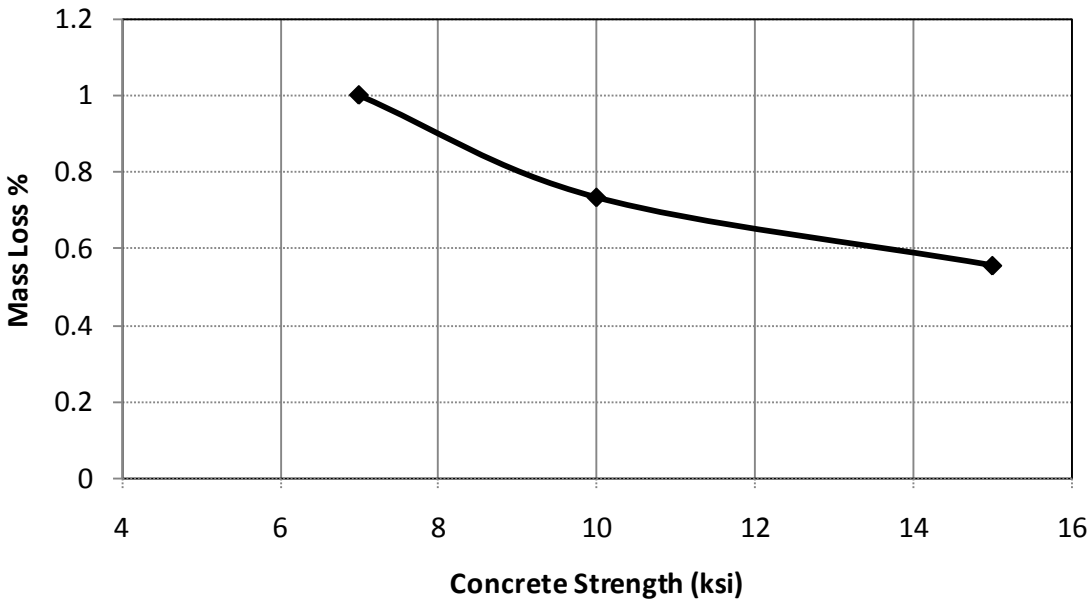

(c) Mass Loss

Figure 20. Time histories for (a) acceleration and (b) velocity; mass loss as a function of concrete strength

6.3 Effect of Steel Reinforcement Properities

The comparison of the response of similar box girder bridge deck using three different steel grades is presented in this section. The concrete uniaxial compressive strength was taken as 10 ksi and it was kept constsnt for the three cases. The steel grades according to ASTM A615 were 50, 70, and 100 ksi (344.7, 482.6, and 689.5 MPa) and the blast loading for this study was 30W located at L1 position.

Figure 21 shows the total energy (kinetic plus strain energies) of the bridge section for the different steel grades. It can be seen from the results that there is no significant difference in the total energy and the vertical velocity induced due to the same explosive size and location. So the steel grade does not significantly affect the damage mechanism. When the blast wave hits first the concrete surface causing damage, then the wave moves back and forth through the concrete element around the steel rebars. In most cases the steel cage does not break and the blast wave energy is first absorbed by concrete which moves back and forth causing the dynamic tensile stresses greater than its dynamic strength, which initiates the fragment process. It is concluded from this section that the reinforcing steel has little influence on the deck behavior and damage mechanism under close-in detonations.

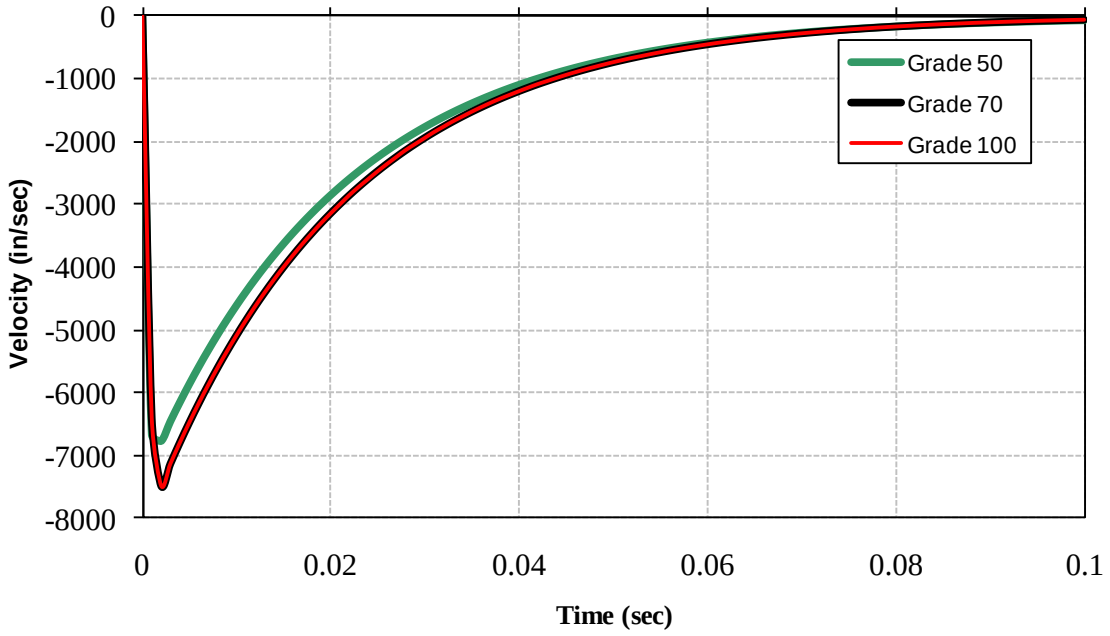

(a) Vertical Velocity

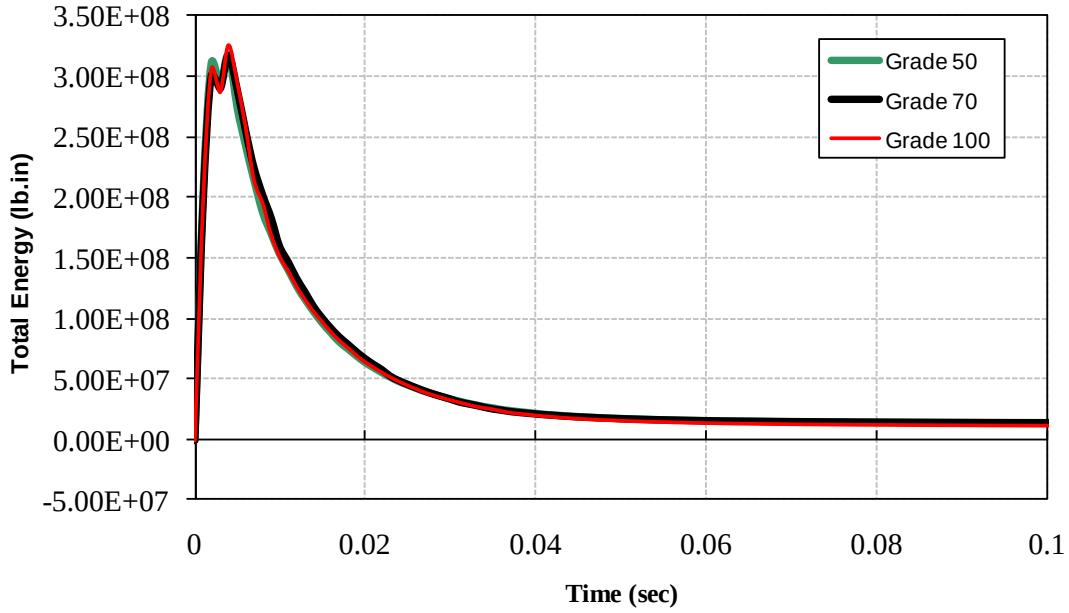

(b) Total Energy

Figure 21. Vertical velocity and total energy time histories with different steel grades

6.4 Effect of Tendon Profile

The post-tensioned low relaxation tendons of grade 270 were used in this study. The effect of tendons shapes on the axial forces, the total bridge energy, and on the damage size were studied. As it can be seen from Fig. 22 that the maximum velocity of the the nearest point to the explosion center for the straight tendons is less than the parabolic one by 13%. The reason for that is the parabolic tendons generates a vertical force component due to the inclination of its profile and that vertical shear force is opposite to the blast load which is acting downword. So using the parabolic tendons contributes in decraesing the maximum velocity as seen in Fig. 22.

Figure 22 (b) shows the effect of tendons shape on the total energy of the whole bridge, as it can be seen that at 0.001 seconds the total energy of the bridge system with parabloic tendons was more than the straight one by 22%. This increase demonstraes the effect of parabloic tendons in absorbing the energy released by the blast loads after miliseconds from the detonation time. After the detonation time by few miliseconds, the energy of the bridge with parabolic tendons dropped to the one with straight tendons and response the became similar until the failure.

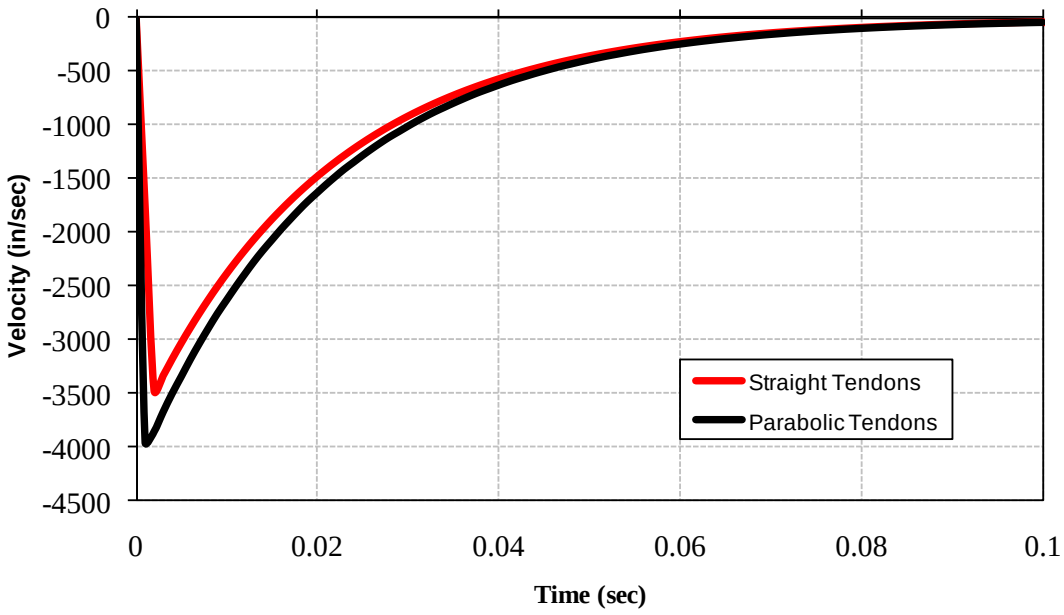

(a) Velocity Profile

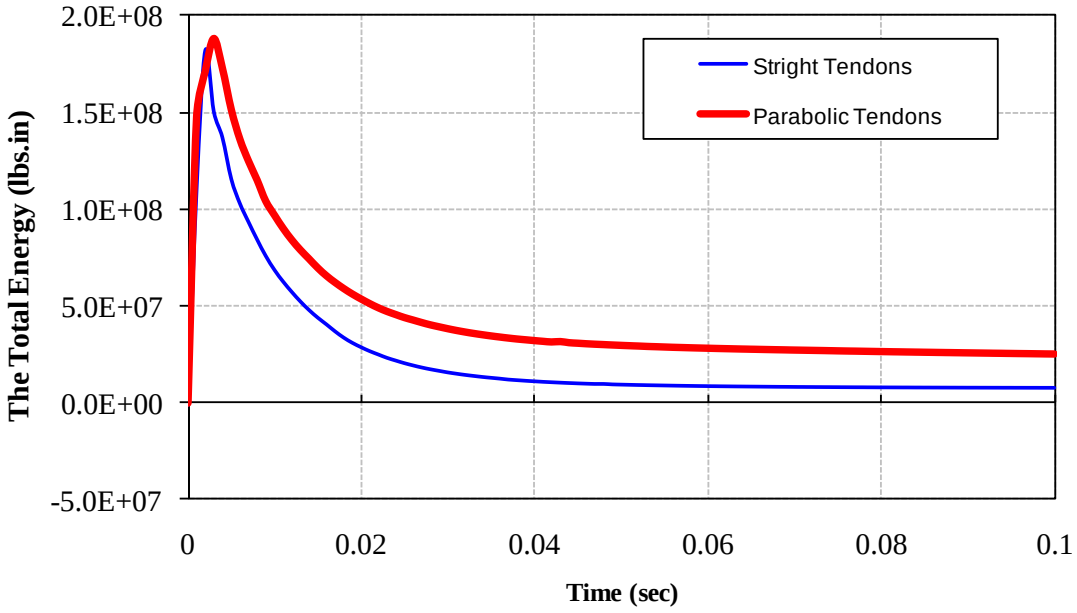

(b) Total Energy

Figure 22. Axial force and the total energy time histories with different tendon profiles

6.5 Effect of Standoff Distance

The effect of the bomb standoff distance on the response of the box girder bridges and on the damage size was considered in this section. Four different standoff distances were studied 30, 40, 60, and 120 inches. Figure 23 shows the time histories of the vertical Acceleration and velocities of one of the elements at the crater perimeter and closest to the ignition point. The responses were traced under blast loads of 10W and concrete compressive strength equal 10 ksi. It can be seen that as the stand off distance increases the effective stresses decrease. In Fig. 23(a). it can be seen that there is no significant difference in the maximum acceleration between the standoff distances 30, and 40 inches. After increasing the standoff distance to 60 and 120 inches, it is noticed a significant change in the acceleration profile is observed. Decreasing the standoff distance from 120 to 30 inches, increased the acceleration by 8.5 times.

Table 13 shows the time history for vertical acceleration, velocity, and displacement for four standoff distances, 30, 40, 60 and 120 inches. The damage size also is shown in Table 13 as an equivalent diamaeter of the crater. An increase in the standoff distance by 25% and 75% led to a decrease in crater diameter by 42 % to no breaching, repectiveley. The conclusion from this section shows the significant effect of the standoff distance on the damage size. It is recommended to protect the these important types of bridges by using common strengthening material like the carbon fiber reinforced polymers (CFRP) to add additional energy absorption mechanism to the whole system of the bridge.

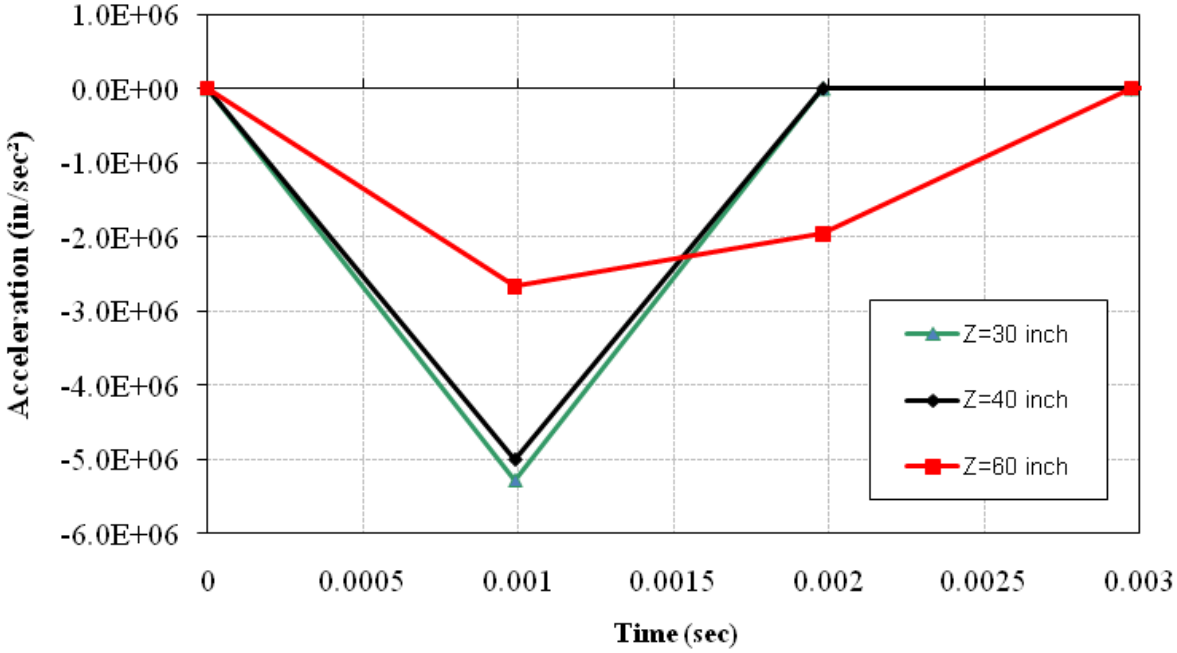

(a) Vertical Acceleration

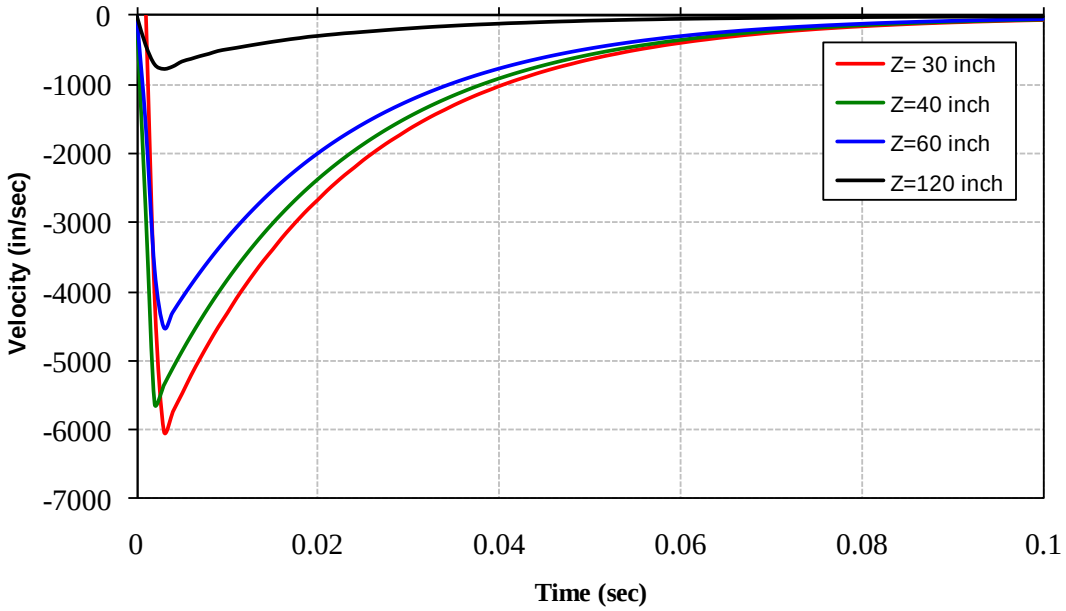

(b) Vertical Velocity

Figure 23. Acceleration and velocity time histories for different standoff distances

Table 13. Maximum responses due to the effect of the standoffs under blast load of 10W

Standoff Distance (in)	Maximum Vertical Acceleration (in/sec^2)	Maximum Vertical Velocity (in/sec)	Damage Size (equivalent diameter) (in)
30	5.26×10^6	6020	450
40	5.00×10^6	5620	263
60	2.67×10^6	4300	153
60	6.25×10^5	750	Scabbing only, no breaching

7. Continous Span Bridge under Blast Load

A two-spans continous box girder bridge was studied under 10 diferent high explosive weights and locations to predict the damage level suffered by the superstructure. The bridge model and boundary conditions are shown in Fig. 24. The bridge was modeled using half- scale with the appropriate symmetry boundary conditions. The tendons profile was chosen to be parabloic as shown in Fig. 25. The bridge was designed using LRFD manual as described in section 5.3 using the same dead and live loads.

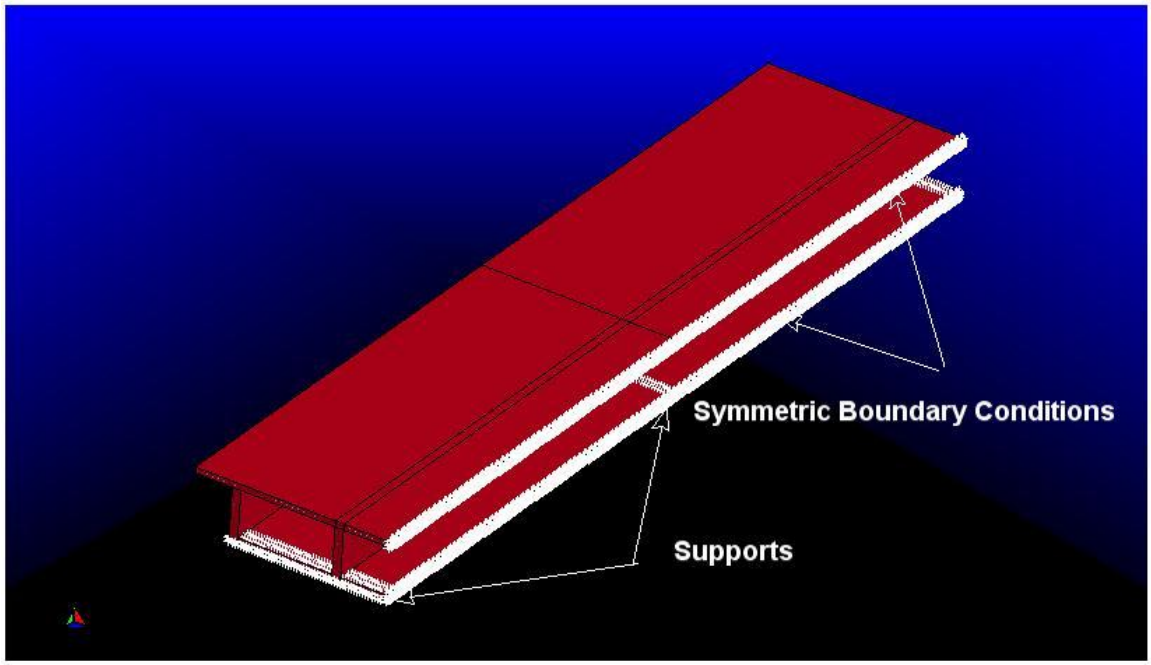

Figure 24. Bridge model and boundary conditions

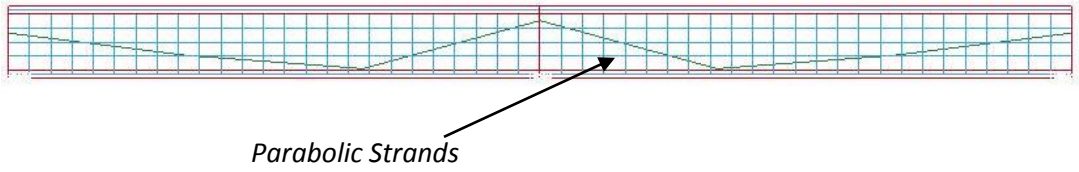

Plan View of the Bridge Cross Section showing the reinforcement profile

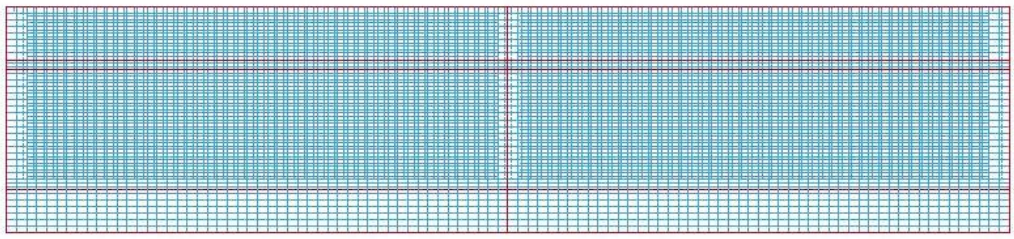

Side View of the Bridge Cross Section

Figure 25. Reinforcement details of the two-span box girder bridge

The continous span bridge was studied under explosive charges 6W, 10W, and 30W which are placed over the support and at the midspan sections. Table 14 summarizes the results in terms of the maximum acceleration under the nearst element to the detonation point, and also shows the damage size as an equivalent diameter of the formed crater. The high explosives were placed at two postions. Two cases in the transverse direction were modeled at the section which is over the support while three cases in the transverse direction for the section which is located at the midspan as shown in the Table 14 below.

Table 14. Maximum responses of continuous bridge under different blast loads and locations

Charge (lb)	HE Location	Vertical Acceleration (in/sec^2)	Maximum effective stresses near the crater (psi)	Damage Size (in) (equivalent diameter)
10W	**M,L1**	1.02e6	27,300	136
30W	**M,L1**	6.7e6	40,100	185
6W	**M,L1**	1.07e5	12,500	117.5
10W	**M,L2**	Global Failure of the upper and lower deck		
30W	**M,L2**	Global Failure the upper and lower deck		
10W	**S,L1**	5.39e4	18,700	140
30W	**S,L1**	1.27e6	22,900	152 *
6W	**S,L1**	5.9e5	10,300	87
10W	**S,L2**	7.38e5	27,500	185**
30W	**S,L2**	6.26e6	54,200	210*

*Partial failure of the support (the web is almost failed at this section)

**Top flange failed, but no failure occurred to the bottom flange

M = Midspan; S = Support at Pier .

8. Proposed Design Criteria

The previous parametric study was performed for 8 locations under different charge weights over the bridge deck. The following section will summarize the statistical analysis and the proposed design criteria for blast resistant design of post-tensioned box girder bridges. Figure 26 shows the crater size in feet versus the scaled distance for all the cases combined, where the damage size was investigated. It is seen that as the scaled distance increases the crater size decreaseds. A logarithemic regression was done to fit the data points, and the following equation was derived to predict the damage size for different scaled distances. This equation should be verified by experiments and should not be used for scaled distances less than 0.1 or more than 0.5. The governing equation for the damage size is:

$$D = -27.95 \ln Z - 13.101$$

where: D is the equivalent damage diameter in feet and Z is the scaled distance in ft/lb$^{1/3}$

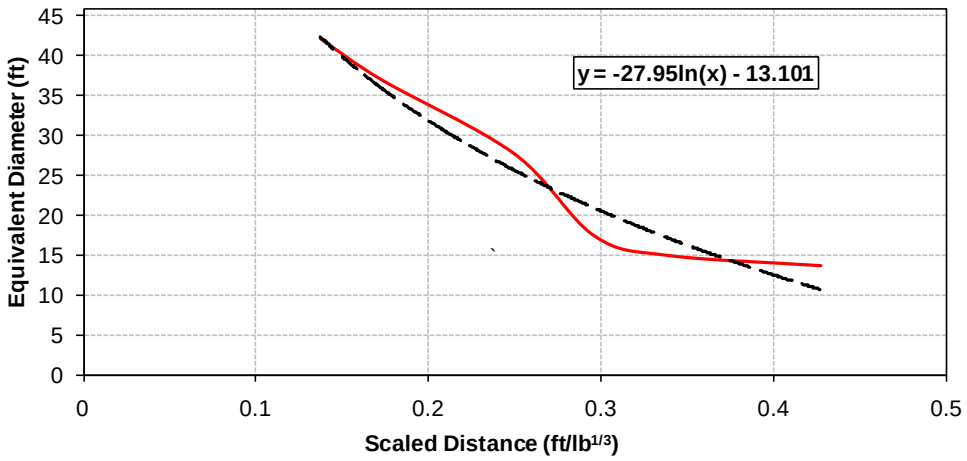

Figure 26. Crater size versus the scaled distance for the box girder bridge

Damage levels versus scaled distances for charge weights placed at the first 4 locations (L1 – L4) are shown in Fig. 27. The damage level is assumed to be the ratio of the the mass loss to the maximum mass loss expeienced by the bridge deck.The general trend for the damage level is decreasing as the sclaed distance increases. The maximum damage level is reached for the loation L1 and load 30W at a scaled distance of 0.1. At lower scaled distances, the damage for loactions L2 and L4 is more than that of location L1.

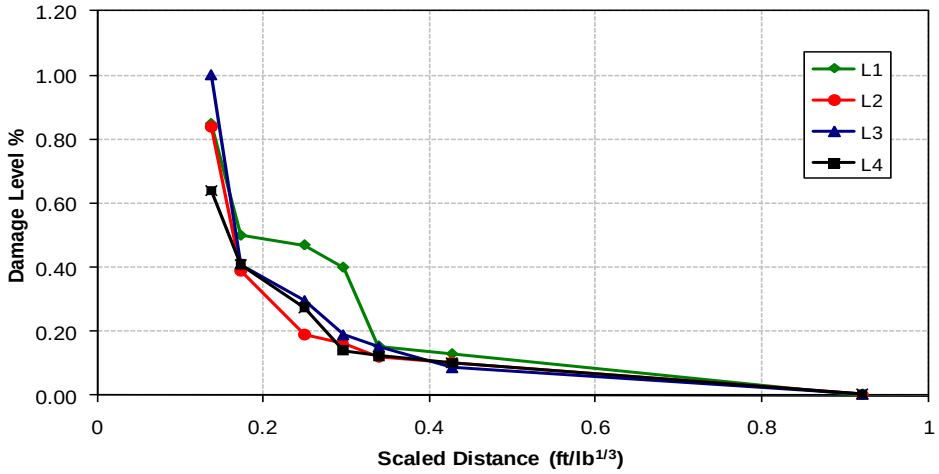

Figure 27. Damage level versus scaled distance for L1 – L4

The results for locations L2 and L3 are shown in Figure 28 with the best fit curves shown for each. From the previous section, it is concluded that the damage size should be controlled after certain amount of the explosive, so a strengthening technique to these types of bridges will be presented in the next section.

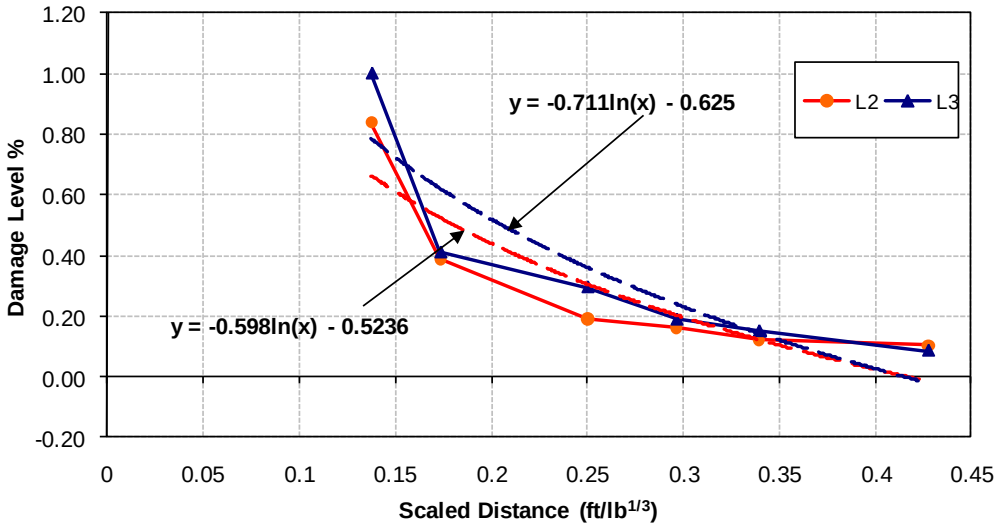

Figure 28. Damage level versus scaled distance

9. Strengthing the Box Girder Bridge using CFRP

The structural characteristics of reinforced concrete box girder bridges strengthened with carbon fiber reinforced polymer (CFRP) composites under blast loads cannot be easily assessed with simple procedure. Experimental tests, specially in the area of blast load, are very expensive in terms of the number of specimens and the required instrmentation. Numerical studies, if properly conducted, provides a reliable and trusted assessment of bridge responses. In this section a

numerical study is conducted on a number of box girder bridges under blast loads to predict the damage level and the correspoding improvements in the response and perfromance.

The CFRP composites are used to strengthen the bridge under certain expolsive charge weights. In this study the charge weights are 10W and 30W, and these espolsives were placed over the bridge deck above the exterior web. Three different cases were studied: the first case was assumed to sterngthened the lower surface of the bridge deck at the midspan section, the second case was to strengthen the upper surface, and the last case was done by placing the CFRP on both sides of the bridge deck as shown in Fig. 29.

The CFRP laminates were modeled using the material model COMPOSITE_DAMAGE available in LS-DYNA with optional brittle failure for composites can be defined. By using the user defined integration rule, which is GIVEN in LS-DYNA by INTEGRATION_SHELL, the consitiutive constants can vary through the shell thickness. Lamination theory was applied to correct the assumption of constant shear strain across the thickness. The interlaminate bond was assumed perfect with no slippage allowed between the element layers. The three layers were assumed oriented at angles equal to 0^0, 90^0, and 0^0 and defined in the SECTION_SHELL card. The properties of the CFRP were derived using the software CADEC - Computer Aided Design Environment for Composites (Barbero, 1995). Table 15. shows the properties of CFRP used in this study. Figure 29 shows the finite element mesh of quarter bridge model and the CFRP on the top and bottom faces. The width of the carbon fiber sheets were taken as 48 inches for the qurter model as shown in Fig. 29.

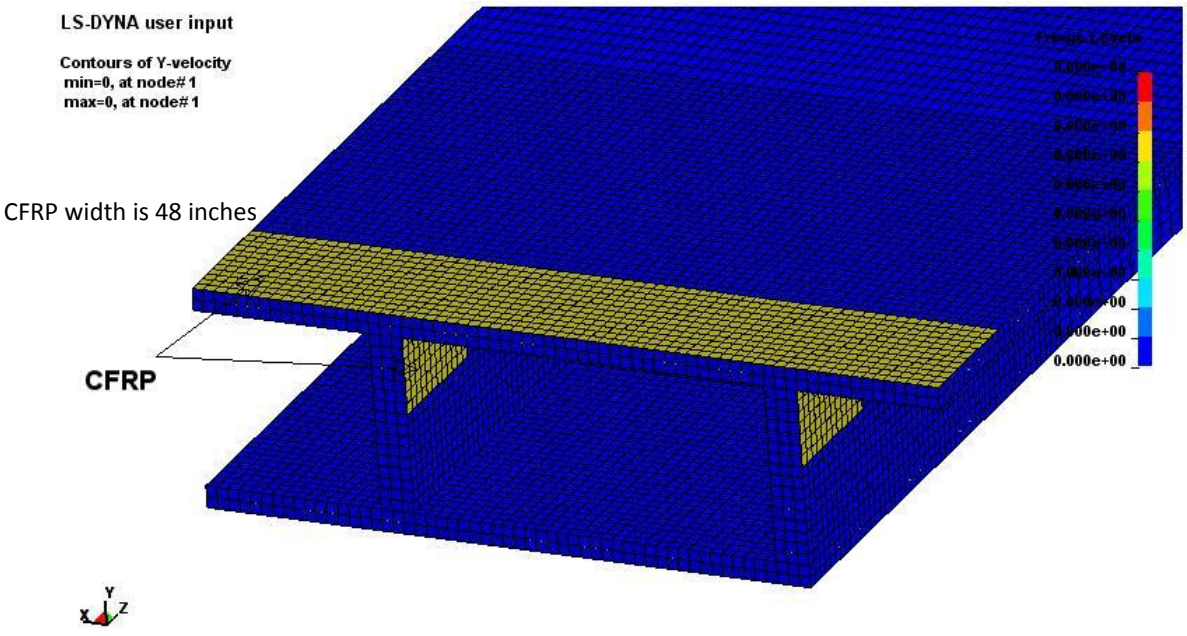

Figure 29. Finite element mesh and the CFRP on both sides of the deck

Table 15. CFRP propertities

Material Type	Poisson's Ration	Thickness [mm (in)]	E MPa (psi)	G MPa (psi)
CFRP	υ_{11}=0.22 $\upsilon_{13=}$0.22 υ_{23}=0.47	1.1 (0.04)	E_{11}=62,100 (9,000,000) E_{22}=4,830 (700,000) E_{33}=4,830 (700,000)	G_{12}=3,270 (473,700) G_{12}=3,270 (473,700) G_{12}=1,860 (270,000)

Figure 30 shows the total energy of the bridge before and after using the CFRP material under blast load of 10W. It can be seen that tha maximum energy was reached at time 0.004 seconds and the values are 2.04×10^8 and 1.22×10^8 lb-in for the case of using CFRP on top, bottom and the reference model, respectively. Using the CFRP laminates in strengthening the top and the bottom surfaces of the bridge deck was effective as it increased the total enery of the bridge deck by 167%. Long-term effects of FRP strengthening was not invistigated in this study, and thus the performance of FRP-retrofitted box girders should include such effects before recommending it for blast-retrofit of post-tensioned box girders in field applications.

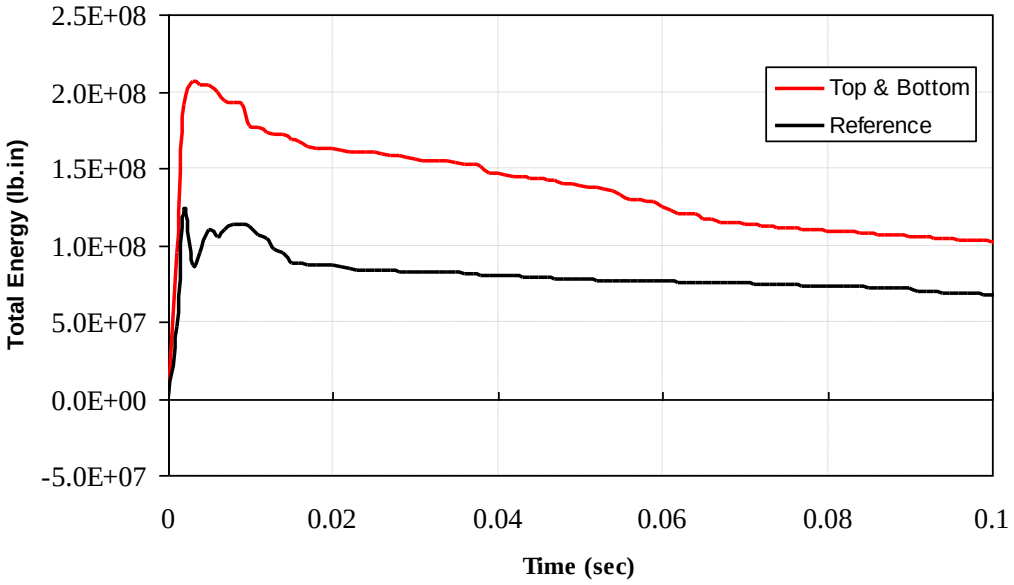

Figure 30. Total energy for the bridge deck for the control and the strengthened cases

The strengthening of the box girder bridge deck using CFRP in three ways (on top surface, on bottom surface, and on the top and bottom surfaces) has a significant effect on the velocity time history. As shown in Fig. 31 the vertical velocity profile for the three strengthening cases of the box girder deck using CFRP, was compared to the reference case, which does not have any strengthening techniques. All the studied cases were for blast load of 10W and placed over the exterior web of the model. The vertical velocity for all the shown cases in Fig 31 are the same until about 0.001 seconds from the detonation time, and then a divergence occurred to the profile behavior.

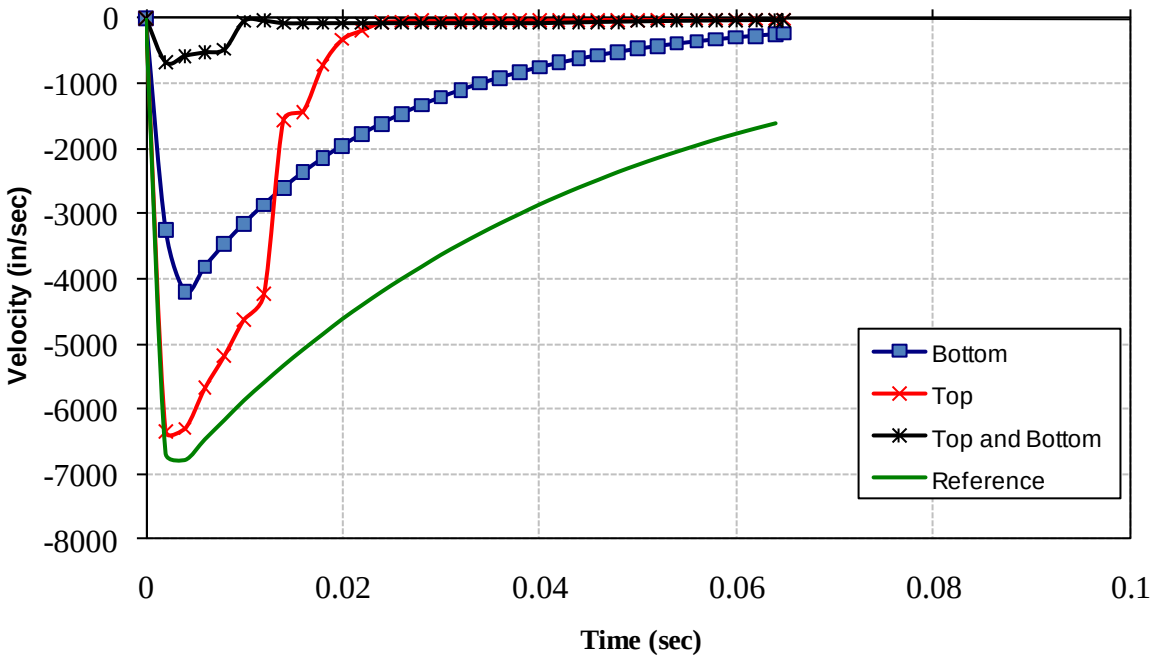

Figure 31. Velocity profile for the strengthened bridge deck

From the damage point of view, Table 16 shows the effect of strengthening the bridge deck using the CFRP in three methods. The maximum velocity was traced at the nearest element under the detonation point. The damage size is measured as the equivalent area of the formed crater. As shown in Table 16, there is a significant effect on decreasing the crater size especially when the carbon fiber was used on the bottom and the top faces of the concrete deck. For the blast load 10W, it is noticed that the crater size decreased from 247 in to 146 inches which indicates 40% decrease in the damage size. Similarly, for the load 30W, it is noticed that the crater size decreased from a global failure case to 196 inches which indicates that CFRP strengthening is effective for these types of decks. The CFRP did not prevent the damage to the deck but it decreased the catastrophic action of close-in detonations.

Table 16. Velocity time history and damage size of the CFRP strengthened cases

Case	Charge Size (lb)	Maximum Velocity (in/sec)	Damage Size/ Crater Diameter (in)
Control	10W	4650	247
Control	30W	6780	394
Bottom	10W	4050	152
Bottom	30W	4210	232
Top	10W	4420	159
Top	30W	6340	201
Top and Bottom	10W	765	146
Top and Bottom	30W	766	196

From the analysis of LS-DYNA results it is noticed that using CFRP absorbed some energy after the detonation time by few seconds and that appeared in the decrease of the damage size. But after the detonation the CFRP reached its maximum tensile strength rapidly as it behaved as a brittle material. The sheets were destroyed and a debonding occurred, then the remaining energy was transferred to the concrete deck resulting in cracking and damage process to start. Figure 32 shows the damage suffered by the bridge deck in the case of top and bottom strengthening under 10W loading. It is seen that using CFRP on the top and the bottom faces of the deck decreases the velocity of the nearest element to the detonation by over 80% which means that this technique is performing the best among the three, and could economically decrease the damage to these types of bridges.

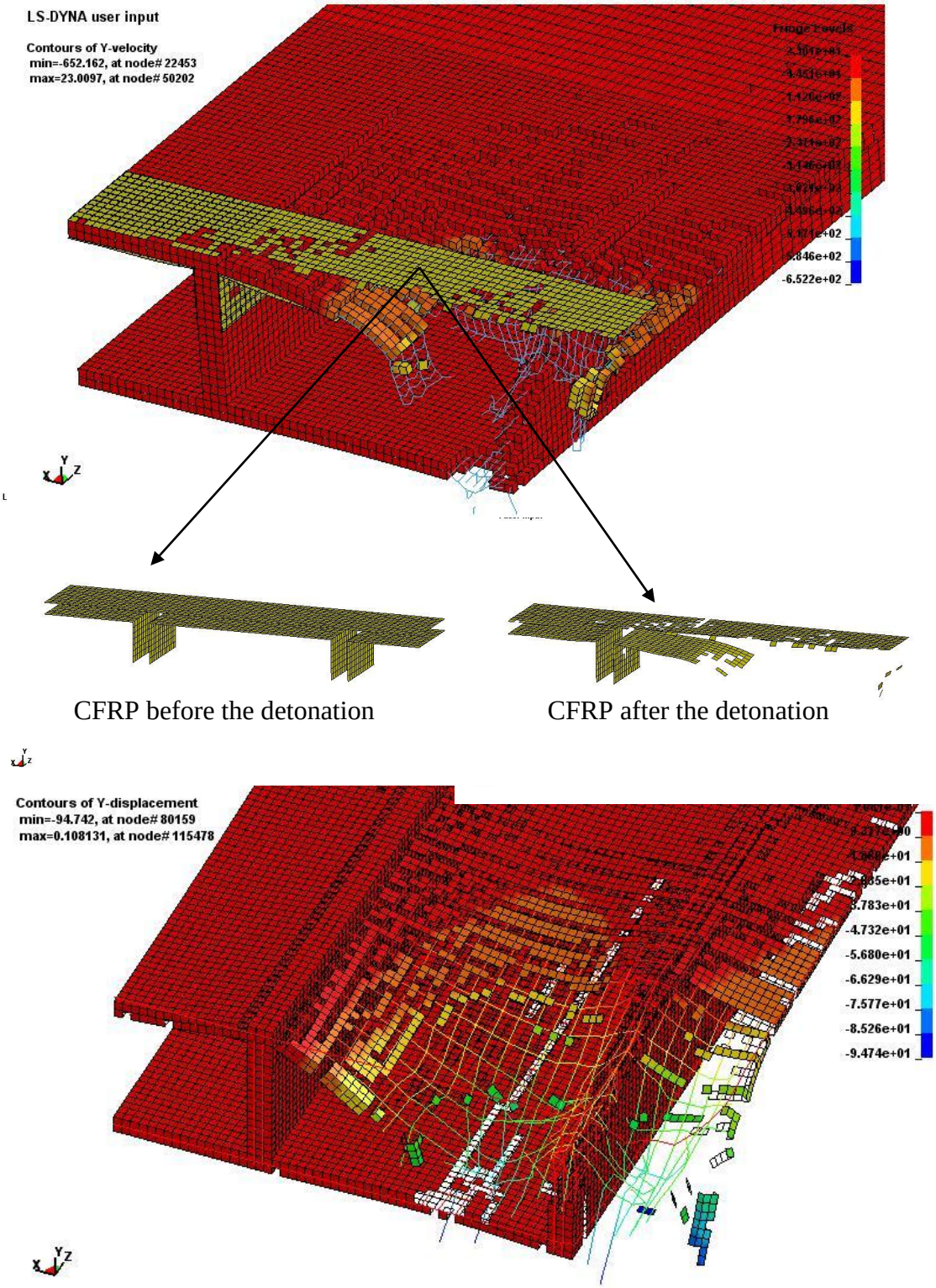

Figure 32. Damage before strengthening using the CFRP sheets

10. Summary

In this research, a literature review of the effect of blast loads on bridges is presented. The review indicates a need to establish design criteria for post-tensioned box girder bridges subjected to blast loads, based on numerical and analytical results. This design criterion would predict the relation between the charge size and the damage type (no damage, spall, and breach). For these needs, numerical models based on the nonlinear explicit finite element method were developed to predict the damage type. Specific conclusions and recommendations are presented in the next section.

10.1 Conclusions

1. The acceleration at the closest point to the detonation center (or to the closest point of the reinforcement when the concrete damage occurs very early) is the most important factor in design of bridges under close- in detonations.
2. The acceleration value is the fastest value that decays compared to velocity and displacement.
3. The concrete elements failed very quickly regardless of the concrete compressive strength, and the reinforcement did not fail, but suffered large deformations.
4. The strain rate effect must be taken into consideration in the design of bridges under close-in detonations. In some of the cases studied the increase was 8 times the uniaxial concrete strength due to the dynamic effect.
5. The steel grades did not affect the failure pattern significantly of the bridge section under different blast loads.
6. No damage occurred to the bridge below blast load of 0.2W.
7. A complete failure of the box girder bridge occurred after blast load of 30W.
8. There is a difference in the response if the detonation occurred over the vertical web rather than between the vertical webs. The former is better in resisting the load in terms of the damage size.
9. Increasing the uniaxial compressive strength of concrete by 200% decreased the damage and the mass loss by almost 50%.
10. Increasing the standoff distance from 30 inches to 120 inches results in the damage size decreasing form breaching (section loss) case to scabbing (spalling of concrete from the tension side) case. Long-term field performance of FRP retrofit were not investigated in this study, and thus a conclusive design recommendation cannot be made.
11. Using the carbon fiber reinforced polymer CFRP on both the top and bottom surfaces of the bridge concrete deck, increased the blast resistance of the bridge system and decreased the damage size.
12. According to the parametric study, a logarithmic equation was developed to predict the damage size as a function of the scaled standoff distance. This equation must be verified by experiments and has some limitations.

10.2 Recommendations

1. Field experiments should be conducted on the response of post-tensioned concrete box girder bridges under close-in detonations.
2. Additional research is needed to investigate the field application and long-term performance of CFRP composite materials as a blast-retrofit alternative as one of the proposed techniques in increasing the blast resistance for post-tensioned box girder bridges.
3. Further studies on box girder bridges are recommended to study the effect of close-in detonations from the soffit of the bridge and include the interaction between columns, the box girder, and the foundations.
4. Additional LS-DYNA simulations that are verified using field experiments are needed to create data sets that include all significant parameters that cover the problem domain. These results can be used to develop an artificial neural network (ANN) model which can be implemented into a fast-running high-fidelity design code for predicting the local and global response of post-tensioned box girder bridges under blast.

11. References

Alagusundaramoorthy P., Harik I.E., M.ASCE, and Choo C.C. (2006). Structural Behavior of FRP Composites Bridge Deck Panels. *Journal of Bridge Engineering*, 11, (4), July, 384-393.

ASCE (1997). Design of Blast Resistant Buildings in Petro-Chemical Facilities. American Society of Civil Engineers.

Barbero, E. (1995). CADEC-Computer Aided Design Environment for Composites. University of West Virginia.

Baylot, J., Roy, J., and Hall. J. (2002). Prediction Method for Response of Steel Bridge Beams and Girders to Blast and Fragment Load. *Transportation Research Record*.

Betra, R.C., and Hassan N.M. (2008). Blast Resistance of Unidirectional Fiber Reinforced Composites. *Composites engineering*, part B 39, 513-536.

Broadhouse B.J. (1995). The Winfrith Concrete Model in LS-DYNA3D. *Structural Performance Department, AEA Technology, Winfrith Technology Center.*

Buchan, P.A, and Chen J.F. (2007). Blast resistance of FRP composites and Polymer Strengthened Concrete and Masonry Structures- A state –of-the-Art Review. *Composites Engineering*, part B, 38, 509-522.

Cimo, R. (2007). Analytical Modeling to Predict Bridge Performance under Blast Loading. *Master Thesis*, University of Delaware., USA.

Cowper, G.R. and Symonds, P.S. (1957). Strain-Hardening and Strain-Rate Effects in the Impact Loading of Cantilever Beams. *Technical Reports No.28, Division of Applied Mathematics, Brown University*.

Islam, A.K., (2005). Performance of AASHTO Girder Bridges under Blast Loading. FAMU-FSU College of Engineering. Florida, Florida State University.

Kasidit, C., Solomon, C.S, Yim, M.ASCE, and Thomas, H.M.ASCE. (2006). Nonlinear Finite Element Analysis of FRP-Strengthened Reinforced Concrete Bridge. *Journal of Bridge Engineering, ASCE*, 11, (1), 21-32.

LS-DYNA (2007). Livermore Software Technology Corporation, LS-DYNA Nonlinear Dynamic Analysis of Structures. Version 971, Livermore, California, 2007.

Marchanad, K., Willaimson, E.B and Winget , D.G. (2004). Analysis of Blast Loads on Bridge Substructures. Structures under shock and impact VIII. Wessex. Institute of Technology Press, WIT Press.

Mosalam, M.K., and Mosallam, A.S. (2001). Nonlinear Transient Analysis of Reinforced Concrete Slabs Subjected to Blast Loading and Retrofitted with CFRP Composites. *Composites and Structures*, Part B 32, 623-636.

Nago, T., Mendis, P., Gupta, A. and Ramsay, J. (2007). Blast loading and blast effects on the structures-An overview. *Electronic Journal of Structure Engineering*. Special issue Feb., 92-101.

Nam, J.W, Kim, J.H, Kim, S.B, and Byun, K.J. (2009). Analytical Study of Finite Element FRP Retrofitted Concrete Structure under Blast Loads. *International Journal of Damage Mechanics*, 18-July 2009, 461-490.

Ottoson, N.S., (1975). Failure and Elasticity of Concrete. RISO-M1810.

Pelton, J.F. (1993). Bridge Inspections in Bosnia-Operation Grapple. *The Royal Engineering Journal*, 10(2).

Schleyer, G.K and Hsu, S.S. (2000). A Modeling Scheme for Predicting the Response of Elastic-Plastic Structures to Pulse Pressure Loading. *International Journal of Impact Engineering*, .759-777.

Son, J. (2008). Performance of Cable Supported Bridge Decks Subjected to Blast Loads. *Ph.D dissertation*, University of California, Berkeley, USA.

Vultisky, M., and Karniz, Z. (2002). Ship structures subject to high explosive detonation. *In: 7th International LS-DYNA Users Conference*, Michigan, USA: Livermore Software Technology Corporation (LSTC) and Engineering Technology Associates (ETA).

Williamson, E.B, and Marchand, K.A. (2006). Recommendations for Blast-Resistant Design and Retrofit of Typical Highway Bridges", Structure Congress (ASCE), Alexander Bell Drive, Reston, VA, USA.

Winget, D.G, Marchand, K.A, and Williamson, E.B. (2005). Analysis and Design of Critical Bridges Subjected to Blast Loads," *J. Struct. Engrg*, 131,(8), 1243-1255.

Wu C., Oehlers D.J., Rebentrost J., Leach J., and Whittaker A.S. (2009). Blast testing of Ultra-High Performance Fiber and FRP-Retrofitted Concrete Slabs. *Engineering Structures*, 31, 2060-2069.